1-1-2015

Tumor Promoting Functions of Lipid Storage in Clear Cell Renal Cell Carcinoma

Bo Qiu
University of Pennsylvania, boqiu@mail.med.upenn.edu

Tumor Promoting Functions of Lipid Storage in Clear Cell Renal Cell Carcinoma

Abstract
Two hallmarks of clear cell renal cell carcinoma (ccRCC) are constitutive hypoxia inducible factor (HIF) signaling and abundant intracellular lipid droplets (LDs). However, regulation of lipid storage and its role in ccRCC are incompletely understood. In this study, we explored the function of the LD coat protein perilipin 2 (PLIN2) within the context of ccRCC. Transcriptional profiling of primary ccRCC samples revealed that expression of PLIN2 was elevated in tumors and correlated with HIF-2α, but not HIF-1α, activation. HIF-2α dependent PLIN2 expression promoted lipid storage, proliferation, and viability in xenograft tumors. Mechanistically, lipid storage maintained integrity of the endoplasmic reticulum (ER), which is functionally and physically associated with LDs. Specifically, PLIN2 dependent lipid storage suppressed cytotoxic ER stress responses that otherwise result from elevated protein synthetic activity characteristic of ccRCC cells. Thus, in addition to promoting ccRCC proliferation and anabolic metabolism, HIF-2α modulates lipid storage to sustain ER homeostasis, particularly under conditions of nutrient and oxygen limitation, thereby promoting tumor cell survival. We also examined the mechanisms underlying the tumor promoting functions of PLIN2-dependent lipid storage in ccRCC. Most phospholipid and triacylglycerol (TAG) biosynthetic enzymes reside in the ER, and lipids are exchanged between the ER and LD. The phospholipid composition of the ER membrane is tightly regulated to support biosynthetic functions and protein homeostasis within the ER lumen. In addition, perturbation of the phospholipid membrane is sufficient to induce ER stress. We tested the hypothesis that (TAG) synthesis and storage prevents ER stress by guarding against perturbations in ER phospholipid composition. Phospholipid and TAG biosynthesis share a common pathway involving the synthesis of diacylglyerol. We found that ablation of the acyl-CoA:diacylglycerol (DGAT) enzymes necessary for TAG biosynthesis enhances sensitivity of ccRCC cells to conditions that perturb phospholipid homeostasis and trigger ER stress. These include exposure to the saturated fatty acid palmitate, hypoxia, and importantly, growth as a sub-cutaneous xenograft tumor. Collectively, our results reveal a novel function for the well-documented “clear cell” phenotype and identifying ER stress as a targetable vulnerability created by HIF-2α/PLIN2 suppression in this common renal malignancy.

Degree Type
Dissertation

Degree Name
Doctor of Philosophy (PhD)

Graduate Group
Cell & Molecular Biology

First Advisor
M. Celeste Simon

Second Advisor
Constantinos Koumenis

Keywords
Cancer, clear cell renal cell carcinoma, Endoplasmic reticulum, Lipid droplet, Lipid storage

Subject Categories
Biology

TUMOR PROMOTING FUNCTIONS OF LIPID STORAGE

IN CLEAR CELL RENAL CELL CARCINOMA

Bo Qiu

A DISSERTATION

in

Cell and Molecular Biology

Presented to the Faculties of the University of Pennsylvania

in

Partial Fulfillment of the Requirements for the

Degree of Doctor of Philosophy

2015

Supervisor of Dissertation

_____

M. Celeste Simon, Ph.D.

Scientific Director and Investigator, Abramson Family Cancer Research Institute

Professor, Cell and Developmental Biology

Graduate Group Chairperson

_____

Daniel S. Kessler, Ph.D.

Associate Professor of Cell and Developmental Biology

Dissertation Committee

Constantinos Koumenis, Professor, Radiation Oncology

Morris Birnbaum, Emeritus Professor of Medicine

Kathryn E. Wellen, Assistant Professor, Cancer Biology

Zoltan Arany, Associate Professor of Medicine

TUMOR PROMOTING FUNCTIONS OF LIPID STORAGE IN CLEAR CELL RENAL CELL

CARCINOMA

ACKNOWLEDGMENT

Note: excerpts from the following manuscript were included in this document (with permission from the American Association of Cancer Research):

Qiu, B., Ackerman, D., Sanchez, D.J., Li, B., Ochocki, J.D., Grazioli, A., Bobrovnikova-Marjon, E., Diehl, J.A., Keith, B., and Simon, M.C. (2015). HIF2alpha-Dependent Lipid Storage Promotes Endoplasmic Reticulum Homeostasis in Clear-Cell Renal Cell Carcinoma. Cancer Discov *5*, 652-667.

Note: excerpts from the following manuscript were included in this document (with permission from Elsevier):

Qiu, B. and Simon, M.C. (2015). Oncogenes strike a balance between cellular growth and homeostasis. Semin Cell Dev Biol. 2015. doi: 10.1016/j.semcdb.2015.08.005.

ABSTRACT

TUMOR PROMOTING FUNCTIONS OF LIPID STORAGE

IN CLEAR CELL RENAL CELL CARCINOMA

Bo Qiu

M. Celeste Simon

Two hallmarks of clear cell renal cell carcinoma (ccRCC) are constitutive hypoxia inducible factor (HIF) signaling and abundant intracellular lipid droplets (LDs). However, regulation of lipid storage and its role in ccRCC are incompletely understood. In this study, we explored the function of the LD coat protein perilipin 2 (*PLIN2*) within the context of ccRCC. Transcriptional profiling of primary ccRCC samples revealed that expression of *PLIN2* was elevated in tumors and correlated with HIF-2α, but not HIF-1α, activation. HIF-2α dependent PLIN2 expression promoted lipid storage, proliferation, and viability in xenograft tumors. Mechanistically, lipid storage maintained integrity of the endoplasmic reticulum (ER), which is functionally and physically associated with LDs. Specifically, PLIN2 dependent lipid storage suppressed cytotoxic ER stress responses that otherwise result from elevated protein synthetic activity characteristic of ccRCC cells. Thus, in addition to promoting ccRCC proliferation and anabolic metabolism, HIF-2α modulates lipid storage to sustain ER homeostasis, particularly under conditions of nutrient and oxygen limitation, thereby promoting tumor cell survival. We also examined the mechanisms underlying the tumor promoting functions of PLIN2-dependent lipid storage in ccRCC. Most phospholipid and triacylglycerol (TAG) biosynthetic enzymes reside in the ER, and lipids are exchanged between the ER and LD. The phospholipid composition of the ER membrane is tightly regulated to support biosynthetic functions and protein homeostasis within the ER lumen. In addition, perturbation of the phospholipid membrane is sufficient to induce ER stress. We tested the hypothesis that (TAG) synthesis and storage prevents ER stress by guarding against perturbations in ER phospholipid composition. Phospholipid and TAG biosynthesis share a common pathway involving the synthesis of diacylglyerol. We found that ablation of the acyl-

CoA:diacylglycerol (DGAT) enzymes necessary for TAG biosynthesis enhances sensitivity of ccRCC cells to conditions that perturb phospholipid homeostasis and trigger ER stress. These include exposure to the saturated fatty acid palmitate, hypoxia, and importantly, growth as a subcutaneous xenograft tumor. Collectively, our results reveal a novel function for the well-documented “clear cell” phenotype and identifying ER stress as a targetable vulnerability created by HIF-2α/PLIN2 suppression in this common renal malignancy.

TABLE OF CONTENTS

ABSTRACT IV

LIST OF TABLES IX

LIST OF ILLUSTRATIONS X

CHAPTER 1: INTRODUCTION 1

Introduction to clear cell renal cell carcinoma (ccRCC) 1

Genetics of ccRCC 1

Lipid storage 4

Oncogene activation and ER stress in cancer 4

Summary 7

CHAPTER 2: MATERIALS AND METHODS 9

Primary patient samples 9

Cell Culture and viability assays 9

Reagents 9

Plasmids, lentivirus production, and viral transduction 10

Xenografts 11

TCGA RNA-seq analysis 11

Microarray analyses 11

Tissue staining and imaging 11

RNA reverse transcription and quantitative RT-PCR analysis 12

BODIPY 493/503 and ER tracker staining 13

Transmission electron microscopy 13

PPRE reporter assay 14

ATP measurement **14**

Western blot analysis **14**

Protein synthesis measurement **15**

Metabolomics analysis **15**

Liquid Chromatography Mass Spectrometry (LC-MS) **15**

CHAPTER 3: HIF-2A DEPENDENT PLIN2 EXPRESSION AND LIPID STORAGE **17**

Introduction **17**
LD coat proteins 17
HIF-2α, lipid storage, and PLIN2 18

Results **20**
PLIN2 is overexpressed in ccRCC patient samples and positively correlated with HIF-2α activation 20
HIF-2α/PLIN2 promote lipid storage and tumor growth in ccRCC xenografts 30
PLIN2 dependent lipid storage is required for ER homeostasis and cell viability in ccRCC cell lines and xenograft tumors 35
PLIN2 dependent lipid storage supports ER homeostasis during oncogene mediated activation of protein synthesis 45
HIF-2α dependent PLIN2 expression and lipid storage promote resistance against pharmacologic ER stress 51

Discussion **57**

CHAPTER 4: DGAT ACTIVITY PROMOTES ER HOMEOSTASIS IN CCRCC **60**

Introduction **60**
Synthesis of TAG and phospholipid 60
Triglyceride storage and ER stress 62
Summary 63

Results **65**
Examining DGAT1 and DGAT2 function in A498 ccRCC cells 65
DGAT activity protects against palmitate-induced lipotoxicity 68
DGAT ablated cells are more sensitive to serum and oxygen deprivation 71
DGAT activity protects against pharmacologic ER stress 73
DGAT activity promotes tumor growth and protects against ER stress in subcutaneous ccRCC xenografts 75

Discussion **77**

CHAPTER 5: CONCLUSION **79**

Tumor promoting functions of lipid storage **79**

Future directions **80**
HIF-2α and PLIN2 expression: gene regulation and metabolic impacts 80
Extending the cytoprotective functions of lipid storage to other settings 82
Targeting oncogene-induced metabolic vulnerabilities 83

List of Tables

Table 1: Expression of triglyceride synthesis genes in primary ccRCC (n=480) compared to normal kidney (n=69) samples.

Table 2: Expression of cholesterol synthesis genes in primary ccRCC (n=480) compared to normal kidney (n=69) samples.

List of Illustrations

Figure 1: *PLIN2* is upregulated in primary ccRCC

Figure 2: *PLIN2* expression correlates with *VHL* inactivation and HIF-2α stabilization

Figure 3: HIF-2α, but not HIF-1α promotes PLIN2 expression in ccRCC cell lines

Figure 4: PPARγ function is not required for PLIN2 expression in ccRCC

Figure 5: HIF-2α dependent *PLIN2* expression and lipid storage promotes xenograft tumor growth.

Figure 6: HIF-2α dependent *PLIN2* expression and lipid storage promotes cell proliferation and viability in xenograft tumors

Figure 7: HIF-2α dependent PLIN2 expression promotes cell viability in nutrient deprived regions of 3D tumor spheroids

Figure 8: PLIN2 is required for lipid storage and cell viability in 786-O cells.

Figure 9: PLIN2 dependent lipid storage promotes ER homeostasis in ccRCC cells and xenograft tumors

Figure 10: PLIN2 is required for lipid storage, cell viability, and maintenance of ER homeostasis in A498 cells

Figure 11: Validation of IRE-1α inhibitor, PERK inhibitor, and ATF6 siRNA in A498 cells

Figure 12: Unfolded protein response promotes cell death upon PLIN2 depletion.

Figure 13: Energetic effects of PLIN2 depletion in ccRCC cell lines and evidence for suppression of β-oxidation in ccRCC tumor tissue

Figure 14: Suppression of mTORC1 ameliorates ER stress and cell death upon PLIN2 depletion

Figure 15: Suppression of protein synthesis ameliorates ER stress and cell death upon PLIN2 depletion

Figure 16: SREBP-dependent lipid synthesis is adaptive in PLIN2 depleted cells

Figure 17: HIF-2α/PLIN2 dependent lipid storage protects ccRCC cells against tunicamycin-induced ER stress

Figure 18: HIF-2α/PLIN2 dependent lipid storage protects ccRCC cells against bortezomib-induced ER stress

Figure 19: Proposed model illustrating the protective function of HIF-2α dependent PLIN2 expression and lipid storage in ccRCC

Figure 20: Model of ER membrane homeostasis.

List of Illustrations (continued)

Figure 21: Perturbations to the cellular lipid profile impact tumor growth.

Figure 22: Ablation of DGAT1 and DGAT2 in A498 cells

Figure 23: DGAT1/2 double ablation reduces TAG storage capacity

Figure 24: DGAT2 ablation enhances, while DGAT1 ablation ameliorates, palmitate-induced cell death.

Figure 25: DGAT1/2 double ablation enhances palmitate-induced lipotoxicity

Figure 26: DGAT activity protects against unsaturated lipid deprivation

Figure 27: DGAT activity protects against pharmacological ER stress

Figure 28: DGAT activity promotes ccRCC xenograft tumor growth

Chapter 1: Introduction

Introduction to clear cell renal cell carcinoma (ccRCC)

Renal cell carcinoma is a heterogeneous class of tumors arising from the kidney, distinguished by various histological and genetic characteristics. Collectively, renal cell carcinoma accounts for approximately 140,000 deaths annually (Siegel et al., 2014). ccRCC is the most common form of kidney cancer worldwide, making up 70% of cases; while papillary and chromophobe renal cell carcinomas make up 10-15% and 5% of all cases, respectively (Frew and Moch, 2015). ccRCC is among the few malignancies increasing in incidence (Siegel et al., 2014), owing largely to an increased rate of incidental detection by imaging studies. Nephrectomy is curative for most cases of localized disease; however, 5-year survival is 20% for patients diagnosed with metastatic disease and 25-30% of individuals initially diagnosed with resectable, local disease later present with metastatic disease (Frew and Moch, 2015). ccRCC tumors are resistant against conventional cytotoxic chemotherapy or radiation, and until 2007, the only approved therapies for metastatic disease included immune-modulatory therapy with high dose IL-2 or IFN-α (Lee-Ying et al., 2014; Sun et al.). While these therapies extend overall survival and are curative in some instances, they are associated with significant systemic toxicities that limit the number of patients that can tolerate such therapy. In recent years, an understanding of the molecular pathogenesis of ccRCC has led to the development of targeted therapies that elicit greater responses and fewer side-effects compared to previous therapies.

Genetics of ccRCC

An understanding of ccRCC tumorigenesis was aided by the identification of von Hippel-Lindau (VHL) familial cancer syndrome, which involves inherited predisposition to ccRCC, hemangioblastomas, and pheochromocytomas (Gossage et al., 2015). The *VHL* tumor suppressor gene was first identified by positional cloning in families with VHL disease (Latif et al., 1993). While VHL-disease cases make up a small portion of all ccRCC cases, multiple studies have indicated that the protein encoded by *VHL* (pVHL) is silenced or mutated in 90% of sporadic

ccRCC tumors (Cancer Genome Atlas Research, 2013; Gordan et al., 2008; Sato et al., 2013). pVHL functions as an adaptor protein within an E3 ligase complex that targets various proteins for proteasomal degradation. pVHL has been demonstrated to regulate a multitude of cellular processes, including oxygen-dependent degradation (ODD) of the hypoxia inducible factor alpha (HIFα) transcription factors, regulation of microtubule stability, maintenance of primary cilium function, and many others (Frew and Moch, 2015).

VHL disease is phenotypically diverse and can be classified into various sub-types based on the spectrum of disease which families present (i.e. ccRCC vs hemangioblastoma vs pheochromocytoma) (Gossage et al., 2015). Initial studies correlating genotype with phenotype revealed that ccRCC disease tracked with families exhibiting *VHL* mutations that disrupt ODD of HIFα subunits (Chen et al., 1995; Hoffman et al., 2001). Subsequent functional studies have confirmed a central role of constitutive HIF signaling in ccRCC and laid the foundation for development of targeted therapies currently used to treat advanced ccRCC (Keith et al., 2012; Kondo et al., 2003; Kondo et al., 2002; Shen and Kaelin, 2013).

HIF-dependent transcriptional responses to hypoxia are driven by heterodimers of HIF-1α or HIF-2α with a shared HIF-1β/ARNT subunit (Majmundar et al., 2010). In the presence of oxygen, HIF-α subunits are targeted for degradation by the oxygen-deponent hydroxylation of proline residues via a family of prolylhydroxyase (PHD) enzymes. Proline-hydroxylated HIFα subunits are recognized by a pVHL-containing E3 ligase complex, ubiquitinated, and targeted for degradation in the 26S proteasome. Under conditions of low oxygen tension, proline hydroxylation is suppressed and HIFα subunits are stabilized.

HIF-dependent transcriptional responses include the synthesis and secretion of vascular endothelial growth factor (VEGFA) and transforming growth factor alpha (TGFα) (Majmundar et al., 2010). Paracrine signaling via VEGFA drives the high rates of angiogenesis characteristic of ccRCC tumors, while autocrine signaling via TGFα contributes to ccRCC cell proliferation in the absence of exogenous, serum-supplied growth factors (Gunaratnam et al., 2003). Pharmacologic

agents that suppress signaling via these growth factor pathways have been approved for the treatment of ccRCC (Lee-Ying et al., 2014). For example, bevacizumab is a VEGF neutralizing antibody and small molecule kinase inhibitors, such as sunitinib, suppresses the signaling events downstream of growth factor receptor activation. HIF-dependent gene expression also contributes directly to enhanced cell proliferation and metabolic alterations that characterize ccRCC (Keith et al., 2012; Li et al., 2014; Majmundar et al., 2010; Schodel et al., 2012). HIF-1α enhances glycolytic flux by inducing genes involved in glucose uptake and glycolysis. In addition, HIF-1α decreases the rate of pyruvate entry into the tricarboxylic acid (TCA) cycle by enhancing expression of pyruvate dehydrogenase kinase 1 (PDK1), an inhibitor of pyruvate dehydrogenase. HIF-2α promotes tumor growth and proliferation via expression of VEGFA, TGFα, and cyclin D1 (Keith et al., 2012; Schodel et al., 2012). While HIF-1α and HIF-2α share several common transcriptional targets, they also exhibit distinct functions (Keith et al., 2012). This is particularly evident in ccRCC, where HIF-1α expression is frequently lost during disease progression, and pre-clinical data indicate that it can repress tumor growth (Raval et al., 2005; Shen et al., 2011). The central role of HIF-2α in ccRCC is supported by findings that 1) all pVHL-null ccRCC maintain HIF-2α expression (Gordan et al., 2008), 2) HIF-2α function is required for ccRCC xenograft growth (Kondo et al., 2003), and 3) polymorphisms in *EPAS1/HIF2α* are associated with increased ccRCC risk in GWAS studies (Purdue et al., 2011).

In hereditary, VHL disease-associated ccRCC, it was apparent that biallelic inactivation of *VHL* was an early event in disease progression (Mandriota et al., 2002). Recent high-throughput sequencing studies have revealed that pVHL loss of function is also an early event in sporadic ccRCC (Gerlinger et al., 2014). Specifically, multi-region biopsies taken from primary and metastatic tissues within the same patient reveal substantial intratumor heterogeneity with respect to DNA mutations. Despite this branched evolution within ccRCC tumors, biallelic inactivation of *VHL* was observed in all regions of the tumors analyzed, suggesting that *VHL* loss occurred early in the progression of disease. Longitudinal monitoring of VHL disease patients has revealed that the clear cell phenotype also develops early in disease progression, coincdiding

with pVHL loss of function and HIF-α stabilization (Mandriota et al., 2002). Despite these observations, the regulation and function of enhanced lipid storage in ccRCC has not been explored.

Lipid storage

ccRCC cells exhibit elevated intracellular lipid and glycogen content, which are washed away during routine tissue processing for histology and result in the "clear cell" appearance. This feature of disease has long aided pathological diagnosis, but its function in ccRCC is unknown. The intracellular lipid droplet consists of a neutral lipid core containing TAG and cholesterol-ester species surrounded by a phospholipid monolayer and associated LD surface proteins (Walther and Farese, 2012). Lipid droplets are ubiquitous organelles within mammalian cells. Energy storage is a primary function of lipid droplets within eukaryotic cells. Lipids liberated from LDs also provide substrates for membrane synthesis and the generation of lipid-derived signaling molecules.

LDs are functionally and physically associated with the endoplasmic reticulum (ER), as lipids and the proteins that synthesize/modify them are exchanged between these organelles via transient membrane bridges (Wilfling et al., 2013). In particular, many of the fatty acid, phospholipid, triglyceride, and cholesterol ester synthesis enzymes reside in the ER. The PAT (Perilipin, Adipophilin, Tip47) family of LD coat proteins regulates both lipid storage and lipolysis. Perilipin (PLIN1) is expressed primarily in adipocytes, while Adipophilin/Adipose Differentiation Related Protein (hereafter referred to as Perilipin 2, PLIN2) and TIP47 (PLIN3) are ubiquitously expressed and function as the predominant LD coat proteins in non-adipose tissue (Greenberg et al., 2011). Additional discussion of lipid droplet coat proteins and neutral lipid synthesis enzymes are included in Chapters 3 and 4, respectively.

Oncogene activation and ER stress in cancer

The clear cell nature of ccRCC is an indicator of profoundly altered cellular metabolism. In normal cells, metabolism is fine tuned to match nutrient, oxygen, and growth factor availability.

On the other hand, oncogenic transformation commits tumor cells to anabolic growth rates that generate metabolic stresses that must be overcome to sustain growth and survival. The ER is a "hub" for both protein and lipid metabolism, and maintenance of ER functions is necessary to support the high rates of anabolic metabolism required for tumor growth. In a cell-intrinsic manner, oncogene activation and cellular transformation commits tumors to growth programs that strain ER homeostasis, including dysregulation of protein and lipid metabolism (Young et al., 2013). Such ER stress is exacerbated by conditions of nutrient and O_2 deprivation characteristic of solid tumor microenvironments, which further disrupt cellular protein and lipid homeostasis (Ackerman and Simon, 2014).

The mechanistic target of rapamycin (mTOR) is a Ser/Thr kinase that functions as a master regulator of cell growth, proliferation, and metabolism (Laplante and Sabatini, 2012). mTOR exists in two distinct complexes (mTORC1 and mTORC2), with different subunit composition and cellular functions. mTORC1 promotes protein synthesis, glycolysis, lipogenesis, and nucleotide biosynthesis . mTORC1 functions as a nutrient and growth factor sensor in normal cells. Growth factor signaling and amino acid availability regulate mTORC1 via distinct mechanisms and both are required for mTORC1 activation (Chantranupong et al., 2015). Immunohistochemical staining for mTORC1 direct targets reveals pathway activation in >80% of cases (Haddad et al., 2015). mTORC1 signaling is likely promoted by multiple mechanisms in ccRCC. First of all, large scale exome sequencing has revealed pathway-activating mutations in approximately 30% of ccRCC tumors (Cancer Genome Atlas Research, 2013). Additionally, autocrine growth factor signaling via HIF-driven TGFα signaling promotes serum-independent mTORC1 activation (Gunaratnam et al., 2003). Indeed, mTORC1 inhibitors are approved as 3rd line therapies for ccRCC.

Perhaps one of the best-characterized functions of mTORC1 is increased protein synthesis through translation initiation and elongation (via phosphorylation of 4E-BP1 and S6K1) (Laplante and Sabatini, 2012). While multiple studies indicated that heightened protein synthesis

contributes to tumorigenesis downstream of mTORC1 (Barna et al., 2008; Faller et al., 2015), it also elicits tonic levels of ER stress that must be overcome (Hart et al., 2012; Ozcan et al., 2008). The ER is a hub for both protein and lipid metabolism, and optimal ER function requires coordination of these processes. In particular, increased ER protein load requires expansion of ER membrane via lipid synthesis, a process that is particularly important under ER stress (Lee et al., 2008). In addition, altered ER lipid content can impair protein-folding capacity (Fu et al., 2011). Multiple laboratories have identified the sterol regulatory element binding proteins (SREBP1/2) as mediators of fatty acid and sterol synthesis gene expression programs downstream of mTORC1 (Duvel et al., 2010; Porstmann et al., 2008).

mTORC1 activation not only enhances the quantity of fatty acids available for replication, but also fine tunes the composition of the fatty acid pool that ultimately gives rise to phospholipid membranes within the cell. Proper desaturation of membrane lipids is absolutely required to sustain organelle functions and cell viability. The stearoyl CoA desaturase enzyme (SCD1) generates unsaturated lipids within the cell. This enzyme, which is an mTORC1/SREBP1 target gene, also requires oxygen for its enzymatic activity (Behrouzian and Buist, 2002). Our lab demonstrated that under hypoxic conditions, where SCD1 is inhibited, mTORC1-driven protein synthesis sensitized tumor cells to serum lipid deprivation and subsequent ER stress (Young et al., 2013). Notably cytotoxic ER stress was suppressed by providing cells with the unsaturated fatty acid oleic acid or by reducing ER protein load using rapamycin or cyxloheximide. These findings were demonstrated in a variety of human cancer cells lines, revealing unsaturated lipid dependence as generalizable tumor cell vulnerability. Consistent with this finding, Griffiths et al showed that ablation of SREBP1 and 2, and thus SCD1 expression, elicited ER stress and cell death under conditions of serum lipid deprivation in various cancer cells (Griffiths et al., 2013).

In response to elevated mis-folded protein load or disruption of ER membrane lipid composition, mammalian cells activate a highly conserved unfolded protein response (UPR) (Volmer et al., 2013; Walter and Ron, 2011). ER stress sensors, including PERK, IRE-1α, and

ATF6, initiate UPR-driven adaptive processes, including a generalized reduction in protein synthesis and selective expression of genes encoding lipid synthetic enzymes, protein-folding chaperones, and components of the ER associated degradation (ERAD) system for enhancing proteasome dependent proteolysis. However, sustained and irremediable ER stress can trigger cell death via a "terminal" UPR (Clarke et al., 2014). The role of the UPR in cancer is complex. A cytoprotective role of the UPR has been demonstrated in various mouse models of cancer (Bobrovnikova-Marjon et al., 2010; Clarke et al., 2014). In particular, enhanced protein synthesis and increased ER protein load has been demonstrated to trigger a cytoprotective UPR downstream of mTORC1 or MYC activation (Hart et al., 2012). In addition, mutations that disrupt terminal UPR signaling, but maintain adaptive UPR functions, can be found within human tumors (Ghosh et al., 2014), further highlighting the importance of controlling ER stress to support tumor growth.

Summary

The central goal of this project was to identify mechanisms promoting lipid storage and the functions it serves in ccRCC. In Chapter 3, we examined the role of LD coat proteins in ccRCC. Transcriptional profiling of primary ccRCC and normal kidney samples revealed that *PLIN2,* but not other perilipin family members, is overexpressed in ccRCC and positively correlated with HIF-2α activation. HIF-2α promoted PLIN2 expression and lipid storage in ccRCC cell lines, and remarkably, PLIN2 activity accounted for a substantial portion of HIF-2α's tumor-promoting effects in xenograft assays. Mechanistically, HIF-2α/PLIN2-dependent lipid storage suppressed cytotoxic ER stress responses that otherwise result from elevated protein synthetic activity characteristic of ccRCC cells. These findings revealed an unexpected function for the "clear cell" phenotype and identify enhanced ER stress as a targetable vulnerability created by HIF-2α suppression in ccRCC. In Chapter 4, we examined the mechanism by which loss of lipid storage affected ER homeostasis and cell viability in ccRCC. For our approach, we suppressed TAG synthesis by ablating the acyl-CoA:diacylglcerol (DGAT) enzymes. We hypothesized that suppression of TAG synthesis would force more toxic fatty acids into the phospholipid pool, which

directly impacts ER membrane homeostasis. This function of DGAT was required for growth of ccRCC cells under various conditions that strain ER homeostasis, including *in vivo* tumor growth, *in vitro* culture conditions that perturb cellular fatty acid homeostasis, and in the presence of pharmacologic agents that increased mis-folded protein load in the ER.

Chapter 2: Materials and methods

Primary patient samples

Fresh frozen ccRCC or matched normal kidney patient samples were obtained from the Cooperative Human Tissue Network (CHTN). Samples were de-identified and handled in accordance with institutional review boards.

Cell Culture and viability assays

Authenticated (short tandem repeat profiling) human ccRCC cell lines 786-O, A498, and RCC4 were obtained from the American Type Culture Collection in 2001. Cells were cultured for a maximum of four weeks before thawing fresh, early passage cells. All cells were confirmed to be mycoplasma negative (MycoAlert) and verified for pVHL and HIFα expression status using western blot analysis. Cells were cultured in Dulbecco's Modified Eagle Medium (DMEM) + 10% FBS. Cell viability was determined using the FITC-Annexin V, PI kit (Cat 556547) from BD Biosciences according to the manufacturer's instructions. Flow cytometry was performed using the BD Accuri C6 instrument and double negative cells were deemed viable.

3D spheroid cultures were generated using the liquid overlay technique. 24 well plates were coated with 1% agarose in DMEM prior to plating 100,000 cells per well in DMEM + 10% FBS. To promote spheroid formation, plates were swirled prior to incubation. Media was changed every 3 days and spheroids were harvested after 9 days. Hypoxic cells were labeled by incubating spheroids with 200μM FITC-conjugated pimonidazole hydrochloride (Hypoxyprobe, Cat HP2) prior to fixation. For BODIPY 493/503 quantification, spheroids were dissociated with Accutase at 37°C for 30 minutes and stained as described below in "BODIPY staining".

Reagents

Oleic Acid (Cat O3008), rapamycin (Cat R8781), tunicamycin (Cat T7765), and brefeldin A (Cat B7651) were purchased from Sigma Aldrich. GSK2656157 PERK inhibitor (Cat 5046510001), 4μ8C IRE-1α inhibitor (Cat 412512), Torin1 (Cat 475991), and cycloheximide (Cat

239763) were purchased from Millipore. siRNA pools targeting human *ATF6* (Cat L-009917), *SREBF1* (Cat L-006891), and *SREBF2* (Cat L-009549) were purchased from Dharmacon. Rotenone (Cat 557368) was purchased from EMD Chemicals. Bortezomib was purchased from Cell Signaling Technologies (Cat 2204S).

Plasmids, lentivirus production, and viral transduction

The lentiviral vector PLKO.1 SCR (Plasmid No. 17920) was obtained from Addgene. pLKO.1 vectors expressing sh*HIF1A_9* (TRCN0000003809), shHIF2A_6 (TRCN0000003806), sh*HIFA_7* (TRCN0000003807), sh*PLIN2_1* (TRCN0000136605), sh*PLIN2_2* (TRCN0000136481), sh*PPARG_2* (TRCN0000001672), and sh*PPARG_3* (TRCN0000001673) were obtained from the Broad Institute TRC shRNA library. The GIPZ vector expressing sh*HIF1A_52* (V3LMM_441752) was obtained from Dharmacon. PLIN2 open reading frame was sub-cloned from MGC sequence verified cDNA (Dharmacon, Clone ID: 3844174) into the PCDH-CMV-MCS-EF1-HYGRO mammalian expression vector. The Doxycycline inducible shHIF2A_7 construct was generated using the "Tet-pLKO-puro" plasmid (Addgene Cat 21915). The indicated TRC library shRNAs against *DGAT1* (sh*DGAT1_9*: TRCN0000036149, sh*DGAT1_1*: TRCN0000036151) and *DGAT2* (sh*DGAT2_4*: TRCN0000005194, sh*DGAT2_5: TRCN0000005195*) were adapted to the "Tet-pLKO-puro" system. DGAT1/2 double ablation was achieved by expressing Dox-inducible sh*DGAT2_5* (Tet-pLKO-puro) and sh*DGAT1_1* (Tet-pLKO-neo, Addgene Plasmid #21916) within the same cells.

Lentivirus was produced by transfecting 293T cells with the indicated expression plasmid, pRSV-Rev, pMDL, and pCMV-VSV-G plasmids using Fugene6 (Promega). Virus was harvested 48 hours after transfection. For viral infection, cells were incubated with medium containing virus and 8μg/ml polybrene for 16 hours. Cells were allowed to recover for 48 hours before antibiotic selection, and surviving pools were utilized for downstream analyses.

Xenografts

Sub-cutaneous xenograft experiments were approved by the Animal Care and Use Committee at the University of Pennsylvania. NIH-III nude mice (Charles River, 4-6 weeks old) were injected in each flank with five million cells in a 1:1 mixture of PBS and Matrigel (BD 356234). Tumor volume was monitored by caliper measurements. After tumors reached 300mm^3, mice were split into cohorts receiving standard chow or Doxycycline chow (625 mg/kg, Harlan Labs Cat TD05125) *ad libitum.* After 11 days on the indicated chow, animals were sacrificed by CO_2 inhalation and xenograft tumors were dissected for downstream analyses.

TCGA RNA-seq analysis

Level 3 RNA-seq data for 480 ccRCC and 69 normal kidney samples was downloaded from the TCGA on April 2, 2013. Differential gene expression analysis of tumor and normal samples was performed using DeSeq (Bioconductor Version 2.12). Box and whisker plots correspond to 1-99th percentiles (bars), 25-75th percentiles (box), and median (line in box). Differentially expressed genes were subjected to gene set enrichment analysis (GSEA) using the Broad Institute Molecular Signature Database.

Microarray analyses

Classification of primary ccRCC samples into *VHL* WT, H1H2, and H2 sub-groups and microarray analysis was previously performed by our laboratory (Gordan et al., 2008). Expression data is deposited at the NCBI Gene Expression Omnibus (GEO) under GSE11904. Expression profiling of normal kidney, ccRCC, papillary RCC, and chromophobe RCC performed by Jones et al was downloaded from GEO (GSE15641) (Jones et al., 2005).

Tissue staining and imaging

For frozen patient samples, OCT embedded tissue was cut to 10μm sections and fixed in 4% paraformaldehyde (PFA) prior to staining. For xenograft tumors, samples were fixed in 4% PFA, equilibrated in 30% w/v sucrose, and embedded in OCT. 10μm sections were cut for staining. H&E staining was performed as previously described (Gordan et al., 2008).

Oil Red O: A working oil red O solution was generated by diluting a 3.5mg/ml stock (in 100% isopropanol) 6:4 with distilled water. This solution was incubated at room temperature for 30 minutes and filtered in Whatman paper before use. Tissue sections were incubated in 60% isopropanol for 5 minutes, dried at room temperature, and incubated in oil red O staining solution for 1 hour at room temperature. Slides were rinsed in distilled water and counterstained with hematoxylin prior to mounting in Prolong Gold Antifade with DAPI (Life Technologies, Cat P36935).

Immunohistochemistry: Slides were treated in 1% hydrogen peroxide for 30 minutes and blocked in 2% normal goat serum and 4% BSA in Tris buffer with Tween 20. Avidin/Biotin blocking was performed and sections were incubated with primary antibodies overnight at 4°C. Ki67 antibody was used at 1:100 (BD, Cat 550609). Cleaved caspase 3 (Asp175) antibody was used at 1:400 (Cell Signaling, Cat 9661). Slides were incubated in 1:200 dilutions of biotinylated goat anti-mouse (Vector Labs, Cat BA-9200) or anti-rabbit (Vector Labs, Cat BA-1000) secondary antibodies for 1 hour at room temperature. Sections were then processed using the Vectastain Elite ABC kit (Vector Labs, PK-6100) and DAB peroxidase substrate kit (Vector Labs, Cat SK-4100), dehydrated in a standard ethanol/xylenes series, and mounted in 75% v/v Permount (Fischer, Cat SP15-500) in xylenes.

Immunofluorescence: Slides were incubated in 50mM ammonium chloride for 10 minutes, permeabilized with 0.25% Triton X-100 for 10 minutes, and blocked in 2% normal goat serum and 4% BSA for 1 hour. Slides were incubated with cleaved caspase 3 (Asp175) antibody at 1:400 (Cell Signaling, Cat 9661) overnight at 4°C. Secondary Alexa Flour 488 goat anti-rabbit (Life technologies, Cat A-11008) was used at 1:200 for 1 hour at room temperature. Slides were mounted in Prolong Gold Antifade with DAPI before imaging.

RNA reverse transcription and quantitative RT-PCR analysis

Total RNA was isolated using the RNAeasy purification kit (Qiagen). cDNA was synthesized using the Applied Biosystems High Capacity RNA-to-cDNA master mix. qRT-PCR

was performed on a ViiA7 Real Time PCR systems from Applied Biosystems. Pre-designed Taqman primers were obtained from Life Technologies for the following genes: *TBP* (HS01060665_G1), *ACTB* (HS01060665_G1), *VEGFA* (HS00900055_M1), *PLIN2* (HS00605340_M1), *HIF2A/EPAS1* (HS01026149_M1), *HIF1A* (HS00153153_M1), *TGFA* (HS00608187_M1), *PDK1* (HS01561850_M1), *PLIN3* (HS00998416_M1), *BiP/HSPA5* (HS00946084_G1), *XBP1(spliced)* (HS03929085_G1), *CHOP/DDIT3* (HS00358796_G1), *ERO1A/ERO1L* (HS00205880_M1), HERP/*HERPUD1* (HS01124269_M1), *EDEM1* (HS00976004_M1), *ERdj4/DNAJB9* (HS01052402_M1), and *HRD1/SVN1* (HS00381211_M1), *ATF6* (HS00232586_M1), *DGAT1* (HS01017541_M1), and *DGAT2* (HS01045913_M1). SYBR-green primers were utilized for human *ATF3* (Forward: TAGGCTGGAAGAGCCAAAGA, Reverse: TTCTCACAGCTGCAAACACC).

BODIPY 493/503 and ER tracker staining

BODIPY 493/503 (Cat D3922) was purchased from Life Technologies. Live cells were washed twice in PBS and incubated in 2μg/ml BODIPY in PBS for 15 minutes at 37°C. After staining, cells were washed twice in PBS and fixed in 2% PFA for 15 minutes. Fixed cells were washed and re-suspended in Annexin-V binding buffer (BD Cat 556454), passed through a cell strainer, and analyzed on an Accuri C6 flow cytometer under FL-1. ER-Tracker Red (Cat E34250) was purchased from Life Technologies. Live cells were incubated with 1μM ER Tracker on DMEM with 10% FBS for 30 minutes. Cells were washed twice in PBS, re-suspended in PBS with 5% serum, passed through a cell strainer, and analyzed on an Accuri C6 flow cytometer under FL-3. Data analysis was performed using FlowJo software.

Transmission electron microscopy

Cells were fixed with 2.5% glutaraldehyde, 2.0% paraformaldehyde in 0.1M sodium cacodylate buffer, pH7.4, overnight at 4°C. After subsequent buffer washes, the samples were post-fixed in 2.0% osmium tetroxide for 1 hour at room temperature, and then washed again in buffer followed by distilled water. After dehydration through a graded ethanol series, the tissue

was infiltrated and embedded in EMbed-812 (Electron Microscopy Sciences, Fort Washington, PA). Thin sections were stained with uranyl acetate and lead citrate and examined with a JEOL 1010 electron microscope fitted with a Hamamatsu digital camera and AMT Advantage image capture software.

PPRE reporter assay

The PPRE X3-TK-luc plasmid was purchased from Addgene (No. 1015). 30,000 cells were seeded into 24 well plates and transfected with 1μg of PPRE X3-TK-luc and 100ng of Renilla luciferase plasmids using Fugene 6 (Promega). Luciferase activity was measured two days after transfection using the Dual Luciferase assay kit (Promega).

ATP measurement

ATP luminescence assay system (Cat 6016941) was purchased from Perkin Elmer. 100,000 cells were plated into each well of an opaque 96 well plate and analyzed as described by the manufacturer.

Western blot analysis

Cells were lysed in lysis buffer (40mM HEPES, 2mM EDTA, 10mM pyrophosphate, 10mM glycerophosphate, 1% Triton X-100) containing Roche complete ultra protease/phosphatase inhibitor (Cat 05892791001). Nuclear and cytoplasmic fractionation was performed using the Thermo Scientific NE-PER kit (Cat PI-78833). Isolated proteins were resolved by SDS-PAGE and western blot analysis was performed. All primary antibodies were diluted at 1:1000 in 5% w/v non-fat milk, unless otherwise noted. Blots were incubated with primary antibodies overnight at 4°C. HIF-2α (Cat NB100-122) and phospho-serine 724 IRE-1a (Cat NB-100-2323) were purchased from Novus Biologicals. HIF-1α antibody (Cat 610958) was purchased from BD Biosciences. PLIN2 antibody (Cat ab78920) was purchased from Abcam. β-Actin (1:4000, Cat SC-47778), ATF6 (Cat SC-22799), ATF4 (1:2000, Cat SC-200), and DGAT1 (1:1000, Cat SC-32861) antibodies were purchased from Santa Cruz Biotechnology. Cleaved caspase 3 (Cat 9661), PERK (1:4000, Cat 3192), IRE1a (Cat 3294), phospho-threonine 389

S6K1 (Cat 9234), S6K1 (Cat 2708), phosphor-serine 65 4E-BP1 (Cat 9451), 4E-BP1 (Cat 9452), FASN (Cat 3180), ACC (Cat 3696), HDAC1 (1:4000, Cat 5365), and PPARG (Cat 2435) antibodies were purchased from Cell Signaling Technology. Rabbit polyclonal phospho-threonine 980 PERK antibody was a gift from Dr. Alan Diehl. Primary antibodies were detected using horseradish peroxidase conjugated secondary antibodies (Cell Signaling Technologies) followed by exposure to ECL (Pierce).

Protein synthesis measurement

Protein synthesis was measured as described (Schmidt et al., 2009). Briefly, cells were pulsed with puromycin (30 min, 10µg/ml) and chased in puromycin free media (1 hr). Whole cell lysates were subjected to western blot analysis using anti-puromycin antibody (Millipore, Cat MABE343) at 1:20,000.

Metabolomics analysis

Mass spectrometry based metabolomics analysis was performed in conjunction with Metabolon, as previously described (Li et al., 2014).

Liquid Chromatography Mass Spectrometry (LC-MS)

Total lipid was purified from cultured cells by the Folch method, as previously described (Folch et al., 1957). Briefly, pelleted cells were incubated with 2 ml methanol, 1.5 ml PBS, and 20 µl of internal standard (Ceramide $^{13}C_2$, D_2). Homogenate was mixed by vortexing and 4 ml of chloroform was added to each sample. Samples was placed in an orbital shaker for 20 minutes before centrifuging at 2000xg for 5 minutes. The bottom layer was transferred and dried under nitrogen. 100ul of mobile phase solvent was addeded to each sample (Acetonitrile: Isopropanol: water at 5:3:2) and vortexed for 30 seconds. After incubating for 1 minute, samples were transferred to HPLC vials.

For LC-MS, a Thermo Scientific LTQ-Orbitrap-XL was used at a resolution of 60,000. The samples were analyzed on a Waters nano-ACQUITY UPLC system (Waters Corp., Milford, MA, USA). A Waters XBridge BEH130 C18 column (100 µm × 150 mm, 1.7 µm pore size; Waters

Corp) was employed for reversed phase separation with 3 µL injections. The flow-rate was 1.5 µL/min, solvent A was (40:60; v/v) water/acetonitrile with 0.1% formic acid, 10 mM ammonium formate and solvent B was (10:90; v/v) acetonitrile/isopropanol with 0.1% formic acid, 10 mM ammonium formate. The gradient was as follows: 32% B at 0 min, 32% B at 6 min, 45% B at 10min, 52% B at 11 min, 60% B at 17 min, 70% B at 20 min, 75% B at 27 min, 97 % at 29 min, 70 % B at 36 min, 32 % at 38 min, and 32% B at 45 min. Separations were performed at 50 °C. For LC-HRMS analysis, a recently calibrated LTQ XL-Orbitrap hybrid mass spectrometer (Thermo Fisher) was used in positive ion mode with a Michrom captive spray ESI source. The operating conditions were: spray voltage at 1.5 kV; capillary temperature at 200 °C; capillary voltage at 0 V, tube lens 80 V. Data were analyzed using Theromo Scientific™ Xcalibur™ software.

Chapter 3: HIF-2α dependent PLIN2 expression and lipid storage

Introduction

LD coat proteins

The PAT family of LD coat proteins impacts the structure and function of LDs (Bickel et al., 2009). The most studied LD coat protein is PLIN1, which is the predominant PAT family member expressed in adipocytes. Interestingly, PLIN2 and PLIN3 are expressed during development and differentiation of adipocytes, but are ultimately replaced by PLIN1 is mature adipose (Martinez-Botas et al., 2000; Tansey et al., 2001). In addition to providing structure to the LD, PLIN1 regulates the removal of lipids from the neutral LD via lipolysis. Adipocytes exhibit a low level of basal lipolysis, but can greatly enhance rates of neutral lipid hydrolysis upon β-adrenergic stimulus. PLIN1 impacts both basal and stimulated lipolysis. Under basal conditions, PLIN1 suppresses the activity of adipose triglyceride lipase (ATGL). However, upon adrenergic stimulus, protein kinase A (PKA)-mediated phosphorylation of PLIN1 is required for maximal activation of neutral lipid hydrolysis. Thus, *Plin1* deficient mice exhibit reduced adiposity secondary to enhanced basal lipolysis, but are impaired in increasing serum lipid concentrations under β-adrenergic stimulus (Martinez-Botas et al., 2000; Tansey et al., 2001).

PLIN2 and PLIN3 are the predominant LD coat proteins outside of adipose tissue. The regulation and functions of PLIN2 and PLIN3 have been examined primarily in the context of physiologic and pathophysiologic states of lipid accumulation, including hepatic steatosis and foamy macrophage formation (Greenberg et al., 2011). In these settings, increased lipid levels are sensed by the peroxisome proliferator-activated receptor (PPAR) family of transcription factors, including PPARα and PPARγ, which are activated by lipophilic ligands. Upon activation, these transcription factors coordinately upregulate both PLIN2 and PLIN3. PLIN2 is stable only when bound to the surface of lipid droplets, while PLIN3 is stable in the cytosol and localizes to LDs upon lipid loading. While the biophysical principles underlying LD budding from the ER are

incompletely understood, it is hypothesized that PLIN2 and/or PLIN3 localization to the nascent LD facilitates organelle stability and budding from the ER (Thiam et al., 2013).

Recently, the dynamic nature of the LD has come into focus and it has become increasingly clear that PLIN2 is not merely a marker of lipid accumulation. Instead, gain and loss of function studies have revealed that PLIN2 impacts the dynamic regulation of lipid entry and exit from the LD. For instance, overexpression of PLIN2 in cultured fibroblasts, hepatocytes, or in murine liver is sufficient to drive lipid storage, lipid uptake, and de novo lipogenesis (Imamura et al., 2002; Sun et al., 2012). Similarly, acute ablation of hepatic Plin2 expression in mouse models of fatty liver reduced *de novo* fatty acid synthesis and TAG content. PLIN2 also stabilizes neutral lipid stores by suppressing LD localization and activation of ATGL (Sapiro et al., 2009). Recent work reveals that selective degradation of PLIN2 by chaperone-mediated autophagy is required for activation of lipolysis under nutrient limited conditions (Kaushik and Cuervo, 2015).

Global deletion of *Plin1* or *Plin2* in mice reveals some functional compensation within the PAT family, but clearly indicates that each protein also has distinct, non-redundant functions. For instance, Plin2 can coat the surface of LDs in *Plin1* null adipocytes (Martinez-Botas et al., 2000; Tansey et al., 2001). Nonetheless, the mice exhibit reduced adiposity, increased basal lipolysis, and impaired β-adrenergic induced lipolysis. *Plin2* knockout animals are completely viable and do not exhibit overt phenotypes under basal conditions. Indeed, Plin3 coats the LDs the hepatocytes of these animals. Nonetheless, *Plin2* null mice exhibit reduced hepatic TAG content and are protected against hepatic steatosis and insulin resistance when fed a high fat diet (Chang et al., 2006; Chang et al., 2010). These results indicate that Plin3 is not able to fully compensate for Plin2 loss.

HIF-2α, lipid storage, and PLIN2

Multiple studies report that PLIN2 upregulated in ccRCC compared to normal kidney tissue (Tun et al., 2010; Yao et al., 2007), and urinary protein content of PLIN2 has been reported as a biomarker of ccRCC (Morrissey et al., 2015). In addition, an association between constitutive

HIF activation and enhanced lipid storage has been documented before. First of all, Plin2 expression is positively correlated with HIF-2α activation in mouse hepatocytes *in vivo* (Rankin et al., 2009). In murine models of hepatocyte *VHL* deletion, enhanced lipid storage and *Plin2* upregulation are observed. Notably, co-deletion of *Epas1/HIF2α* abrogated this phenotype. Furthermore, our microarray data suggest that HIF-2α promotes *PLIN2* mRNA expression in ccRCC cells *in vitro* (Hu et al., 2003). These observations suggest a potential functional relationship between two hallmarks of ccRCC: HIF activation and enhanced lipid storage.

Results

PLIN2 is overexpressed in ccRCC patient samples and positively correlated with HIF-2α activation

To confirm the contribution of neutral lipid storage to the "clear cell" phenotype in our archived ccRCC tissues, we performed oil red O staining of primary tumor and matched normal kidney samples and observed enhanced neutral lipid staining in ccRCC tumor cells (Fig. 1A). Potential mediators of enhanced lipid storage were identified by analyzing RNA-seq data released by The Cancer Genome Atlas (TCGA) comparing primary ccRCC (n=480) and normal kidney (n=69) tissues (Cancer Genome Atlas Research, 2013). Focusing on expression of the PAT family of lipid droplet coat proteins, we observed that *PLIN2* was overexpressed in tumors across all stages of disease (Fig. 1B). In contrast, mRNA expression of other perilipin family members was not enhanced in ccRCC (Fig. 1C). *PLIN2* upregulation was confirmed in an independent set of matched ccRCC (n=10) and normal kidneys (n=10) from our archived samples (Fig. 1D). Analysis of "Triglyceride Synthesis" and "Cholesterol Synthesis" gene-sets within the TCGA RNA-seq dataset, as defined by the Broad Institute Molecular Signatures database, revealed differential expression of many lipogenic genes (Tables 1-2). Some fatty acid and triglyceride synthesis genes were upregulated within tumor tissues (i.e. *ACLY*, *ELOVL2*, *LPCAT1*), while many others were downregulated (i.e. multiple *ACSL* and *AGPAT* family members) (Table 1). On the other hand, the expression of most cholesterol biosynthetic enzymes was decreased in tumor tissue relative to normal kidney (Table 2). Although altered expression of triglyceride and cholesterol synthesis enzymes may impact lipid synthesis and storage in ccRCC, we focused our attention on *PLIN2* for multiple reasons. First of all, functional studies in murine models of hepatosteatosis have revealed that Plin2 upregulation is necessary for lipid storage and enhanced *de novo* lipid synthesis, even if other lipogenic genes were overexpressed (i.e. *Elovl3*, *Fasn*, *Scd1*) (Imai et al., 2012; Imamura et al., 2002). Secondly, overexpression of Plin2 alone was sufficient to drive lipid synthesis and storage in murine liver and mouse embryonic fibroblasts (Imamura et al., 2002; Sun et al., 2012). Taken together with the observation that HIF-

2α activation and PLIN2 expression are positively correlated in various settings, these findings suggested a functional connection between two hallmarks of ccRCC—constitutive HIF activity and heightened neutral lipid storage.

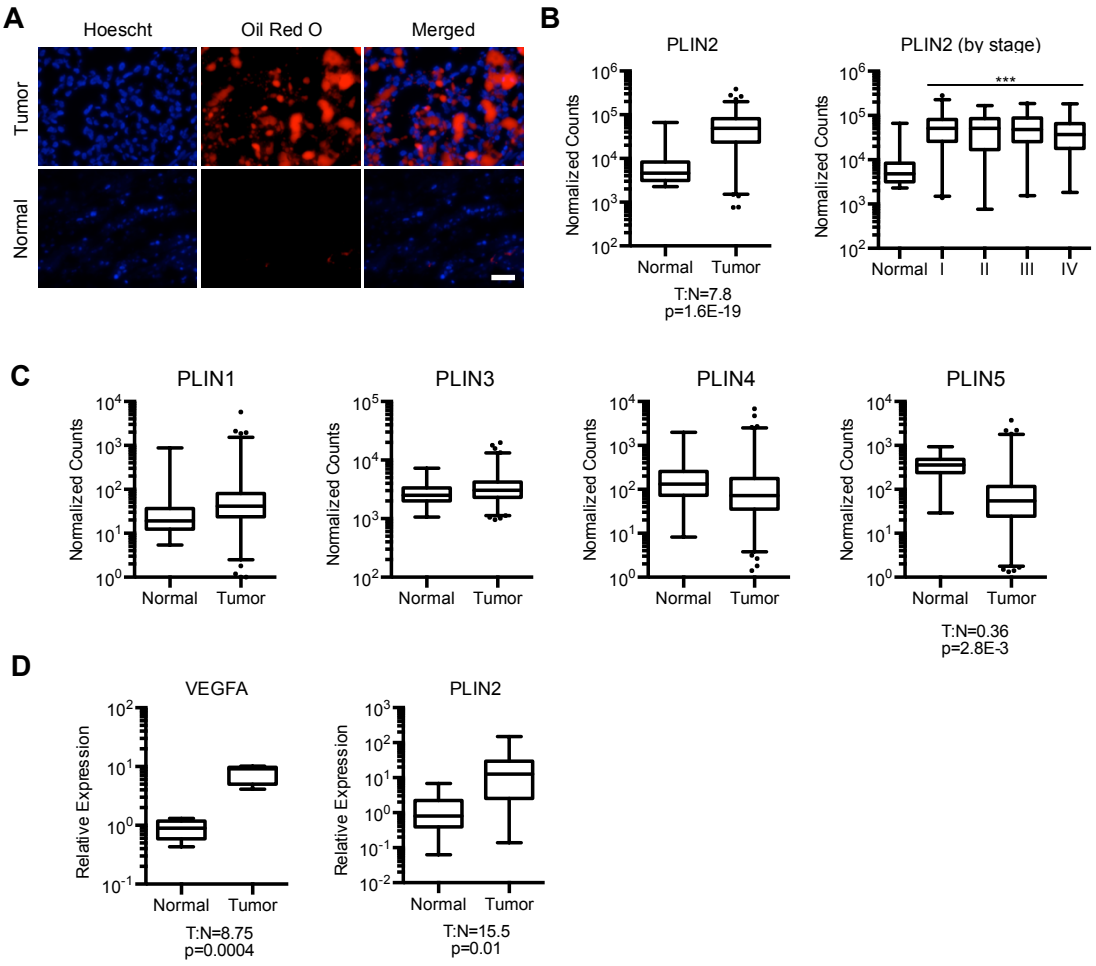

Figure 1: *PLIN2* is upregulated in primary ccRCC

A) Oil red O staining of matched primary ccRCC and normal kidney samples. Scale bar = 50 µm.

B) Normalized RNA-seq reads of *PLIN2* in ccRCC (n=480) and normal kidney (n=69) samples. Tumors were also analyzed for *PLIN2* expression according to tumor stage. RNA-seq data was obtained from The Cancer Genome Atlas (TCGA), and p-values determined by DEseq. Whiskers denote the 1st and 99th percentiles.

C) Normalized RNA-seq reads for genes encoding the PAT family of LD coat proteins in ccRCC (n=480) and normal kidney (n=69) samples. Data obtained from The Cancer Genome Atlas (TCGA). p-values were determined by DEseq.

D) Quantitative RT-PCR (qRT-PCR) analysis of *VEGFA* and *PLIN2* in matched ccRCC (n=10) and normal kidney (n=10) samples obtained from the Cooperative Human Tissue Network (CHTN). Whiskers denote the 1st and 99th percentiles.

Gene Symbol	Fold Change (Tumor vs. Normal)	Adjusted p-value	Description
AGPAT9	**-5.65**	**6.33E-17**	**1-acylglycerol-3-phosphate O-acyltransferase 9**
ACSL6	**-5.00**	**4.79E-04**	**acyl-CoA synthetase long-chain family member 6**
GPD1	**-3.04**	**3.38E-09**	**glycerol-3-phosphate dehydrogenase 1 (soluble)**
ELOVL3	-3.01	9.53E-02	ELOVL fatty acid elongase 3
GPD1L	**-2.79**	**3.15E-10**	**glycerol-3-phosphate dehydrogenase 1-like**
GK	**-2.77**	**8.34E-13**	**glycerol kinase**
ACSL4	**-2.68**	**5.18E-28**	**acyl-CoA synthetase long-chain family member 4**
LPIN2	**-2.05**	**9.80E-17**	**lipin 2**
ACSL3	**-1.91**	**4.01E-13**	**acyl-CoA synthetase long-chain family member 3**
LPIN1	**-1.84**	**3.12E-07**	**lipin 1**
ACSL1	**-1.71**	**3.66E-07**	**acyl-CoA synthetase long-chain family member 1**
AGPAT4	**-1.70**	**3.68E-03**	**1-acylglycerol-3-phosphate O-acyltransferase 4**
ACACA	**-1.58**	**1.68E-05**	**acetyl-CoA carboxylase alpha**
GPAM	**-1.58**	**1.26E-02**	**glycerol-3-phosphate acyltransferase, mitochondrial**
ELOVL6	**-1.57**	**4.25E-03**	**ELOVL fatty acid elongase 6**
DGAT2	-1.47	5.66E-01	diacylglycerol O-acyltransferase 2
AGPAT3	**-1.32**	**4.13E-02**	**1-acylglycerol-3-phosphate O-acyltransferase 3**
AGPAT2	**-1.14**	**4.38E-02**	**1-acylglycerol-3-phosphate O-acyltransferase 2**
DGAT1	-1.13	2.19E-01	diacylglycerol O-acyltransferase 1
TECR	-1.12	3.34E-01	trans-2,3-enoyl-CoA reductase
AGPAT1	-1.08	5.86E-01	1-acylglycerol-3-phosphate O-acyltransferase 1
ELOVL4	1.02	1.00E+00	ELOVL fatty acid elongase 4
LCLAT1	1.02	8.01E-01	lysocardiolipin acyltransferase 1
ELOVL1	1.06	8.48E-01	ELOVL fatty acid elongase 1
AGPAT6	1.10	5.16E-01	1-acylglycerol-3-phosphate O-acyltransferase 6
FASN	1.12	6.36E-01	fatty acid synthase
SLC25A1	1.19	1.96E-01	solute carrier family 25 (mitochondrial carrier; citrate transporter), member 1
LPCAT4	1.19	6.13E-01	lysophosphatidylcholine acyltransferase 4
AGPAT5	**1.32**	**3.09E-02**	**1-acylglycerol-3-phosphate O-acyltransferase 5**
ACSL5	**1.48**	**5.47E-03**	**acyl-CoA synthetase long-chain family member 5**
ELOVL7	**1.50**	**9.07E-04**	**ELOVL fatty acid elongase 7**
ELOVL5	**1.74**	**2.50E-08**	**ELOVL fatty acid elongase 5**
ACLY	**2.62**	**4.09E-12**	**ATP citrate lyase**
GPAT2	2.69	1.15E-01	glycerol-3-phosphate acyltransferase 2, mitochondrial
LPIN3	**2.82**	**4.26E-13**	**lipin 3**
LPCAT1	**5.89**	**7.50E-39**	**lysophosphatidylcholine acyltransferase 1**
ELOVL2	**9.32**	**1.04E-06**	**ELOVL fatty acid elongase 2**

Table 1: Expression of triglyceride synthesis genes in primary ccRCC (n=480) compared to normal kidney (n=69) samples. RNA-seq data was obtained from The Cancer Genome Atlas (TCGA), and p-values determined by DEseq. Genes of interest were obtained from the "Triglyceride Synthesis" gene set from the MSigDB (Broad Institute). Data are sorted by fold change and significantly altered genes ($p<0.05$) are shown in bold.

Gene Symbol	Fold Change (Tumor vs. Normal)	Adjusted p-value	Description
TM7SF2	**-2.10289**	**1.82E-09**	**transmembrane 7 superfamily member 2**
HMGCR	**-2.07684**	**2.51E-12**	**3-hydroxy-3-methylglutaryl-CoA reductase**
FDFT1	**-2.04116**	**1.96E-16**	**farnesyl-diphosphate farnesyltransferase 1**
IDI1	**-2.03994**	**4.50E-11**	**isopentenyl-diphosphate delta isomerase 1**
CYP51A1	**-2.02077**	**9.62E-15**	**Cytochrome P450, Family 51, Subfamily A, Polypeptide 1**
SOAT2	-1.84305	0.548695	Sterol O-acyltransferase (acyl-Coenzyme A: cholesterol acyltransferase) 2
SC5DL	**-1.666**	**0.000194949**	**sterol-C5-desaturase**
DHCR7	**-1.59281**	**1.13E-05**	**7-dehydrocholesterol reductase**
SQLE	**-1.58155**	**0.000378643**	**squalene epoxidase**
HMGCS1	**-1.53447**	**7.50E-05**	**3-Hydroxy-3-Methylglutaryl-CoA Synthase 1 (Soluble)**
DHCR24	**-1.52765**	**7.19E-06**	**24-dehydrocholesterol reductase**
LSS	**-1.35662**	**0.0168087**	**lanosterol synthase (2,3-oxidosqualene-lanosterol cyclase)**
EBP	**-1.34193**	**0.0115545**	**emopamil binding protein (sterol isomerase)**
GGPS1	-1.16436	0.210802	geranylgeranyl diphosphate synthase 1
MVK	-1.09057	0.322348	mevalonate kinase
LBR	-1.02221	0.903213	lamin B receptor
FDPS	-1.01414	0.981354	farnesyl diphosphate synthase
IDI2	1.01563	0.964958	isopentenyl-diphosphate delta isomerase 2
PMVK	1.0621	0.793446	phosphomevalonate kinase
MVD	1.11229	0.756692	mevalonate (diphospho) decarboxylase
NSDHL	1.12495	0.659622	NAD(P) dependent steroid dehydrogenase-like
SOAT1	1.27231	0.0633827	Sterol O-acyltransferase (acyl-Coenzyme A: cholesterol acyltransferase) 1
HSD17B7	**2.90771**	**1.30E-07**	**hydroxysteroid (17-beta) dehydrogenase 7**

Table 2: Expression of cholesterol synthesis genes in primary ccRCC (n=480) compared to normal kidney (n=69) samples. RNA-seq data was obtained from The Cancer Genome Atlas (TCGA), and p-values determined by DEseq. Genes of interest were obtained from the "Cholesterol Biosynthesis" gene set from the MSigDB (Broad Institute). Data are sorted by fold change and significantly altered genes ($p<0.05$) are shown in bold.

Our analysis of published microarray data profiling gene expression in normal kidney and distinct renal malignancies (Jones et al., 2005) revealed that *PLIN2*, along with a panel of established HIF-2α target genes, is specifically elevated in ccRCC samples (Fig. 2A). Because pVHL loss of function is a defining feature of most ccRCC, we examined whether HIF activation promotes PLIN2 expression. To explore this link in ccRCC patient samples, we performed transcriptome profiling of tumors previously grouped into three categories based on HIF-α staining and *VHL* gene sequencing: *VHL* WT (no HIF-α staining), HIF-1α and HIF-2α expressing ("H1H2"), and HIF-2α only ("H2") (4). This analysis indicated that *PLIN2* mRNA was elevated in both H1H2 (9.7 fold overexpression, p=2.6E4) and H2 (16.7 fold overexpression, p=2.5E-6) tumors when compared to *VHL* WT samples (Fig. 2B). Multiple documented HIF-2α targets in ccRCC exhibited a similar expression pattern (Fig. 2B). Collectively, these observations suggest that *PLIN2* levels increase early in disease progression and correlate with enhanced HIF-2α activity in ccRCC patient samples.

To directly examine the role of HIF-2α in PLIN2 regulation in ccRCC, we depleted HIF-2α from 786-O (H2) and RCC4 (H1H2) ccRCC cell lines using multiple shRNAs and found that *PLIN2* mRNA and protein expression was reduced (Fig. 3A-B). In contrast, *HIF1A* silencing in RCC4 cells actually enhanced *PLIN2* mRNA and protein levels, while decreasing levels of the HIF-1α target pyruvate dehydrogenase kinase 1 (*PDK1)* (Fig. 3B). These results are consistent with the *PLIN2* expression pattern we observed in primary patient samples, where *PLIN2* expression is positively correlated with HIF-2α activation (Fig. 2B). We also determined whether peroxisome proliferator-activated receptor gamma (PPARγ) regulates PLIN2 in ccRCC, as PPARγ is overexpressed in ccRCC tissue and was previously shown to stimulate *PLIN2* transcription in the settings of hepatosteatosis and foam cell formation (Inoue et al., 2001). In A498 cells, which exhibit high levels of both PPARγ and PLIN2, *PPARG* shRNAs reduced PPAR-response element reporter activity, but not PLIN2 levels (Fig. 4A-B). PPARα (*PPARA*) also promotes *PLIN2* transcription in states of lipid accumulation (Greenberg et al., 2011). However, expression of *PPARA* and many of its target genes are reduced in ccRCC compared to normal

kidney tissue (Fig. 4C-D), decreasing the likelihood that it regulates PLIN2 in ccRCC.

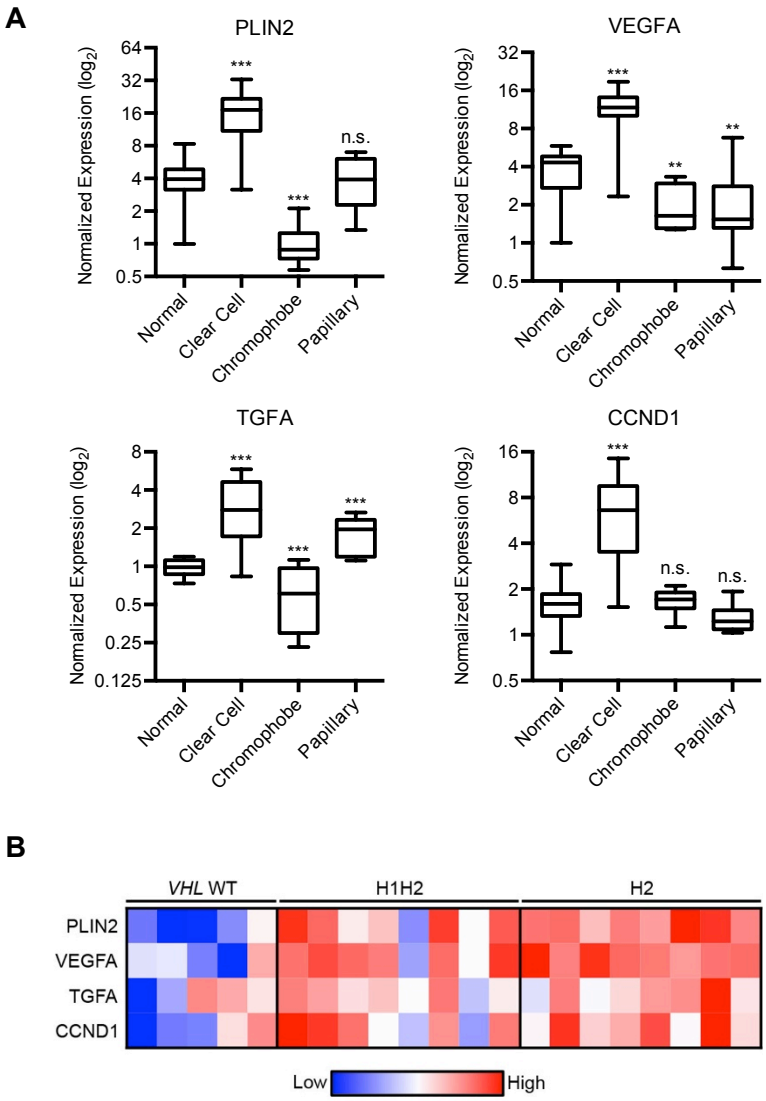

Figure 2: *PLIN2* expression correlates with *VHL* inactivation and HIF-2α stabilization

A) Comparison of gene expression levels of *PLIN2* and multiple known HIF-2α target genes in normal kidney and distinct renal cancer tissues. Normal n=23, ccRCC n=32, Chromophobe n=6, papillary n=11. p-values were adjusted for multiple comparisons. ** p<0.01, *** p<0.001.

B) Microarray analysis of primary ccRCC samples that have been previously classified by *VHL* genotyping and HIF-α immunohistochemical staining to reveal 3 sub-types: *VHL* WT (no HIF-1α or HIF-2α staining and confirmed WT sequence at *VHL* locus, n=5), H1H2 (HIF-1α and HIF-2α staining, n=8), and H2 (HIF-2α staining only, n=8). Expression of *PLIN2* and multiple known HIF-2α target genes in ccRCC are shown. *PLIN2* mRNA was elevated in both H1H2 (9.7 fold overexpression, p=2.6E-4) and H2 (16.7 fold overexpression, p=2.5E-6) tumors compared to *VHL* WT samples. p-values determined by ANOVA.

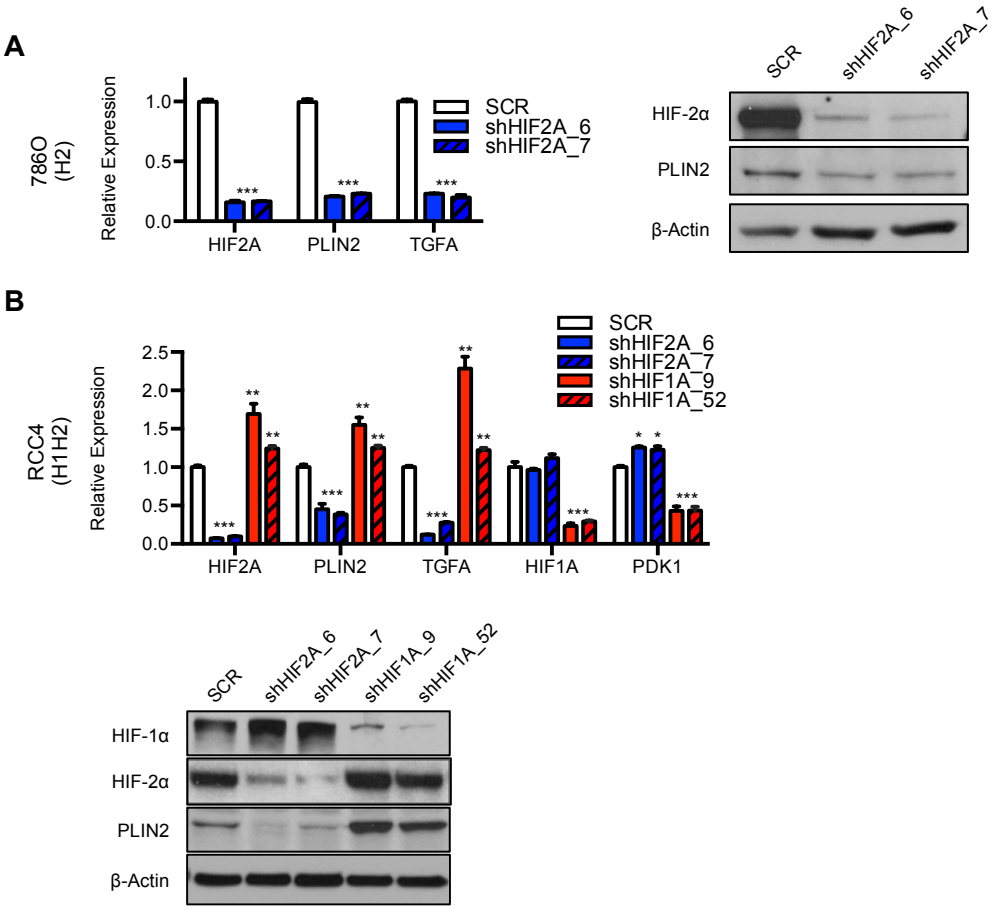

Figure 3: HIF-2α, but not HIF-1α promotes PLIN2 expression in ccRCC cell lines

A) 786-O (H2) ccRCC cells were transduced with two independent shRNAs against *HIF2A* (shHIF2A_6 and 7) or a SCR control. qRT-PCR (left) and western blot analysis (right) of PLIN2 are shown. *TGFA* is included as a positive control for HIF-2α suppression.

B) RCC4 (H1H2) ccRCC cells were transduced with two independent shRNAs against HIF-1α (shHIF1A_9 and 52), HIF-2α (shHIF2A_6 and 7), or a SCR control. qRT-PCR (top) and western blot (bottom) for PLIN2 is shown. *TGFA* and *PDK1* are included as positive controls for HIF-2α and HIF-1α suppression, respectively. Data are representative of three independent experiments. Unless otherwise noted, p-values were determined by student's t-test. * p<0.05, ** p<0.01, *** p<0.001. For qRT-PCR, *TBP* and *ACTB* were utilized as endogenous control genes and relative mRNA expression was determined by normalizing to expression in SCR samples. Error bars denote standard error of the mean (SEM).

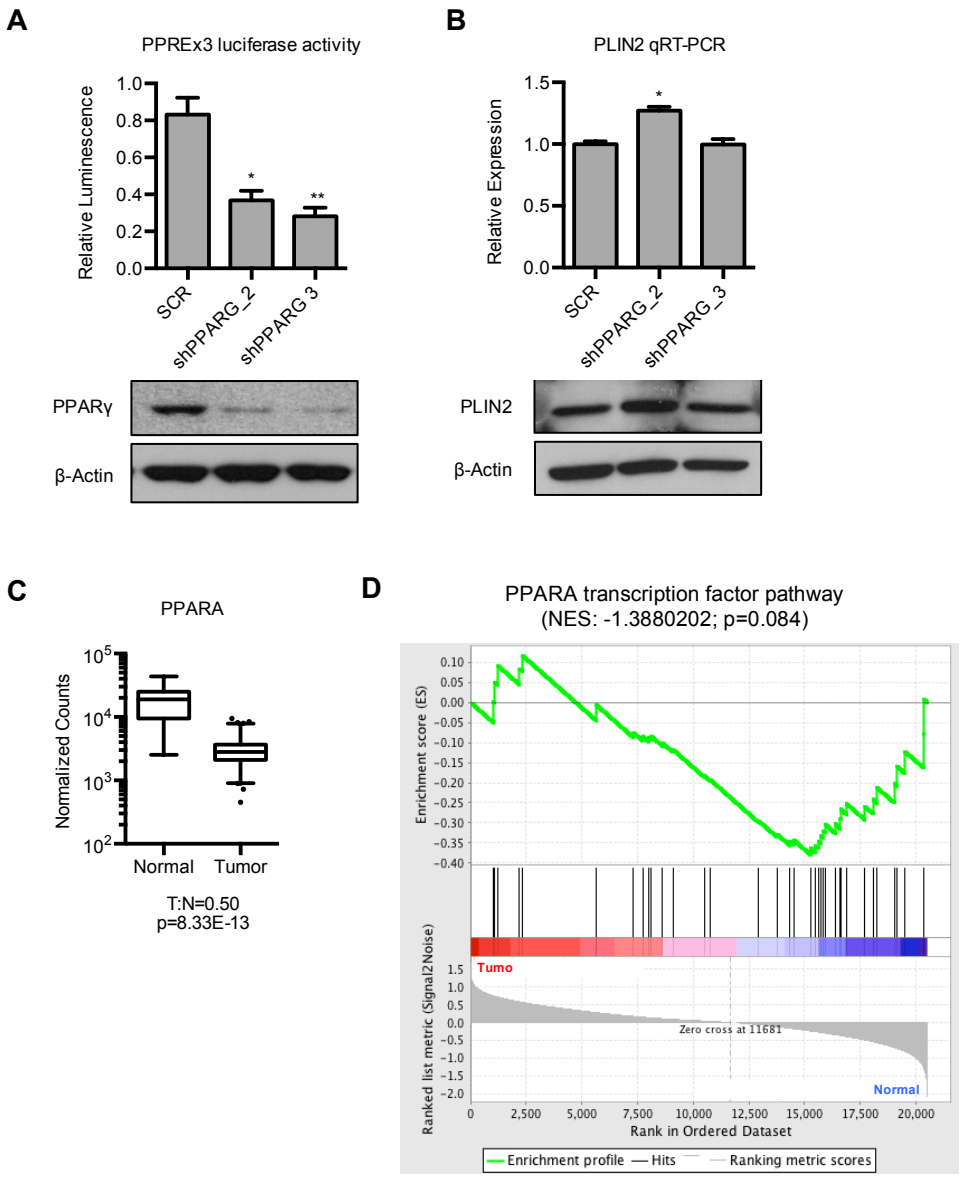

Figure 4: PPARγ function is not required for PLIN2 expression in ccRCC

A) A498 cells were transduced with two independent shRNAs against *PPARG* or a SCR control. PPAR response element reporter activity and western blot for PPARγ are shown.

B) qRT-PCR and western blot analysis for *PLIN2* expression in cells from (A).

C) Normalized RNA-seq reads for *PPARA* in the TCGA data set. Data obtained from The Cancer Genome Atlas (TCGA). p-values were determined by DEseq.

D) Gene set enrichment analysis (GSEA) of differentially expressed genes in ccRCC tumor vs normal kidney samples was performed on the TCGA RNA-seq data set. Results for the "PPARA transcription factor pathway" gene set are shown. * p<0.05. Error bars denote SEM.

These findings suggest that constitutive HIF-2α activity, rather than PPARγ, PPARα, or HIF-1α, regulates PLIN2 in both ccRCC cell lines and primary patient samples.

HIF-2α/PLIN2 promote lipid storage and tumor growth in ccRCC xenografts

PLIN2 is commonly used as a marker of cellular lipid accumulation, but its overexpression is also sufficient to increase lipid synthesis and storage in murine fibroblasts *in vitro* and liver *in vivo* (Imamura et al., 2002; Sun et al., 2012). Given the numerous tumor-promoting processes downstream of HIF-2α, we tested whether PLIN2 restoration alone was sufficient for tumor growth following HIF-2α suppression in multiple model systems. Doxycycline (Dox)-inducible shRNA was used to deplete HIF-2α in 786-O cells constitutively expressing either pCDH empty vector (EV) or an exogenous *PLIN2* cDNA. Xenografts generated from these two cell lines grew at identical rates prior to Dox exposure (data not shown). After administration of Dox-chow to inhibit HIF-2α, EV xenografts exhibited a steady decline in tumor volume and reduced mass at sacrifice, whereas those expressing exogenous PLIN2 demonstrated partial maintenance of both tumor volume and mass (Fig. 5A-B). qRT-PCR analysis confirmed that HIF-2α regulates *PLIN2 in vivo* and exogenous *PLIN2* mRNA levels were maintained following Dox-induced HIF-2α depletion (Fig. 5C). Furthermore, oil red O staining indicted that HIF-2α loss reduced neutral lipid staining, whereas exogenous PLIN2 fully restored lipid storage (Fig. 2B-C). These results indicate that PLIN2 is both necessary and sufficient to promote neutral lipid storage in ccRCC xenografts. Further histological analysis revealed that HIF-2α depletion dramatically decreased tumor cell proliferation, as indicated by Ki67 staining, which was partially restored by exogenous PLIN2 (Fig. 6). We also found that HIF-2α suppression resulted in large areas of tissue necrosis and induction of apoptosis, based on cleaved caspase 3 accumulation, which were both reduced by *PLIN2* expression (Fig. 6).

Despite the complexity of HIF-2α dependent tumorigenesis *in vivo*, including cell extrinsic effects such as angiogenesis, PLIN2 restoration alone significantly restored tumor cell proliferation and viability. We reasoned that enhanced lipid storage imparts a cell intrinsic

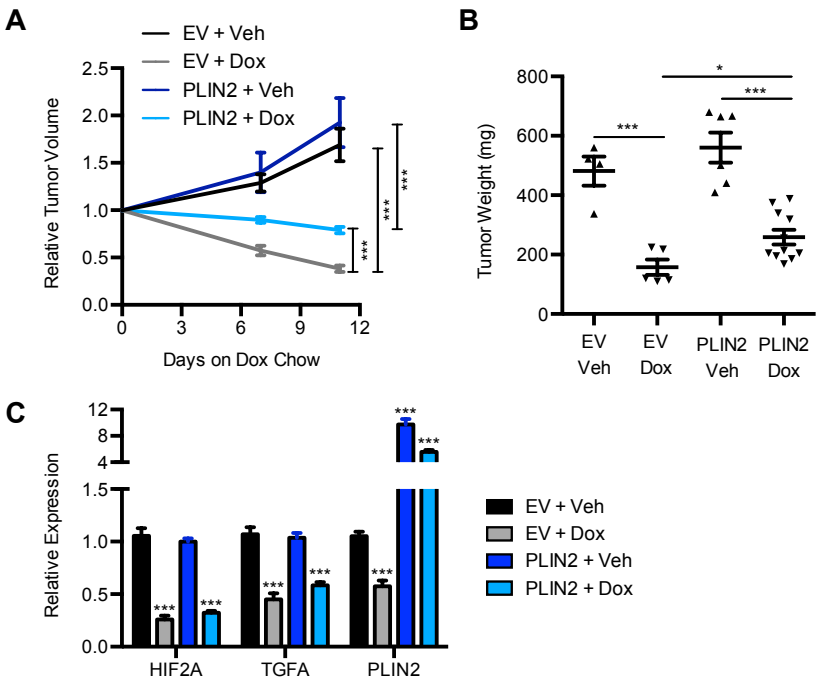

Figure 5: HIF-2α dependent *PLIN2* expression and lipid storage promotes xenograft tumor growth.

A) Sub-cutaneous tumors of 786-O cells expressing Dox-inducible shHIF2A_7, along with either empty vector or exogenous *PLIN2*, were generated in NIH-III nude mice. Once tumor volume reached 300mm^3, a cohort received Dox-chow (625 mg/kg). Relative tumor volume was monitored until 11 days of Dox treatment.

B) Tumor weights at harvest were determined.

C) qRT-PCR analysis for *HIF-2α*, *TGFA,* and *PLIN2* was performed. EV Veh, n=4; EV Dox, n=5; PLIN2 Veh n=6; PLIN2 Dox, n=9. For qRT-PCR, *TBP* and *ACTB* were utilized as endogenous control genes and relative mRNA expression was determined by normalizing to expression in EV Veh samples.

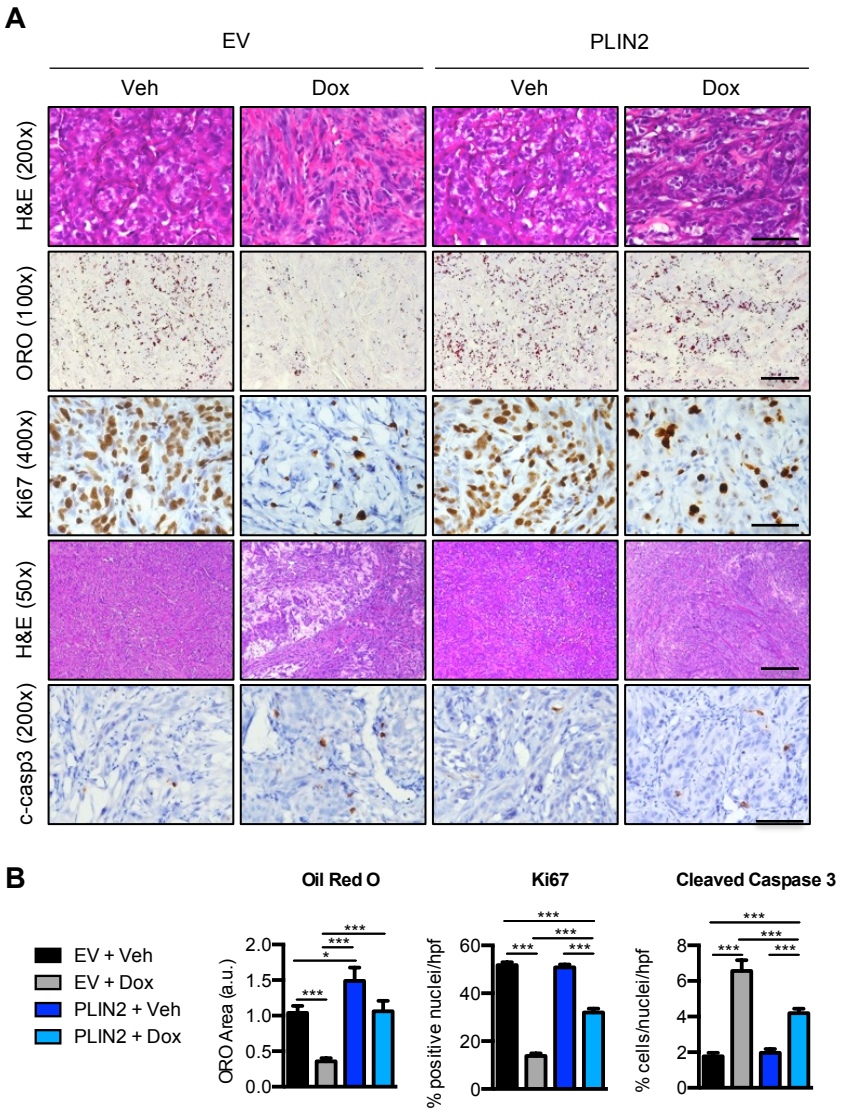

Figure 6: HIF-2α dependent *PLIN2* expression and lipid storage promotes cell proliferation and viability in xenograft tumors

A) Histological analysis of tumors is shown. Scale bars: 50x=400μm, 100x=200μm, 200x=100μm, 400x=50μm.

B) Oil red O area per field was determined using Image J. Percentage of cells per field that exhibited nuclear Ki67 or cleaved caspase 3 expression is shown. For each graph, 30 fields per tumor type were quantified. p-values were determined by two-way ANOVA with Bonferroni correction. * $p<0.05$, ** $p<0.01$, *** $p<0.001$. Error bars denote SEM.

advantage to tumor cells. To test this hypothesis, we generated *in vitro* 3D tumor spheroids using 786-O cells, which recapitulate nutrient and O_2 gradients within solid tumors (Fig. 7A-B). In this assay, HIF-2α inhibition was associated with loss of neutral lipid staining and enhanced cell death, while exogenous PLIN2 expression partially restored lipid storage and reduced cell death (Fig. 7C-D). Thus, multiple tumor model systems suggest an essential role for PLIN2 dependent lipid storage downstream of HIF-2α in ccRCC.

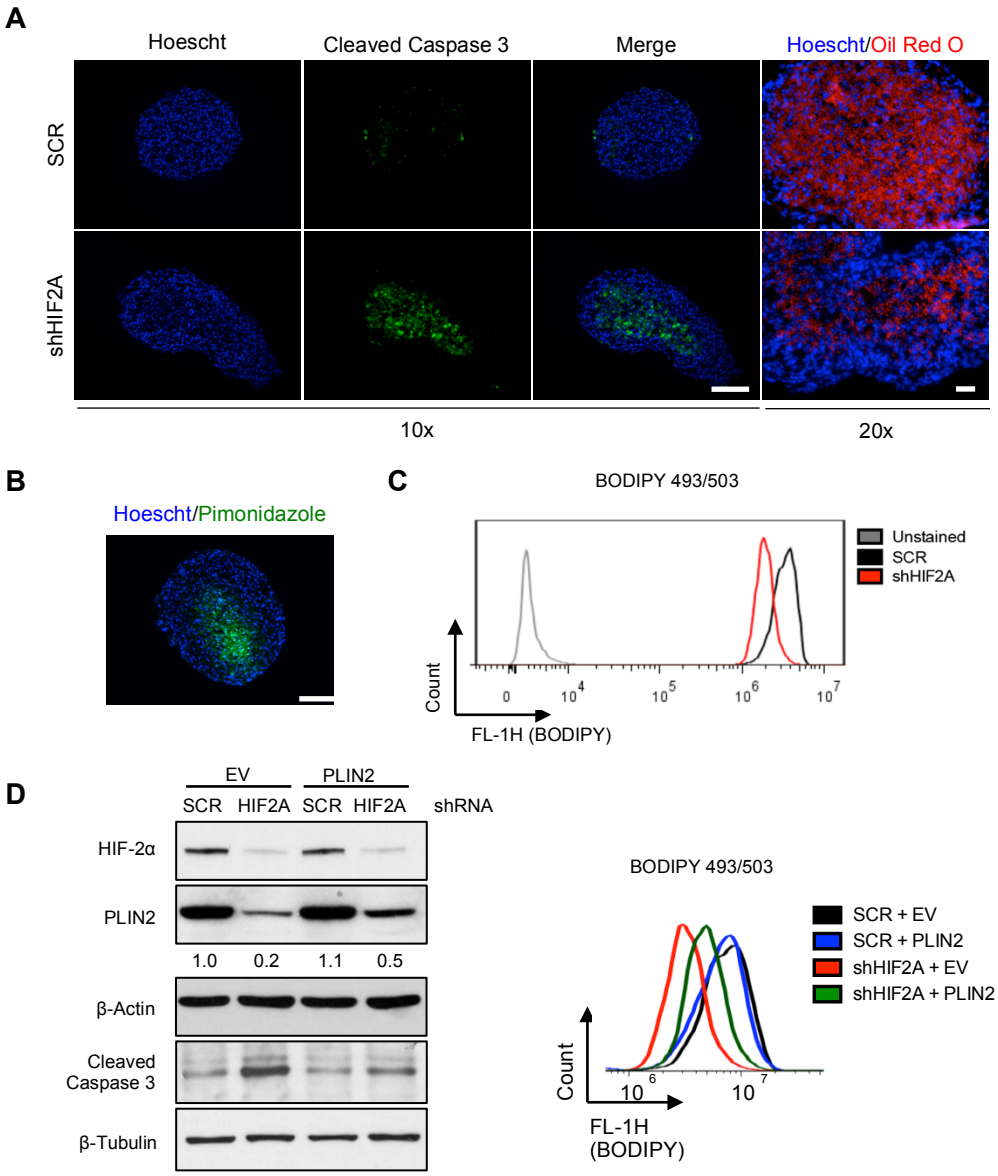

Figure 7: HIF-2α dependent PLIN2 expression promotes cell viability in nutrient deprived regions of 3D tumor spheroids

A) 786-O cells expressing shHIF2A_7 or a SCR control were grown as 3D tumor spheroids using the liquid overlay technique. Sections obtained from spheroids were stained for cleaved caspase 3 and oil red O (left).

B) SCR control spheroids were treated with FITC-conjugated pimonidazole prior to sectioning to identify hypoxic cells. Scale bar = 200μm.

C) BODIPY 493/503 staining of single cell suspensions derived from spheroids described in (A).

D) 3D spheroids were generated from 786-O cells expressing shHIF2A_7 or a SCR control, along with either EV or exogenous PLIN2. Western blot analysis for HIF-2α, PLIN2, and cleaved caspase 3 is shown (left). BODIPY 493/503 was performed on single cell suspensions from dissociated spheroids (right).

PLIN2 dependent lipid storage is required for ER homeostasis and cell viability in ccRCC cell lines and xenograft tumors

The finding that PLIN2 is required for cell viability in ccRCC xenografts was surprising, as acute *PLIN2* depletion experiments have reported no effects on cell viability either *in vivo* or *in vitro* (Bensaad et al., 2014; Imai et al., 2012; Sun et al., 2012). To assess the effects of direct PLIN2 depletion in ccRCC, we expressed multiple shRNAs targeting *PLIN2* or a scrambled control (SCR) in 786-O. We observed a dosage dependent loss of cell viability and proliferation that correlated with degree of *PLIN2* depletion (8A-B). Oil red O staining and BODIPY 493/503 quantification also revealed dosage dependent decreases in neutral lipid levels (Fig. 8C-D). To assess functional lipid storage capacity, cells were treated with oleic acid, a potent inducer of triglyceride synthesis and neutral lipid storage that is selectively toxic for cells incapable of storing it as triglyceride (Listenberger et al., 2003). Consistent with decreased ability to store lipids within LDs, *PLIN2* depleted cells were preferentially sensitized to oleic acid induced cell death (Fig. 8E).

In light of the intimate ER/LD relationship and evidence that altered membrane properties can trigger ER stress (Volmer et al., 2013), we reasoned that decreased lipid storage capacity could disrupt ER homeostasis and trigger the UPR, cell cycle withdrawal (Brewer and Diehl, 2000), and cell death. PLIN2 ablation in 786-O cells elicited dosage dependent activation of UPR sensors PERK, IRE-1α, and ATF6 and induction of multiple UPR target genes (Fig. 9A). Furthermore, ER Tracker imaging and flow cytometry indicated ER expansion in PLIN2 depleted cells (Fig. 9B) and ultra-structural analysis by transmission electron microscopy (TEM) confirmed the presence of dilated and irregularly shaped rough ER (Fig. 9C), both of which are consistent with ER stress (Oslowski and Urano, 2011). Based on these observations, we quantified UPR target gene expression in HIF-2α deficient xenograft tumors. Indeed, multiple UPR targets, including the "terminal" UPR genes *CHOP* and *TXNIP*, were elevated in HIF-2α depleted tumors and decreased by exogenous *PLIN2* expression (Fig. 9D). Lastly, the effects of PLIN2 depletion on cell viability and ER homeostrasis were recapitulated in A498 cells (Fig. 10).

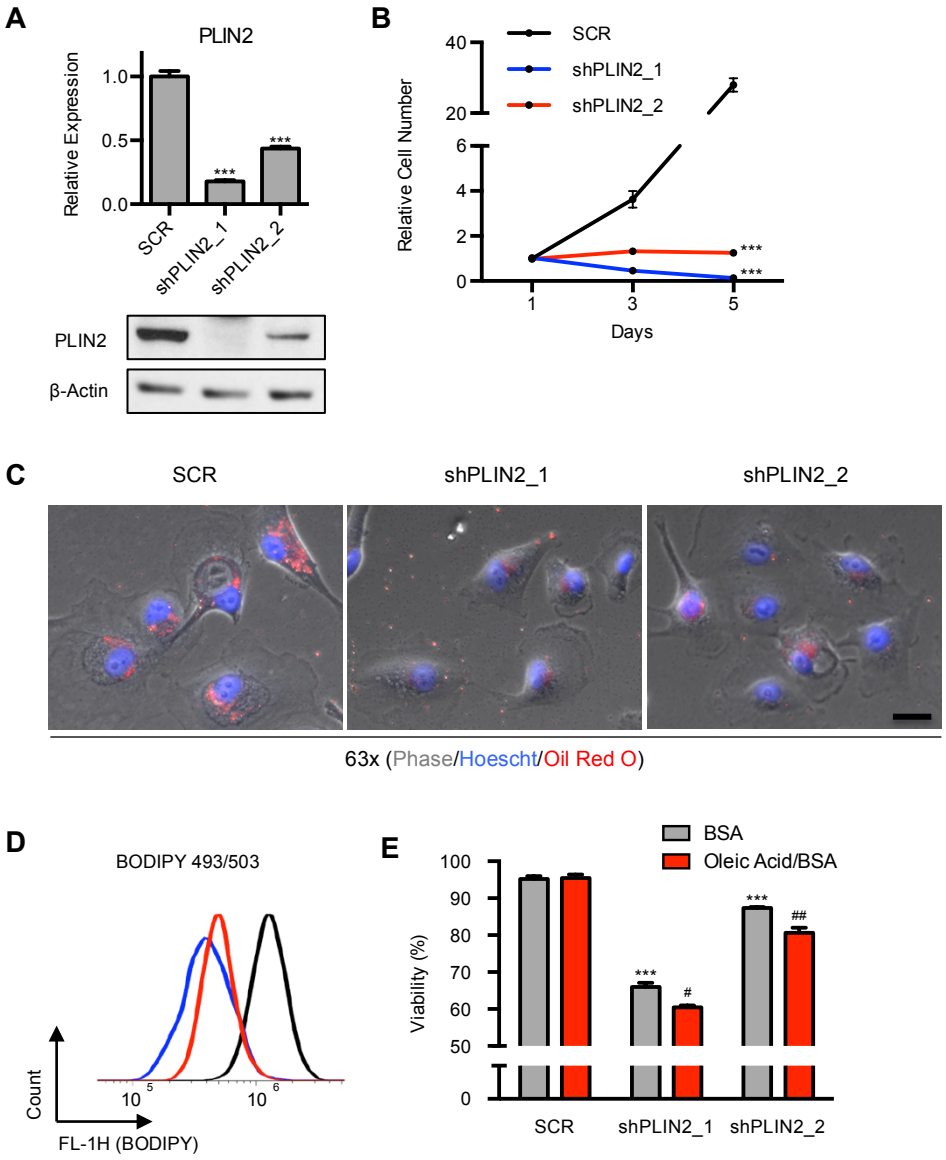

Figure 8: PLIN2 is required for lipid storage and cell viability in 786-O cells.

A) 786-O ccRCC cells were transduced with two independent shRNAs against *PLIN2* (shPLIN2_1, shPLIN2_2) or a SCR control. qRT-PCR and western blot analysis were performed on day 3 post shRNA transduction to assess for PLIN2 suppression. For qRT-PCR, *TBP* and *ACTB* were utilized as endogenous control genes and relative mRNA expression was determined by normalizing to expression in SCR samples. p-values were determined by student's t-test. *** p<0.001.

B) Growth curves for cells described in (A). Day 1 of growth curve corresponds to day 3 post transduction.

C) Oil Red O staining of cells described in (A) was performed on day 3 post transduction. Scale bar = 50μm.

D) Live cells described in (A) were stained with BODIPY 493/503 (2μg/ml) and fluorescence was measured by flow cytometry. A histogram of BODIPY 493/503 fluorescence is shown.

E) Beginning on day 3 post transduction, cells from (A) were treated with BSA alone or BSA conjugated with oleic acid (30μM). Viability was determined by annexin/PI staining after 24 hours of treatment. Data are representative of three independent experiments. p-values were determined by two-way ANOVA with Bonferroni correction. Asterisks denote comparison with SCR BSA. *** $p<0.001$. Pound signs denote comparison of Oleic Acid with BSA treated conditions within each cell line. # $p<0.05$, ## $p<0.01$. Error bars denote SEM.

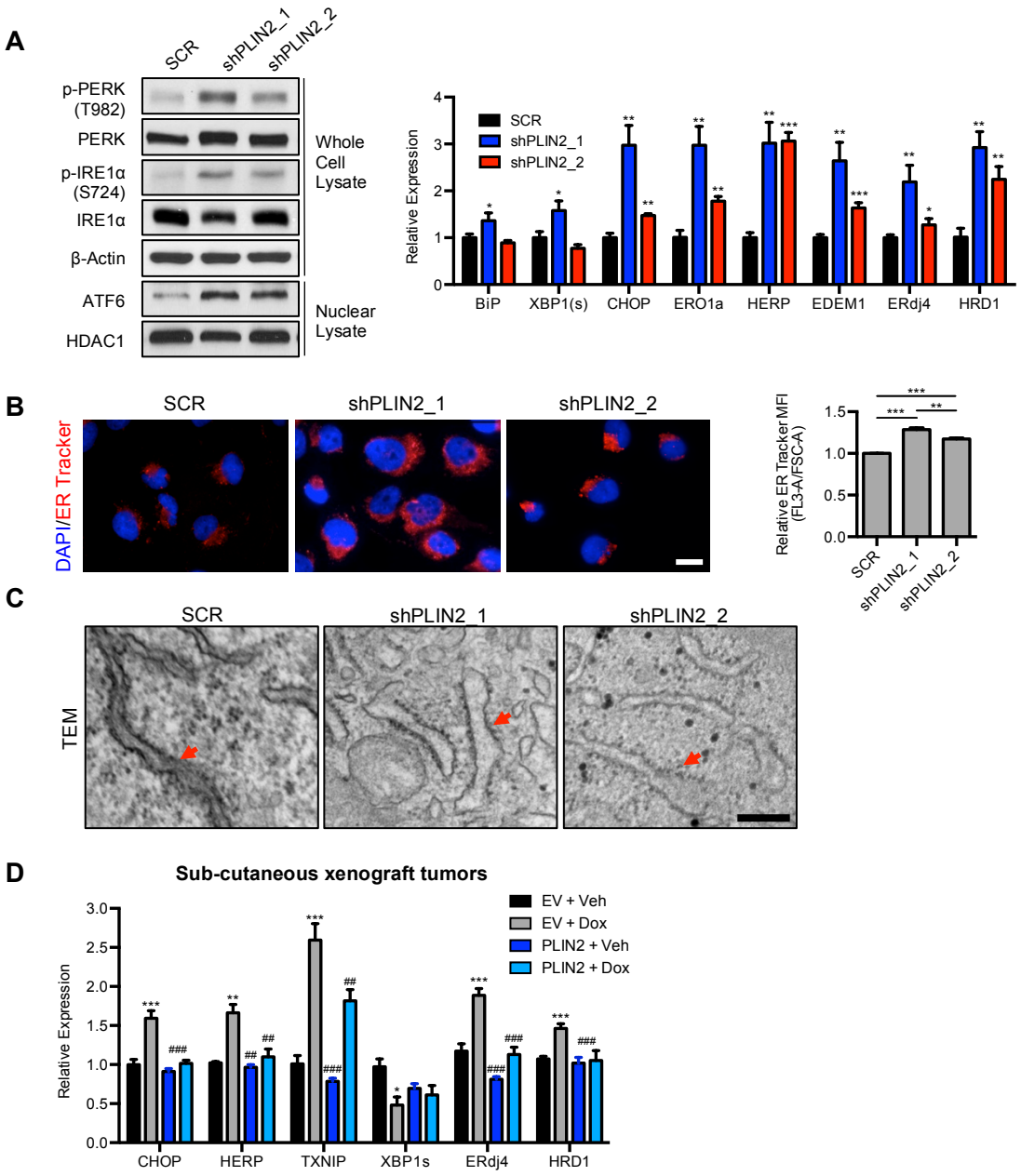

Figure 9: PLIN2 dependent lipid storage promotes ER homeostasis in ccRCC cells and xenograft tumors

A) Western blot for UPR sensors was performed in 786-O cells expressing independent shRNAs against *PLIN2* (shPLIN2_1, shPLIN2_2) or a SCR control (left, day 3 post transduction). Corresponding qRT-PCR analysis of UPR target genes is shown (right, day 4 post transduction). Data are representative of three independent experiments. p-values were determined by student's t-test.

B) ER Tracker Red (500 nM) staining of live cells described in (A) was performed (day 4 post transduction). Representative images (left) and quantification of ER Tracker fluorescence are shown (right). Fluorescence was normalized to forward scatter for each event to account for differences in cell size. Scale bar = 50μm. p-values were determined by student's t-test.

C) Transmission electron microscopy of control and PLIN2 depleted cells is shown (day 4 post transduction). Red arrows denote rough ER. Scale bar=200 nm.
D) qRT-PCR of xenograft tumor RNA assessing expression of UPR target genes. p-values were determined by two-way ANOVA with Bonferroni correction. Asterisks denote comparison with EV Veh. * $p<0.05$, ** $p<0.01$, *** $p<0.001$. Pound signs denote comparison with EV Dox. ## $p<0.01$, ### $p<0.001$. Error bars denote SEM.

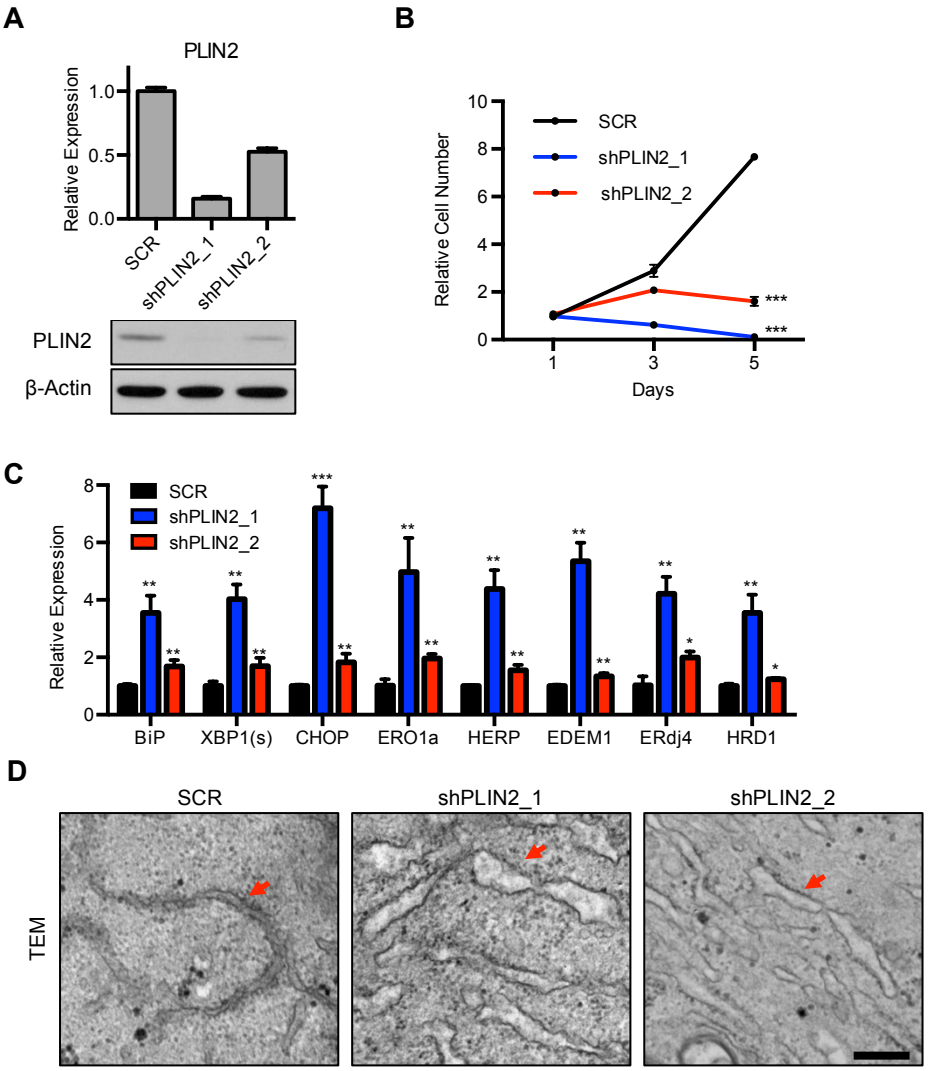

Figure 10: PLIN2 is required for lipid storage, cell viability, and maintenance of ER homeostasis in A498 cells

A) A498 ccRCC cells were transduced with two independent shRNAs against *PLIN2* (shPLIN2_1, shPLIN2_2) or a SCR control. qRT-PCR and western blot analysis were performed on day 3 post shRNA transduction to assess for PLIN2 suppression.

B) Growth curves were obtained for cells described in (A). Day 1 of growth curve corresponds to 3 days post transduction.

C) qRT-PCR analysis of UPR target genes in A498 cells expressing independent shRNAs against *PLIN2* (shPLIN2_1, shPLIN2_2) or a SCR control (day 4 post transduction).

D) Transmission electron microscopy of control and PLIN2 depleted cells is shown (day 4 post transduction). Red arrows denote rough ER. Scale bar: 250 nm. p-values were determined by student's t-test. Error bars denote SEM.

To determine if UPR activation promotes cell death upon PLIN2 loss in ccRCC, we utilized previously characterized small molecule PERK and IRE-1α inhibitors, along with siRNA against *ATF6*, to suppress UPR signaling (Atkins et al., 2013; Cross et al., 2012). These tools were validated in A498 cells, based on UPR sensor phosphorylation status and target gene expression (Fig. 11). In 786-O cells, PERK inhibition reduced *ATF3* levels (a PERK/ATF4 target) in *PLIN2* depleted cells, but enhanced cell death and expression of multiple IRE-1α and ATF6 target genes (Fig. 12A). Whereas IRE-1α and ATF6 suppression each modestly restored cell viability, combined suppression of both yielded enhanced cell survival (Fig. 12B). In A498 cells, ATF6 promoted cell death downstream of PLIN2 inhibition (Fig. 12C). While the specific UPR-sensor(s) mediating cell death varies between cell lines, our results indicate that PLIN2 is required for maintenance of ER homeostasis and prevention of cytotoxic ER stress in ccRCC. Next, we examined the potential sources of ER stress that could explain the enhanced requirement for PLIN2-mediated ER homeostasis in ccRCC.

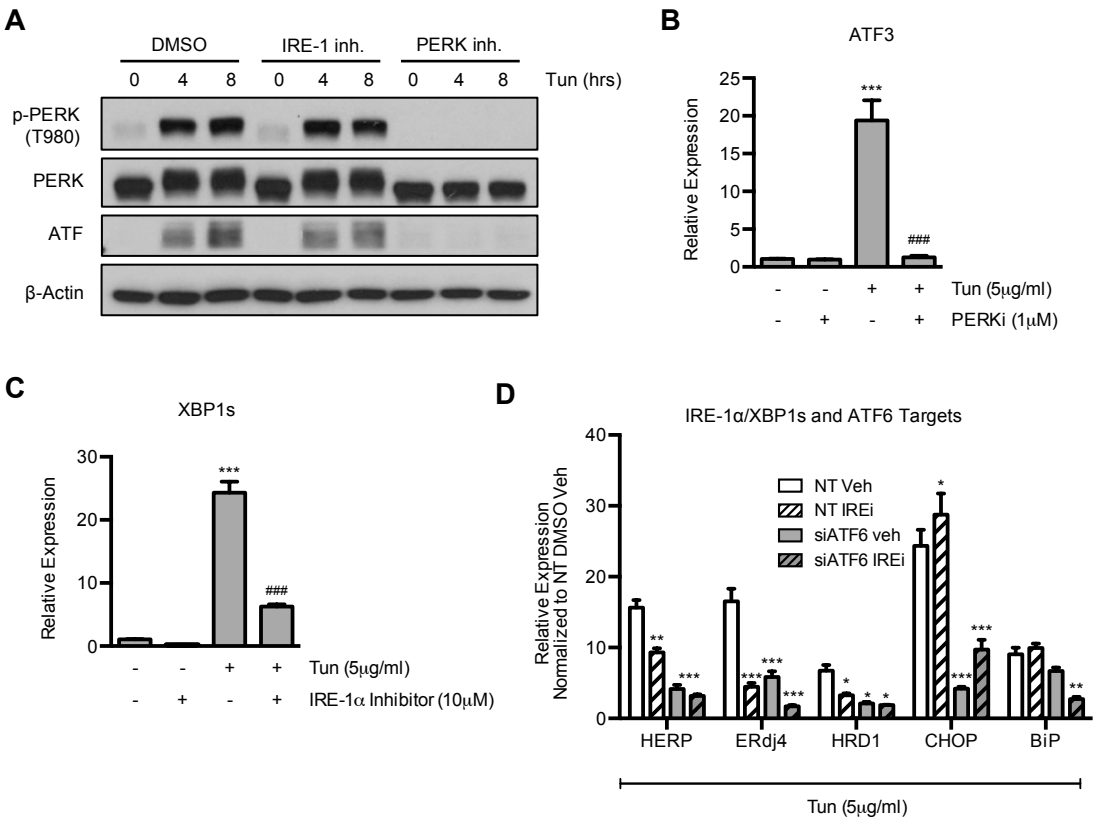

Figure 11: Validation of IRE-1α inhibitor, PERK inhibitor, and ATF6 siRNA in A498 cells

A) Cells were treated with tunicamycin (5μg/ml) or DMSO vehicle, along with IRE-1α (10μM) or PERK (1μM) inhibitor. Western blot analysis of phosphorylated PERK and its downstream target ATF4 is shown.

B) Cells were treated with tunicamycin or DMSO vehicle, with or without PERK inhibitor, for 4 hours. qRT-PCR for ATF3, a PERK specific target, is shown. Values were normalized to expression in cells receiving no Tunicamycin or inhibitor.

C) Cells were treated with tunicamycin or DMSO control, with or without IRE-1α inhibitor, for 4 hours. qRT-PCR for spliced XBP1, an IRE-1α target, is shown. Values were normalized to expression in cells receiving no Tunicamycin or inhibitor. For (B) and (C), astericks denote comparison with cells receiving no Tunicamycin or inhibitor. Pound signs denote comparison with cells receiving Tunicamycin alone.

D) Cells were transfected with non-targeting (NT) or ATF6 directed siRNA. At 3 days post transfection, cells were treated with tunicamycin or DMSO control, with or without IRE-1α inhibitor, for 4 hours. qRT-PCR for multiple genes co-regulated by both IRE-1α and ATF6 is shown. Data are representative of three independent experiments. For qRT-PCR, *TBP* and *ACTB* were utilized as endogenous control genes. p-values were determined by two-way ANOVA with Bonferroni correction. * p<0.05, ** p<0.01, *** p<0.001. ### p<0.001. Error bars denote SEM.

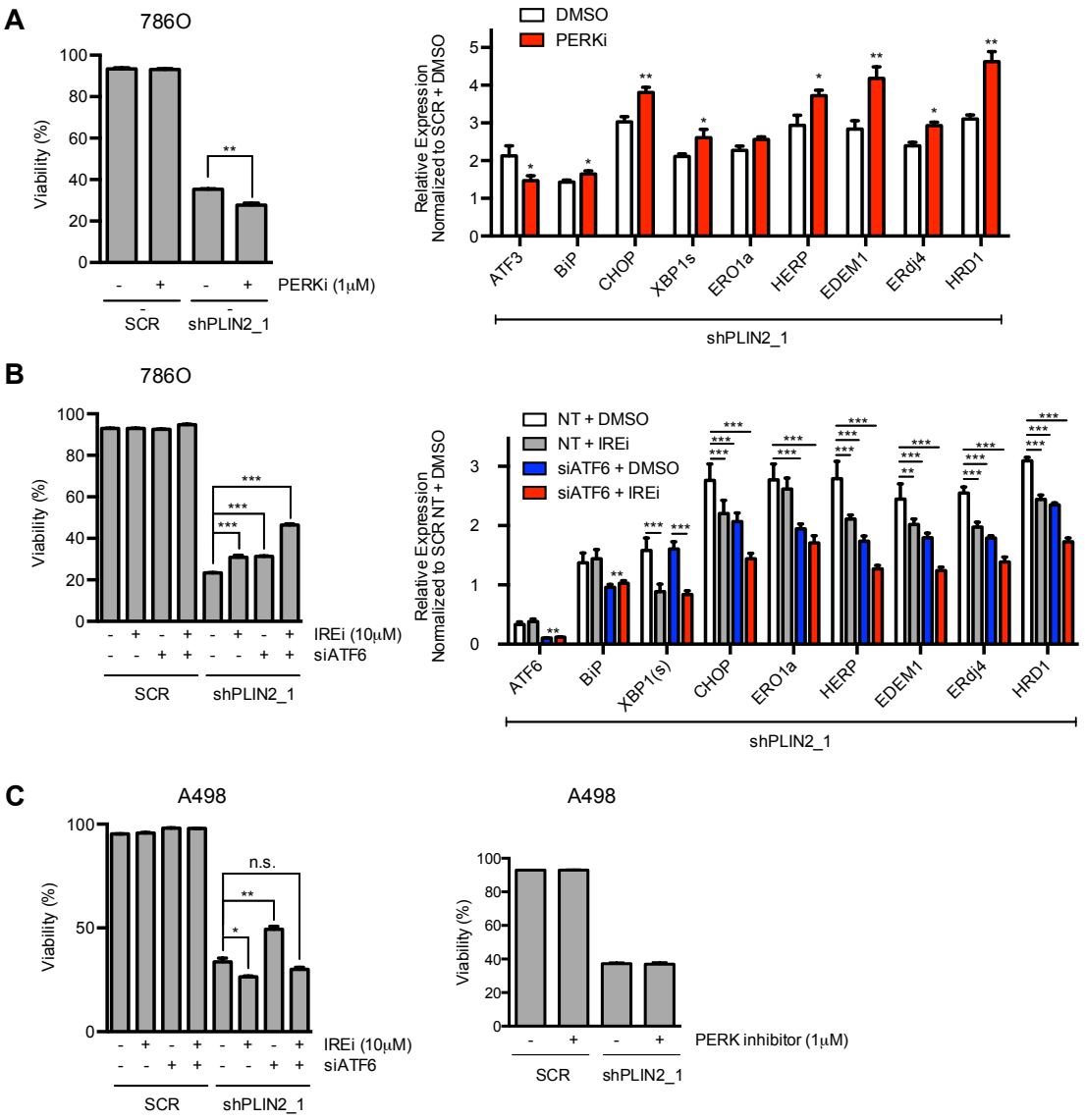

Figure 12: Unfolded protein response promotes cell death upon PLIN2 depletion.

A) 786-O cells expressing shPLIN2_1 or SCR control were treated with PERK inhibitor (1μM) or DMSO vehicle beginning on day 3 post transduction. Cell viability was determined by annexin/PI staining after 48 hours of drug treatment and qRT-PCR analysis of UPR target gene expression was performed after 24 hours of drug treatment. For qRT-PCR, *TBP* and *ACTB* were utilized as endogenous control genes and relative mRNA expression was determined by normalizing to expression in SCR samples. Data are representative of three independent experiments. p-values were determined by student's t-test. * $p<0.05$, ** $p<0.01$, *** $p<0.001$.

B) 786-O cells expressing shPLIN2_1 or SCR shRNA were transfected with non-targeting (NT) or ATF6 directed siRNA (day 2 post transduction) and subsequently treated with IRE-1α inhibitor (10μM) or DMSO vehicle (day 3 post transduction). Cell viability was determined by annexin/PI staining after 48 hours of drug treatment (left) and qRT-PCR analysis of UPR target gene expression was performed after 24 hours of drug treatment (right). Data are representative of three independent experiments. p-values were

determined by two-way ANOVA with Bonferroni correction. ** $p<0.01$, *** $p<0.001$. Error bars denote SEM.

C) Analysis of A498 cells was performed, as described in (A) and (B). Annexin/PI results are shown.

PLIN2 dependent lipid storage supports ER homeostasis during oncogene mediated activation of protein synthesis

The observation that ccRCC cells require PLIN2 for proliferation and viability was surprising, because 1) *Plin2* knockout mice are viable (Chang et al., 2006), 2) *Plin2* deficient macrophages do not exhibit enhanced sensitivity to cholesterol loading, which requires lipid storage to alleviate ER stress (Son et al., 2012), and 3) acute *Plin2* suppression fails to elicit cell death in steatotic hepatocytes (Imai et al., 2012; Sun et al., 2012), MCF7 breast cancer cells, or U87 glioblastoma cells (Bensaad et al., 2014). One potential advantage of lipid storage in ccRCC is the ability to derive energy from fatty acid breakdown via β-oxidation. However, in contrast to the electron transport chain inhibitor rotenone, PLIN2 depletion did not affect ATP levels in multiple ccRCC cell lines (Fig. 13A). Furthermore, transcription factors that promote renal tubular cell β-oxidation, including *PPARA* and PPARγ coactivator 1-alpha (*PPARGC1A*), were substantially downregulated in primary ccRCCs compared to normal kidney (Fig. 13B). The Carnitine/Acyl-carnitine Transporter (*CAT*) and mitochondrial β-oxidation enzymes were also underexpressed in ccRCC tissues (Fig. 13B-C). In agreement with these findings, metabolomic analysis of primary ccRCC and normal kidney tissues revealed elevation of acyl-carnitine levels in tumors (Fig. 13D). These features of ccRCC mirror genetic CAT deficiency, which manifests as acyl-carnitine build up secondary to reduced β-oxidation flux (Roschinger et al., 2000).Furthermore, a recent study indicates that HIF-2α suppresses peroxisomal β-oxidation via selective autophagy of peroxisomes (Walter et al., 2014). Thus, alterations to β-oxidation are unlikely to explain the effects of PLIN2 depletion in ccRCC.

Next, we explored whether enhanced tumor anabolic processes, downstream of oncogenic activation, contribute to the requirement for PLIN2 dependent lipid storage in ccRCC. Particularly, increased protein and lipid synthesis via mTORC1 could result in a greater requirement for lipid storage to maintain ER homeostasis, as the ER functions as a “hub” for both protein and lipid production. We focused on mTORC1 because 1) 30% of ccRCC harbor activating mutations in the mTOR pathway (Cancer Genome Atlas Research, 2013), 2) most

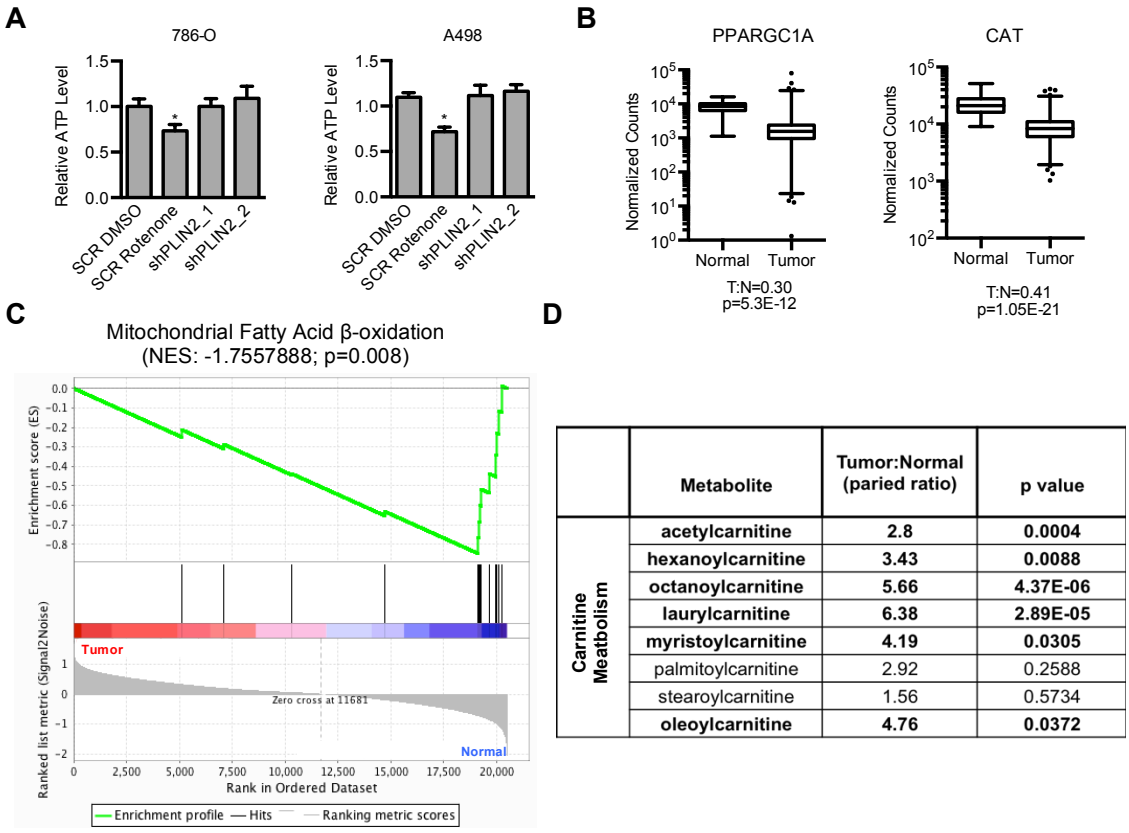

	Metabolite	Tumor:Normal (paried ratio)	p value
Carnitine Meatbolism	**acetylcarnitine**	**2.8**	**0.0004**
	hexanoylcarnitine	**3.43**	**0.0088**
	octanoylcarnitine	**5.66**	**4.37E-06**
	laurylcarnitine	**6.38**	**2.89E-05**
	myristoylcarnitine	**4.19**	**0.0305**
	palmitoylcarnitine	2.92	0.2588
	stearoylcarnitine	1.56	0.5734
	oleoylcarnitine	**4.76**	**0.0372**

Figure 13: Energetic effects of PLIN2 depletion in ccRCC cell lines and evidence for suppression of β-oxidation in ccRCC tumor tissue

A) Luminescence based ATP quantification was performed in 786-O (left) and A498 (right) cells expressing shPLIN2_1, shPLIN2_2, or a SCR control on day 3 post transduction. Values were normalized to luminescence in SCR DMSO samples. Rotenone treatment of SCR control cells is included as a positive control. p-values were determined by two-way ANOVA with Bonferroni correction. * $p<0.05$.

B) Normalized RNA-seq reads for peroxisome proliferator-activated receptor gamma coactivator 1-alpha (left, *PPARGC1A*) and carnitine acyl-carnitine transferase (right, *CAT*) in the TCGA data set. Data obtained from The Cancer Genome Atlas (TCGA). Whiskers denote 1st and 99th percentiles.

C) Gene set enrichment analysis (GSEA) of differentially expressed genes in ccRCC tumor vs normal kidney samples was performed on the TCGA RNA-seq data set. Results for the "mitochondrial fatty acid β-oxidation" gene set are shown. $p<0.05$.

D) Relative concentration of acyl-carnitines in 20 primary ccRCC tumors compared to matched adjacent normal kidney samples. Metabolites were extracted from frozen tissue samples and analyzed by the Thermo-Finnigan GC-MS and LC-MS/MS systems. p-values were determined by Welch's t-test. Significantly altered metabolites ($p<0.05$) are shown in bold.

tumors exhibit elevated mTORC1 activity (p-S6K1, p4EBP1 staining) (Gordan et al., 2008; Haddad et al., 2015), and 3) mTORC1 can stimulate both protein and lipid synthesis (Laplante and Sabatini, 2012). The effects of small molecule mTOR inhibitors on protein and lipid synthesis were characterized in ccRCC cells. As expected (Peterson et al., 2011), Torin1 was more potent than rapamycin in suppressing protein synthesis and lipogenic enzyme gene expression in ccRCC cells (Fig. 14A-B). In both 786-O and A498 cells, rapamycin and Torin1 treatment enhanced viability and reduced UPR gene expression following PLIN2 depletion, with Torin1 being more potent (Fig. 14C-D). Notably, the magnitude of restored viability upon mTOR suppression was greater than that observed upon UPR inhibition in both 786-O and A498 cells (Fig. 12). We reasoned that this was due to amelioration of ER stress, rather than merely UPR signaling itself.

Given that Torin1 suppresses both protein and lipid synthesis, we measured the relative contribution of these activities toward Torin1 dependent effects. Suppression of protein synthesis using the translation inhibitor cycloheximide (CHX) restored cell viability and ameliorated ER stress in PLIN2 depleted 786-O and A498 cells (Fig. 15A-B). On the other hand, silencing of sterol regulatory element-binding proteins 1 and 2 (SREBP1/2), mediators of lipid synthesis downstream of mTORC1, selectively reduced viability in PLIN2 depleted cells (Fig. 16A-B). Consistent with an adaptive function of SREBP1/2 activation in cells experiencing ER stress (Kammoun et al., 2009; Walter and Ron, 2011), PLIN2 depletion induced multiple lipid synthesis enzymes in an SREBP1/2-dependent manner (Fig. 16A-B). Ultimately, CHX treatment restored cell viability in PLIN2 depleted cells, even when SREBP1 and 2 were inhibited, reflecting the aggregate activities of Torin1 (Fig. 14A-B). These findings suggest that protein synthesis is a prominent source of ER stress and cell death in the setting of PLIN2 depletion.

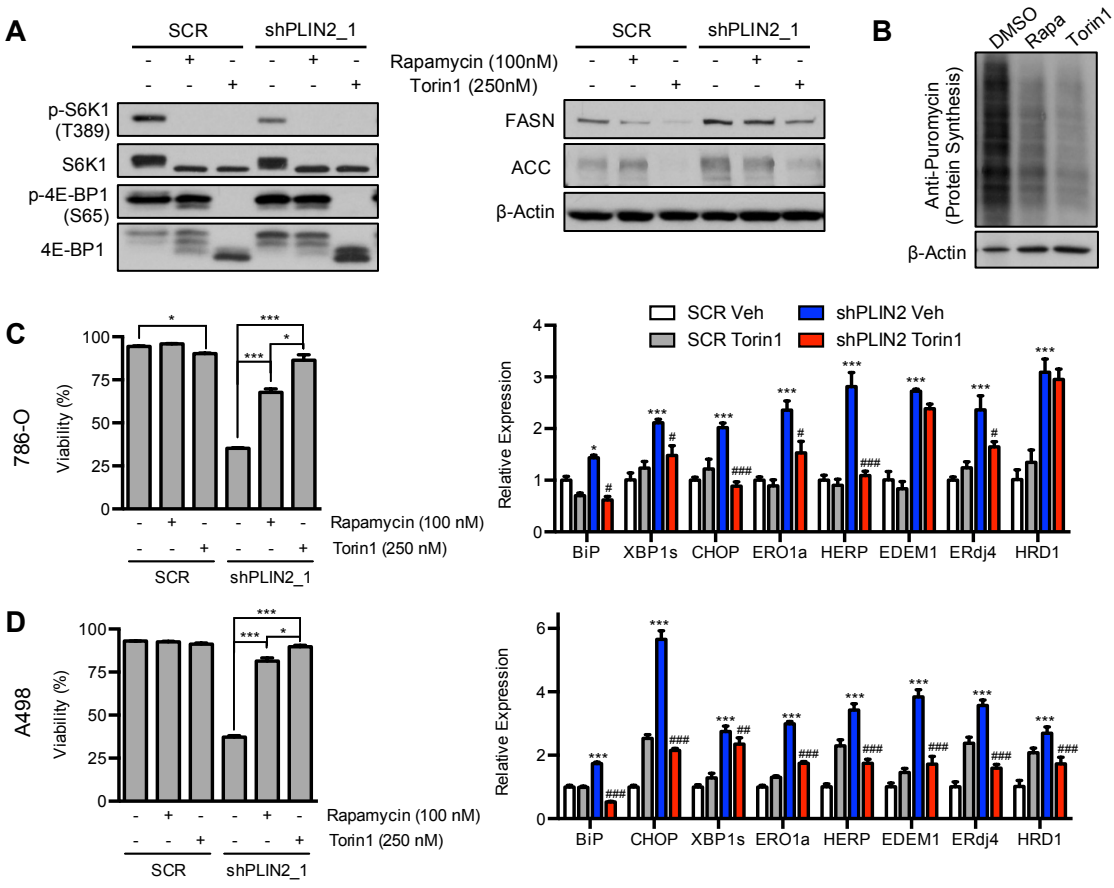

Figure 14: Suppression of mTORC1 ameliorates ER stress and cell death upon PLIN2 depletion

A) 786-O cells expressing shPLIN2_1 or SCR control were treated with rapamycin (100 nM) or Torin1 (250 nM) for 48 hours. Western blot analysis of direct targets of mTORC1 kinase (left) and mTORC1 regulated fatty acid synthesis enzymes (right) are shown.

B) Protein synthesis activity was measured in 786-O cells treated with rapamycin, Torin1, or DMSO vehicle for 48 hours. Cells were pulsed with puromycin (30 min, 10μg/ml) and chased in puromycin free media (1 hr) to allow puromycin incorporation into nascent peptides. Whole cell lysates were subjected to western blot analysis using an anti-puromycin antibody (clone 12D10).

C) 786-O cells expressing shPLIN2_1 or SCR control were treated with rapamycin, Torin1, or DMSO vehicle starting on day 3 post transduction and cell viability was determined by annexin/PI staining after 48 hours of drug treatment (left). qRT-PCR comparing UPR target gene expression in cells treated with Torin1 was performed after 24 hours of drug treatment.

D) A498 cells were treated as described in (C).

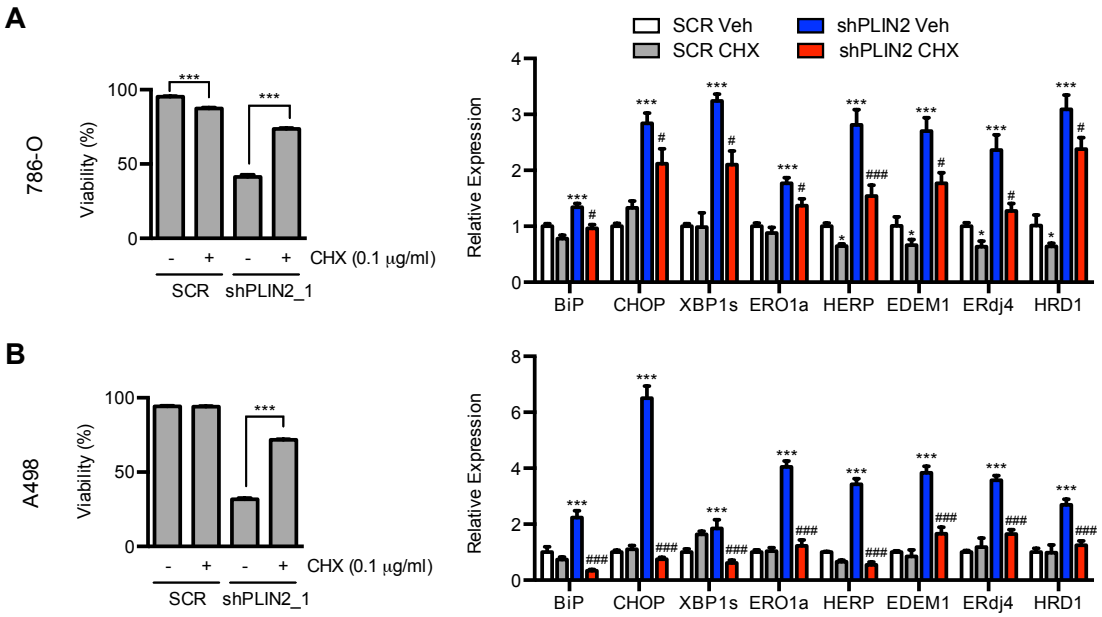

Figure 15: Suppression of protein synthesis ameliorates ER stress and cell death upon PLIN2 depletion

A) Figure 7: 786-O cells expressing shPLIN2_1 or SCR shRNA were treated with cycloheximide or DMSO vehicle starting on day 3 post transduction and cell viability was determined by annexin/PI staining after 48 hours of drug treatment (left). qRT-PCR for UPR target genes was performed after 24 hours of drug treatment (right).

B) A498 cells were treated and analyzed as described in (D). Data are representative of three independent experiments. p-values were determined by student's t-test for annexin/PI assays and two-way ANOVA with Bonferroni correction for qRT-PCR. For qRT-PCR, *TBP* and *ACTB* were utilized as endogenous control genes and relative mRNA expression was determined by normalizing to expression in SCR Veh samples. Asterisks denote statistical comparison with SCR Veh. * $p<0.05$, *** $p<0.001$. Pound signs denote statistical comparison with shPLIN2 Veh. # $p<0.05$, ### $p<0.001$. Error bars denote SEM.

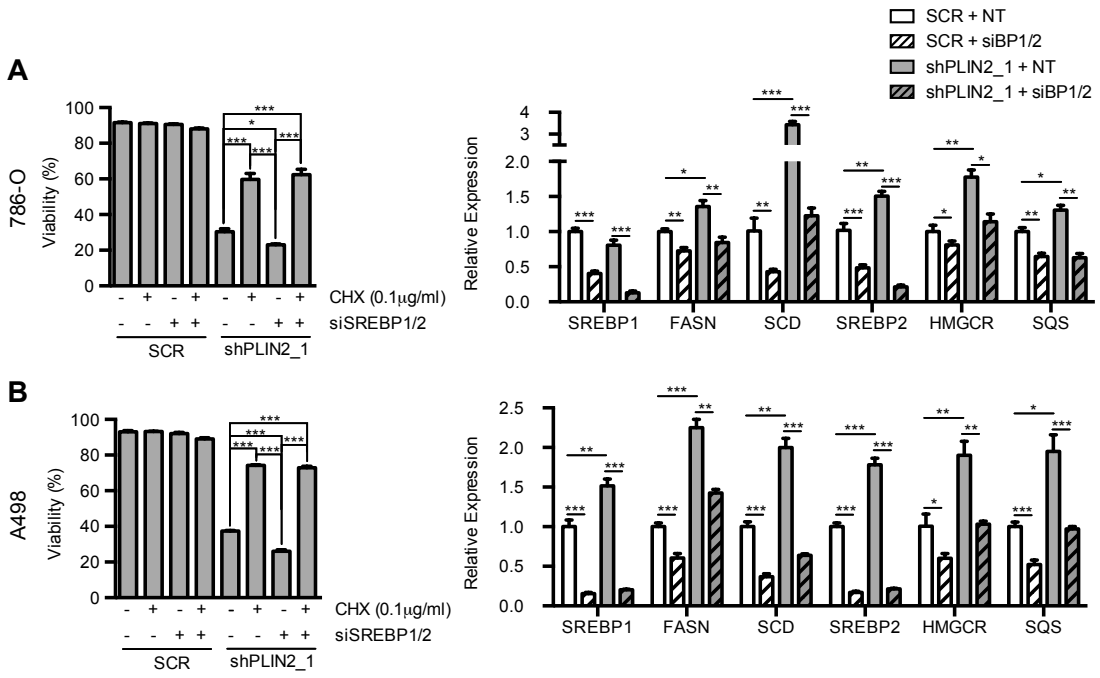

Figure 16: SREBP-dependent lipid synthesis is adaptive in PLIN2 depleted cells

A) 786-O cells expressing shPLIN2_1 or SCR shRNA were transfected with non-targeting (NT) or SREBP1 and SREBP2 directed siRNAs (siBP1/2) (day 1 post transduction) and subsequently treated with CHX (0.1 μg/ml) or DMSO vehicle (day 2 post transduction). Annexin/PI staining was performed 3 days after drug treatment (day 5 post transduction) and qRT-PCR was performed 2 days after drug treatment (day 4 post transduction).

B) A498 cells were treated as described in (C). Data are representative of three independent experiments. p-values were determined by two-way ANOVA with Bonferroni correction. * $p<0.05$, ** $p<0.01$, *** $p<0.001$. Error bars denote SEM.

HIF-2α dependent PLIN2 expression and lipid storage promote resistance against pharmacologic ER stress

Given that reduction of ER protein load alleviated ER stress in PLIN2 depleted cells, we determined if such cells would also be more sensitive to agents that increase mis-folded protein load. Of note, PLIN2 depleted cells were more sensitive to tunicamycin treatment, which inhibits N-linked glycosylation, compared to controls (Fig. 17A). We performed similar experiments to determine if HIF-2α/PLIN2 mediated lipid storage is similarly protective against pharmacological ER stress. A498 cells expressing *HIF2A* shRNA exhibited reduced BODIPY staining, whereas exogenous PLIN2 expression was sufficient to restore neutral lipid levels (Fig. 17B). Upon treatment with tunicamycin, HIF-2α depleted cells exhibited a 3-fold enhancement of cell death that was partially ameliorated by restoring PLIN2 dependent lipid storage (Fig. 17C).

PLIN2 also protected ccRCC cells from the proteasome inhibitor Bortezomib (Fig. 18A), an FDA approved therapy for multiple myeloma that functions partly through ER stress induction (Obeng et al., 2006). Specifically, expression of the IRE-1α substrate spliced *XBP1* is positively correlated with patient response to Bortezomib and functional studies demonstrate a role for the UPR target gene *CHOP* in Bortezomib-mediated cell death (38, 39). Consistent with a cytotoxic function of ER stress in Bortezomib treated ccRCC cells, the enhanced efficacy of Bortezomib in PLIN2 depleted cells was associated with elevated levels of spliced *XBP1* and *CHOP* (Fig. 18B). Furthermore, HIF-2α depleted cells demonstrated enhanced sensitivity to Bortezomib that was ameliorated by exogenous PLIN2 (Fig. 18C). Next, we tested whether nutrient and/or O_2 deprivation—ER stress inducing conditions found within the tumor microenvironment—could further enhance Bortezomib-induced cell death. Indeed, previous work indicates that hypoxia can enhance anti-tumor activity of Bortezomib via ER stress induction (Fels et al., 2008). Growth under conditions of serum and/or O_2 deprivation enhanced Bortezomib induced cell death, most prominently in PLIN2 depleted cells (Fig. 18D). Under each condition tested, expression of the terminal UPR gene *CHOP* was also positively correlated with degree of cell death (Fig. 18E).

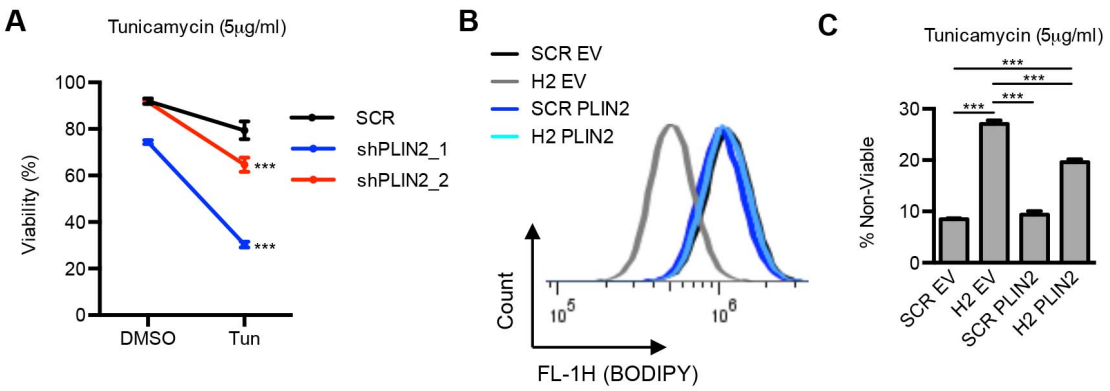

Figure 17: HIF-2α/PLIN2 dependent lipid storage protects ccRCC cells against tunicamycin-induced ER stress

A) A498 cells expressing shPLIN2_1, shPLIN2_2, or SCR control were treated with tunicamycin or DMSO at 2 days post transduction. Cell viability was determined by annexin/PI staining after 48 hours of drug treatment. Asterisks denote statistical comparison of viability under tunicamycin treatment. Tunicamycin-induced reduction in viability was significantly different between shPLIN2 and SCR cells: shPLIN2_1 vs SCR, $p<0.01$; shPLIN2_2 vs SCR, $p<0.01$.

B) A498 cells expressing shHIF2A_7 or SCR control, along with either exogenous PLIN2 or an empty vector (EV), were stained with BODIPY 493/503 (2μg/ml). Histograms indicating BODIPY fluorescence was generated by flow cytometry.

C) Cells described in (B) were treated with tunicamycin or DMSO control for 48 hours and viability was determined by annexin/PI staining.

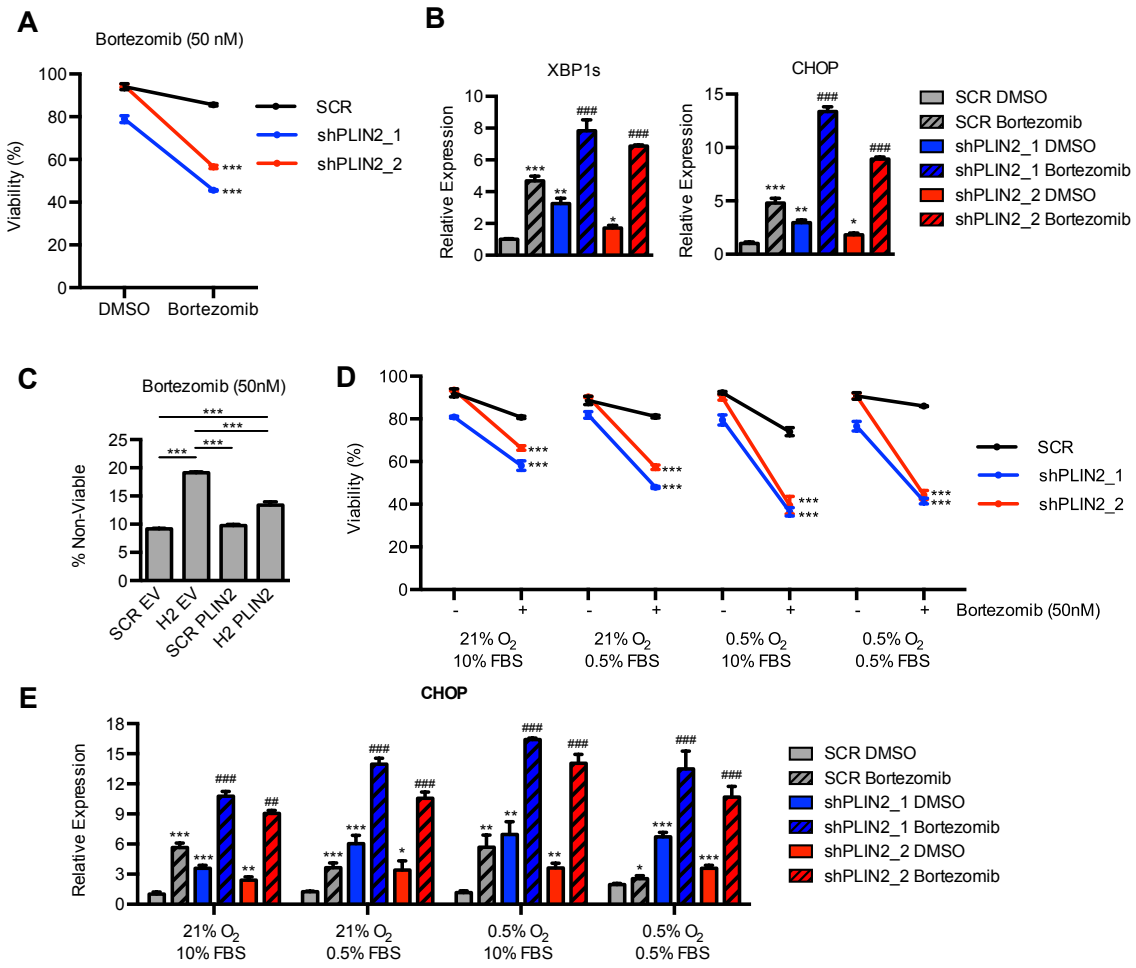

Figure 18: HIF-2α/PLIN2 dependent lipid storage protects ccRCC cells against bortezomib-induced ER stress

A) A498 cells expressing shPLIN2_1, shPLIN2_2, or SCR control were treated with Bortezomib or DMSO at 3 days post transduction. Cell viability was determined by annexin/PI staining after 24 hours of drug treatment. Asterisks denote statistical comparison of viability under Bortezomib treatment. Bortezomib-induced reduction in viability was significantly different between shPLIN2 and SCR cells: shPLIN2_1 vs SCR, p<0.001 shPLIN2_2 vs SCR, p<0.001

B) *XBP1s* and *CHOP* expression in cells from (A) was determined by qRT-PCR. Asterisks denote comparison with SCR DMSO. Pound signs denote comparison with SCR Bortezomib. For qRT-PCR, *TBP* and *ACTB* were utilized as endogenous control genes and relative mRNA expression was determined by normalizing to expression in SCR DMSO samples.

C) The indicated cells were treated with Bortezomib or DMSO control for 24 hours and viability was determined by annexin/PI staining.

D) A498 cells expressing shPLIN2_1, shPLIN2_2, or SCR control were treated with Bortezomib or DMSO at 3 days post transduction and incubated under the designated serum and oxygen conditions. Cell viability was determined by annexin/PI staining after 24 hours of drug treatment. Astericks denote comparison with SCR Bortezomib. Under each serum and oxygen condition, Bortezomib-induced reduction in viability was

significantly different between shPLIN2 and SCR cells: shPLIN2_1 vs SCR, $p<0.001$ shPLIN2_2 vs SCR, $p<0.001$

E) A498 cells expressing shPLIN2_1, shPLIN2_2, or SCR control were treated with Bortezomib or DMSO at 3 days post transduction and incubated under the designated serum and oxygen conditions. *CHOP* expression was measured after 24 hours of drug treatment. For qRT-PCR, *TBP* and *ACTB* were utilized as endogenous control genes and relative mRNA expression was determined by normalizing to expression in SCR DMSO samples. Data are representative of three independent experiments. p-values were determined by two-way ANOVA with Bonferroni correction. Asterisks denote comparison with SCR DMSO. * $p<0.05$, ** $p<0.01$, *** $p<0.001$. Pound signs denote comparison with SCR Bortezomib. # $p<0.05$, ## $p<0.01$, ### $p<0.001$. Error bars denote SEM.

Collectively, we suggest a model in which HIF-2α/PLIN2 dependent lipid storage promotes ER homeostasis and prevents cytotoxic ER stress in ccRCC cells (Fig. 19). This phenotype promotes cell viability under multiple conditions that perturb ER homeostasis, including growth under limited nutrient/O_2 delivery within solid tumors, enhanced protein synthesis downstream of oncogenic activation, and exposure to pharmacological ER stress inducing drugs.

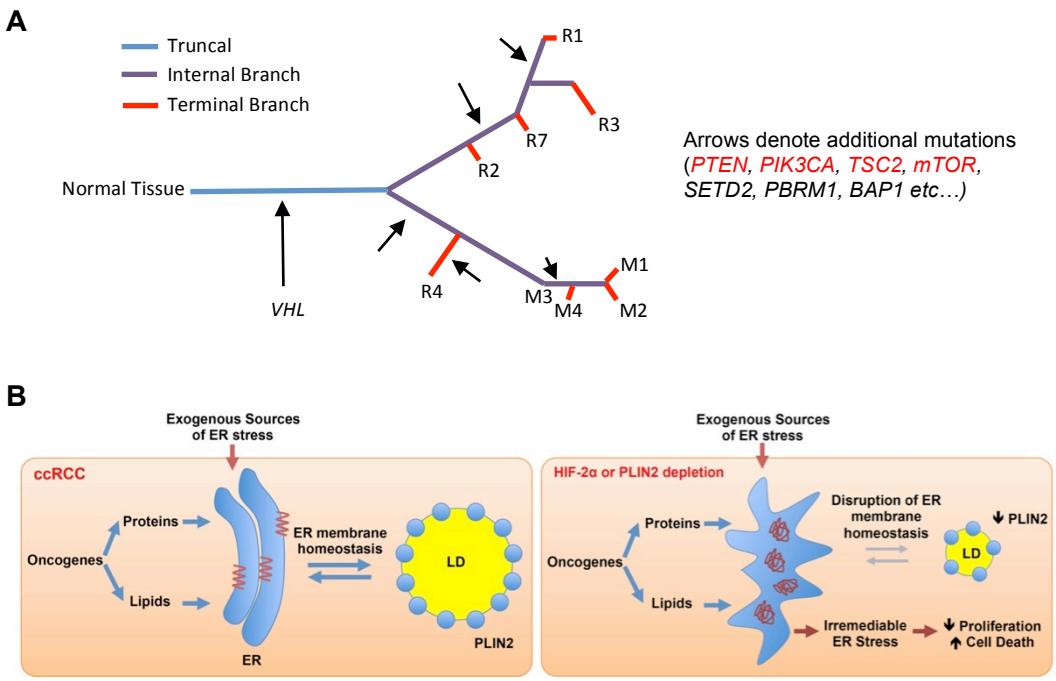

Figure 19: Proposed model illustrating the protective function of HIF-2α dependent PLIN2 expression and lipid storage in ccRCC

A) A model for sporadic ccRCC tumorigenesis, based on published conclusions (Gerlinger et al., 2014). Multi-region sequencing of the same tumor reveals extensive intratumoral heterogeneity, as indicated by branched evolution of recurrent mutations found in ccRCC. In all regions of the tumors analyzed, biallelic inactivation of *VHL* was observed, indicating that it is an early, truncal event in the progression of ccRCC. Subsequent mutations are necessary for tumor progression, including activating mutations in the mTORC1 pathway in many cases (shown in red).

B) Our data suggest a model in which enhanced lipid storage occurs early in disease progression, downstream of *VHL* loss, HIF-2α stabilization, and increased PLIN2 expression. PLIN2-dependent lipid storage promotes ER homeostasis and cell viability under conditions that increase ER stress, including heightened protein synthesis, growth in nutrient/oxygen scarce conditions, and upon exposure to pharmacologic ER stress-inducing agents. For instance, mTORC1 driven protein synthesis and unregulated growth generates cell intrinsic and extrinsic stresses. We suggest that enhanced lipid storage promotes ER membrane homeostasis and allows tumors to tolerate the metabolic stresses that come with mTORC1 activation.

Discussion

Despite the longstanding observation that ccRCC tumor cells exhibit abundant intracellular LDs, a clear function for this phenotype had not been identified. In this study, we explored the role of LD coat proteins in ccRCC progression. Analysis of multiple cohorts of primary ccRCC patient samples revealed *PLIN2* overexpression in tumor samples and suggested a functional relationship between pVHL loss, constitutive HIF-2α activation, and *PLIN2* accumulation. While previous reports indicated that *PLIN2* expression and lipid storage correlated with HIF-2α activation, it was unknown whether PLIN2 was a driver of this phenotype, or a passenger of broader metabolic changes. Our findings indicate that PLIN2 is both necessary and sufficient to promote lipid storage in ccRCC cell lines. Mechanistically, HIF-2α dependent PLIN2 expression and lipid storage is required for maintenance of ER homeostasis and prevention of cytotoxic ER stress.

The significant requirement for PLIN2 in ccRCC cells was intriguing, as *Plin2 -/-* mice are viable and acute *PLIN2* depletion studies in settings of lipid accumulation (i.e. hepatosteatosis or foam cell formation) have (Chang et al., 2010; Son et al., 2012; Sztalryd et al., 2006). We provide two potential explanations for this observation. First of all, in physiological scenarios, PPAR family members coordinately enhance expression of PLIN2 and other PAT LD coat proteins (Greenberg et al., 2011). In these settings, PLIN2 loss of function is associated with compensatory upregulation of other LD coat proteins (Chang et al., 2010; Sztalryd et al., 2006). However, we determined that *PLIN2* is upregulated in ccRCC due to HIF-2α activation, rather than by PPARγ or PPARα. Moreover, *PLIN2* is overexpressed independently of other PAT LD coat proteins in ccRCC, likely explaining why functional compensation cannot be achieved after PLIN2 depletion. Secondly, our results suggest that an enhanced requirement for PLIN2 dependent lipid storage and ER homeostasis could arise from heightened ER stress downstream of oncogene activation. These include cell intrinsic stress from enhanced protein synthesis and cell extrinsic stress due to commitment to a growth rate that outstrips nutrient and O_2 delivery.

Our results fit within an emerging theme in which oncogenic transformation coordinately induces both anabolic processes to increase proliferation and homeostatic pathways that maintain cell viability. These include proteasome activity downstream of mTORC1, autophagy downstream of MYC overexpression (Hart et al., 2012), and lipid/protein scavenging by RAS transformed tumors (Commisso et al., 2013; Kamphorst et al., 2013). Thus, different oncogenes appear to solve the problem of balancing proliferation and cellular homeostasis in unique ways. In the case of ccRCC, we suggest a model in which HIF-2α dependent lipid storage occurs early in disease progression and functions to buffer tumor cells against cell intrinsic and extrinsic sources of ER stress. In ccRCC, the heightened proliferation and anabolic metabolism is driven by HIF-2α dependent processes such as autocrine growth factor signaling via TGFα and VEGFA, mTORC1 stimulation, and cell cycle progression, and independent oncogenic events that activate mitogenic pathways (Cancer Genome Atlas Research, 2013; Elorza et al., 2012; Schodel et al., 2012). Although enhanced lipid storage is a hallmark feature of ccRCC, this phenotype is observed in other malignancies, including Burkitts lymphoma, hepatocellular carcinoma, and advanced prostate cancer (Bozza and Viola, 2010; Yue et al., 2014). While the underlying mechanisms of lipid storage and the function it serves may vary between cancer types, additional studies into the role of lipid storage in cancer are warranted.

Our results indicate that heightened protein synthesis is a prominent source of ER stress in PLIN2 deficient ccRCC cells. While the initial perturbation to ER homeostasis in such cells is likely due to alterations in ER lipid content, the cumulative level of ER stress likely arises from dysregulation of both protein and lipid metabolism, which independently trigger the UPR (Volmer et al., 2013). In addition, disruption of ER lipid composition can further impair protein-folding capacity and enhance ER stress (Fu et al., 2011). Mechanistically, PLIN2 promotes neutral lipid content through at least two, non-mutually exclusive, mechanisms: enhancing lipid storage and suppressing lipolysis. Our observation that oleic acid is selectively toxic to PLIN2 depleted cells suggests that at least a portion of the PLIN2 deficient phenotype arises from loss of the ability to package lipids into LDs. This phenotype is also observed in mouse embryonic fibroblasts that are

deficient in enzymes (diacylglyceride-acyltransferases, DGATs) that are required to incorporate oleic acid into triglycerides (Listenberger et al., 2003). It remains to be tested how PLIN2 affects lipolysis in ccRCC.

Lastly, our finding that loss of HIF-2α/PLIN2 dependent lipid storage enhances sensitivity to ER stress inducing agents has implications for ccRCC therapy. A therapeutic index has previously been demonstrated for the proteasome inhibitor Bortezomib in multiple myeloma, where heightened immunoglobulin synthesis within ER renders cells more sensitive to pharmacological ER stress (Obeng et al., 2006). A small phase II clinical trial evaluating Bortezomib mono-therapy for advanced renal cancer revealed partial responses in only 12% (3/25) of ccRCC patients (Kondagunta et al., 2004). HIF-2α/PLIN2 dependent lipid storage and ER stress resistance could contribute to this limited response rate.

Chapter 4: DGAT activity promotes ER homeostasis in ccRCC

Introduction

Our observations in Chapter 3 suggest that lipid storage capacity maintains ER homeostasis in ccRCC cells. To elucidate a mechanistic connection between lipid storage and ER homeostasis in ccRCC, we turned our attention to the cellular pathways responsible for generating triacylglycerol (TAG), the primary mode for fatty acid storage within LDs. Synthesis of TAGs and phospholipids share a common pathway that includes the synthesis of diacylglyerol (DAG). As with any membrane compartment within the mammalian cell, the phospholipid composition of the ER membrane must be tightly regulated to support organelle function, prevent ER stress, and maintain cell viability (Ariyama et al., 2010; van Meer et al., 2008). On the other hand, neutral TAGs can be stored within the dense neutral lipid core of the LD. Thus, we hypothesize that partitioning of fatty acids into TAG can be cytoprotective by buffering against changes in the phospholipid composition (Fig. 20).

Synthesis of TAG and phospholipid

Here, we will review the enzymatic reactions involved in DAG, phospholipid, and TAG synthesis. Both phospholipids and TAG include a glycerol backbone. Glycerol-3-phosphate is obtained from hydrolysis of extracellular TAG or synthesis from the glycolytic intermediate dihydroxyacetone phosphate (DHAP) (Currie et al., 2013). The sequential transfer of fatty acids from acyl-CoA to glycerol-3-phosphate and subsequent dephosphorylation by lipin (phosphatide phosphatase) generates DAG. Various glycerol-3-phosphate acyltransferse (GPAT) and acylglycerolphosphate acyltransferase (AGPAT) proteins catalyze these reactions (Yen et al., 2008).

Synthesis of phospholipids occurs via the addition of polar head groups (i.e. phosphocholine, phosphoethanolamine) to DAG. TAG synthesis is catalyzed by the addition of a third acyl chain to the DAG molecule by either of two acyl-CoA:diacyglyerol acyltransferase (DGAT) enzymes DGAT1 and DGAT2. Despite catalyzing the same reaction, DGAT1 and DGAT2 belong to distinct

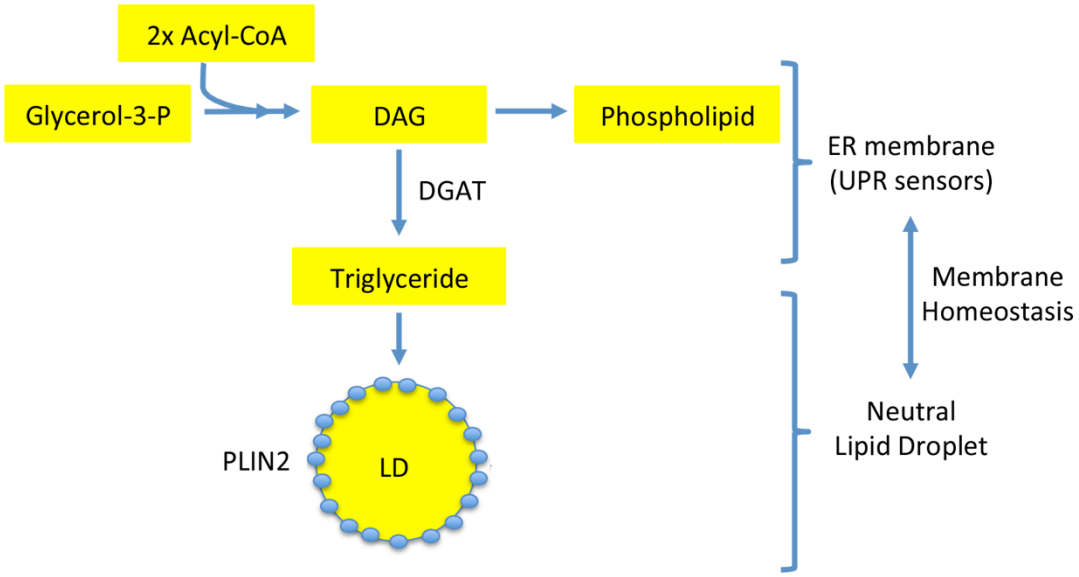

Figure 20: Model of ER membrane homeostasis. The phospholipid composition of the ER membrane must be maintained to support organelle function and prevent ER stress. For instance, perturbations in unsaturation of phospholipid fatty acid chains can trigger the ER stress and activate UPR sensors, which reside in the ER bilayer. On the other hand, neutral TAG can be stored within the LD, away from the ER bilayer. We hypothesize that TAG synthesis allows cells to tolerate perturbations to the fatty acid pool (hypoxia, serum deprivation, etc…) and sustain ER lipid composition to support viability.

gene families and are not structurally related. Major differences between the two enzymes include tissue distribution and sub-cellular localization. In mice, Dgat1 is the primary enzyme in intestines and macrophages (Koliwad et al., 2010; Smith et al., 2000), while Dgat2 is primarily responsible for TAG synthesis in the liver and adipose (Choi et al., 2007; Stone et al., 2004). Mouse studies demonstrate that global deletion of *Dgat1* is associated with poor dietary lipid uptake and a 50% reduction in whole body TAG, but is compatible with life (Koliwad et al., 2010). *Dgat2* ablation results in perinatal lethality, primarily due to dehydration secondary to a skin-barrier defect (Stone et al., 2004). In addition, whole animal TAG are reduced by 90% and plasma lipid and glucose concentrations are perturbed, indicating a more profound energetic function of mouse Dgat2. With regard to sub-cellular localization, DGAT1 is a multi-pass transmembrane protein that is confined to the ER, while DGAT2 can be found within the ER or LDs. LD localization of DGAT2 is facilitated by a transmembrane loop that does not cross to the ER lumen, allowing for association with the phospholipid monolayer of LDs upon exposure of cells to high lipid concentrations (Wilfling et al., 2013).

Triglyceride storage and ER stress

Altered tumor lipid metabolism is not only a question of increasing the quantity of lipid that must be generated to duplicate the contents of the cell. Homeostatic processes are also required to maintain the proper lipid composition within each sub-cellular compartment to support organelle function and cell viability. We focus our attention on the ER, a hub for both protein and lipid metabolism. Proteins that are vital to tumor cell functions, including growth factor receptors and secreted signaling proteins, are synthesized within the ER. In addition, the lipid synthetic reactions described in the section above largely take place within the ER membrane. As a result, proper maintenance of ER phospholipid composition is vital to sustaining cellular functions that support growth and proliferation (Clarke et al., 2014). For example, it is evident that perturbation of ER phospholipid membrane composition can impair protein-folding capacity within the ER lumen (Fu et al., 2011). In addition, exposure to pharmacologic ER stress inducing agents, including tunicamycin and bortezomib, are correlated with an increase in TAG storage (Lee et al.,

2012; Rutkowski et al., 2008). However, the functional connection between TAG synthesis and ER stress are unknown.

The fatty acid composition of phospholipids must be regulated to maintain membrane fluidity (Fig. 21). The cellular fatty acid pool that contributes to phospholipid synthesis is generated by a combination of factors, including 1) lipid synthesis, 2) lipid uptake and 3) modification of fatty acids via elongation and/or desaturation. The tumor microenvironment can affect fatty acid composition by affecting the availability of 1) exogenous lipids (i.e. free fatty acids, lysophospholipids, and lipoproteins), 2) nutrients required for lipid synthesis (i.e. glucose and/or glutamine), and 3) oxygen required to produce unsaturated fatty acids (Fig. 21). Our results in Chapter 3 suggest that TAG synthesis may support tumor growth under these conditions that elicit lipotoxic stress.

Summary

In this chapter, we utilize genetic and pharmacologic methods of ablating cellular DGAT activity to dissect the contribution of TAG synthesis in settings of lipotoxic stress relevant to tumor growth. These include growth within the *in vivo* tumor microenvironment, which is characterized by limited nutrient and oxygen delivery, in addition to various *in vitro* culture systems that mimic sources of lipotoxic stress. Throughout this chapter, we utilize activation of the UPR as a read-out for ER stress downstream of phospholipid membrane dysfunction.

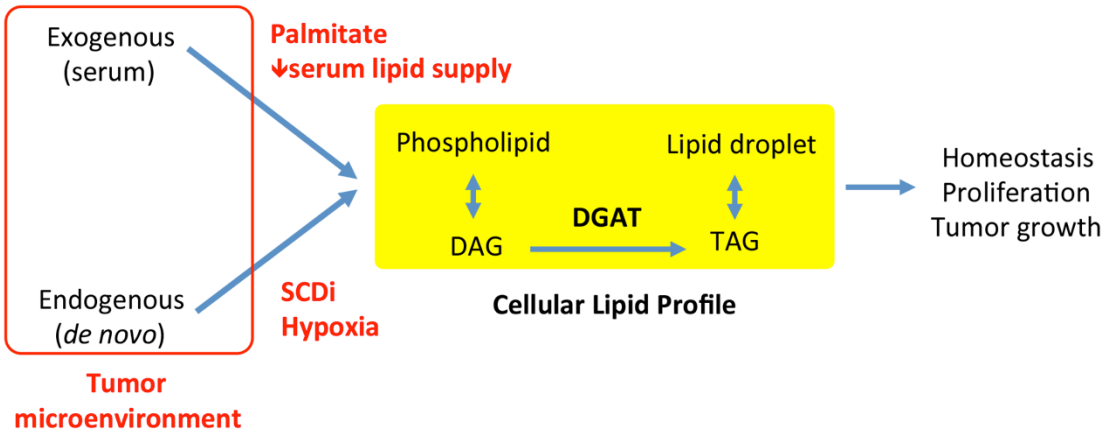

Figure 21: Perturbations to the cellular lipid profile impact tumor growth. Various perturbations that impact the fatty acid composition within a tumor cell are shown in red. These are the systems utilized in this chapter to examine the tumor promoting functions of DGAT-dependent TAG synthesis and storage. As outlined in Figure 20, we hypothesize that DGAT activity promotes ER homeostasis, cell proliferation, and tumor growth by preventing maladaptive changes to the phospholipid pool.

Results

Examining DGAT1 and DGAT2 function in A498 ccRCC cells

To identify the contributions of DGAT1 and DGAT2 to TAG synthesis in A498 ccRCC cells, we generated cells expressing Dox-inducible shRNAs against *DGAT1* or *DGAT2*. qRT-PCR analysis confirmed suppression of *DGAT1* or *DGAT2* upon Dox treatment (Fig. 22A). In addition, western blot analysis confirmed the ablation of DGAT1 protein (Fig. 22B). Note that while DGAT2 protein ablation could not be assessed due to the absence of a reliable antibody, subsequent functional studies confirmed the suppression of DGAT function. Interestingly, *DGAT1* ablation was associated with an increase in *DGAT2* mRNA (Fig. 22A). To determine the functional effects of DGAT1 and DGAT2 ablation, cellular TAG content was determined by LC-MS. TAG content was found to be positively correlated to *DGAT2* mRNA expression in A498 cells: a reduction of TAG in *DGAT2* ablated cells and an increase in *DGAT1* ablated cells (Fig. 22C). The compensatory increase in *DGAT2* mRNA concentrations was unanticipated, as it has not been observed in previous experiments examining acute DGAT ablation. Nonetheless, our central goal was to reduce total cellular DGAT activity. To identify the effects of dual-DGAT1/2 ablation, we generated A498 cells expressing Dox-inducible shRNA against both *DGAT1* and *DGAT2*. We first validated the suppression of mRNA levels of both *DGAT1* and *DGAT2* upon doxycycline treatment (Fig. 23A). DGAT1/2 ablated cells exhibited reduced TAG and increased DAG concentrations, consistent with suppression of cellular DGAT activity (Fig. 23B). These results suggest that DGAT2 activity is required for the increase in TAG content observed in DGAT1 ablated cells. To assess functional lipid storage capacity, cells were evaluated for neutral lipid content after exposure to oleic acid, a potent inducer of triglyceride synthesis and storage. BODIPY 493/503 staining and quantification by flow cytometry revealed that DGAT1/2 ablation largely abrogated the induction of neutral lipid content in oleic acid treated cells (Fig. 23C).

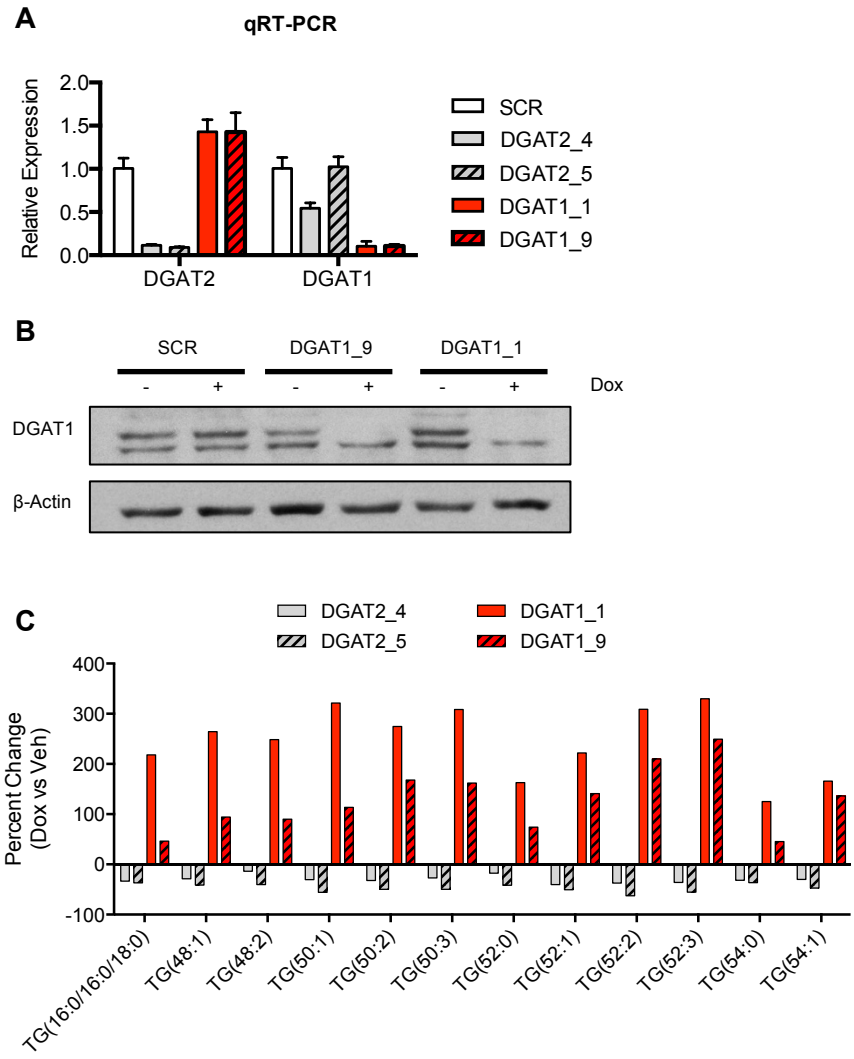

Figure 22: Ablation of DGAT1 and DGAT2 in A498 cells

A) A498 cells expressing dox-inducible SCR shRNA, shDGAT2_4, shDGAT2_5, shDGAT1_1, or shDGAT1_9 were treated with doxycycline (1µg/ml) for 4 days. qRT-PCR analysis of *DGAT2* or *DGAT1* is shown. *TBP* and *ACTB* were utilized as endogenous control genes and relative mRNA expression was determined by normalizing to expression in SCR cells.

B) Western blot analysis of SCR and shDGAT1 cells descibred in (A).

C) LC-MS was performed to determine the effect of DGAT2 or DGAT1 ablation on cellular triglyceride content. Percent change corresponds to change elicited by dox-induced shRNA expression.

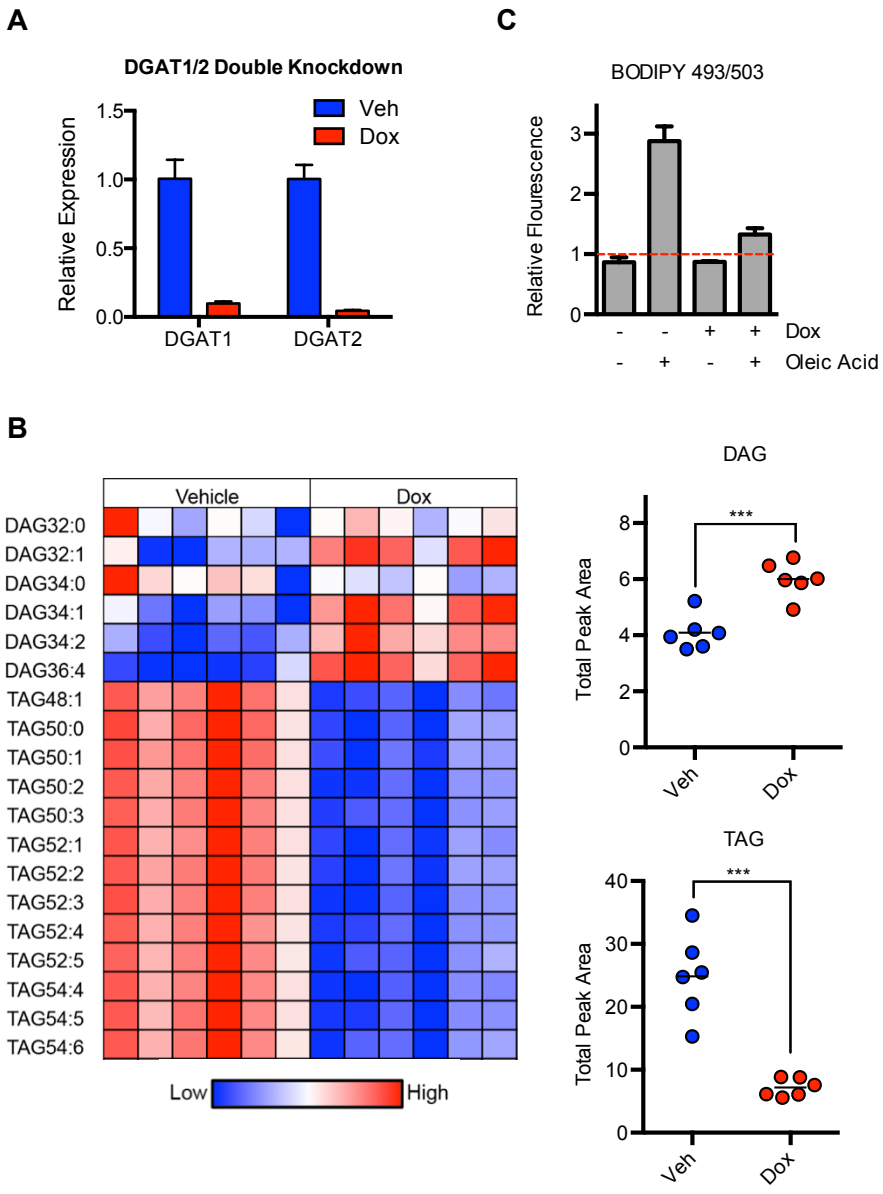

Figure 23: DGAT1/2 double ablation reduces TAG storage capacity

A) A498 cells expressing dox-inducible shDGAT2_5 and shDGAT1_1 were generated. mRNA expression of *DGAT1* and *DGAT2* was determined by qRT-PCR after 4 days of doxycycline (1µg/ml) treatment.

B) LC-MS analysis of lipids extracted from cells in (A). Peak area for each species was normalized to cell number in each sample. Heat map corresponds to relative metabolite content for each DAG or TAG species (left). Total normalized peak area for the DAG and TAG species was calculated using the species shown in the heat map (right). p-values were determined by student's t-test. *** $p<0.001$.

C) Cells in (A) were treated with BSA or oleic acid conjugated BSA for 24 hours. Neutral lipid content was determined by BODIPY 493/503 (2µg/ml) staining and flow cytometry.

DGAT activity protects against palmitate-induced lipotoxicity

Exposure to the saturated fatty acid palmitate is a well-established model of lipotoxicity (Listenberger et al., 2003). Doxycycline-induced *DGAT2* ablation sensitized A498 cells to palmitate-induced cell death (Fig. 24A), while *DGAT1* ablation actually yielded a protective effect (Fig. 24B). The effects of *DGAT1* ablation were recapitulated with a pharmacologic DGAT1 inhibitor T863 (Fig. 24C). These findings were consistent with the neutral lipid storage capacity (TAG content) in the single DGAT1 or DGAT2 ablated cells (Fig. 22C). Cells in which DGAT1 and DGAT2 were suppressed were more sensitive to palmitate-induced cell death, indicating that the protective effect of DGAT1 ablation requires DGAT2 function (Fig. 25A). Taken together, our results suggest that overall TAG storage capacity is inversely related to palmitate-induced cytotoxicity, suggesting a protective function for TAG synthesis under lipotoxic stress.

Perturbation of ER phospholipid composition, including disruption of unsaturated:saturated lipid content, is sufficient to trigger ER stress and UPR signaling (Ariyama et al., 2010; Volmer et al., 2013). Indeed, increased palmitate-induced cell death in DGAT1/2 ablated cells was also associated with an greater expression of UPR target genes (Fig. 25B), consistent with enhanced ER stress. LC-MS was performed to determine if enhanced ER stress and cell death were correlated with perturbation in the ER membrane lipid composition in DGAT1/2 ablated cells. Normalized peak areas for the most abundant phosphotidylcholine (PC) species was calculated. To gain insight into phospholipid composition, the percentage of PC species with zero, one, or two double bonds (DB=0, 1, or 2) was calculated for each condition. As expected, palmitate treatment enhanced the proportion of fully saturated PCs (DB=0) in both vehicle and doxycycline treated cells (Fig. 25C). However, palmitate treatment elicited a greater enhancement of PC saturation in DGAT1/2 ablated cells (Fig. 25C). Palmitate-treated DGAT1/2 ablated cells also exhibited a more substantial reduction in the percentage of species with 1 or 2 double bonds (DB=1 or DB=2) (Fig. 25C). Thus, the protective effects of DGAT activity under palmitate treatment were associated with preservation of phospholipid membrane homeostasis and prevention of ER stress.

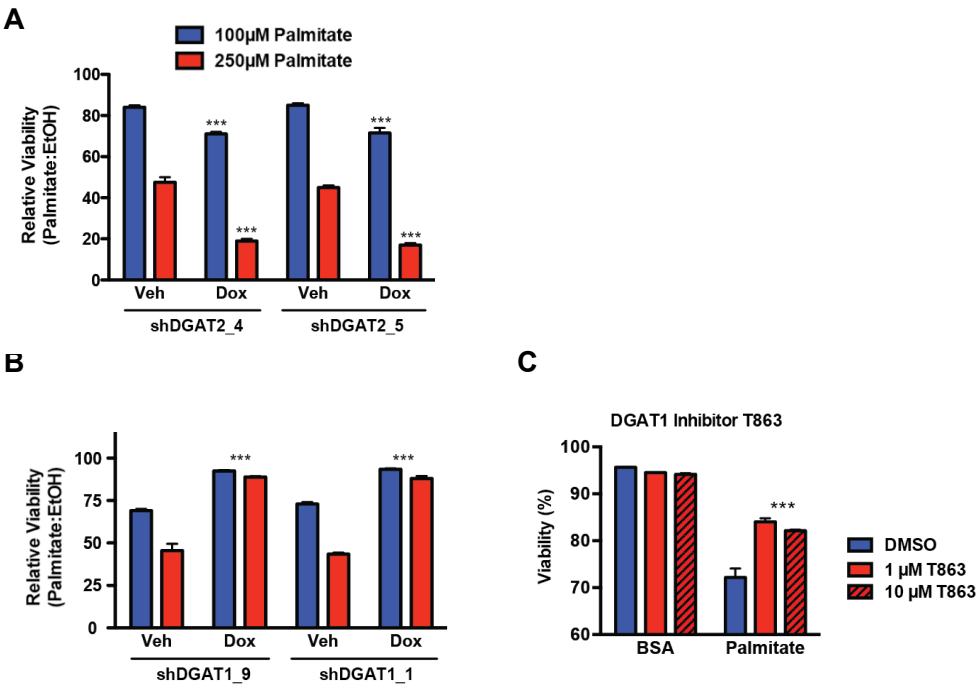

Figure 24: DGAT2 ablation enhances, while DGAT1 ablation ameliorates, palmitate-induced cell death.

A) A498 cells expressing dox-inducible shDGAT2_4 or shDGAT2_5 were treated with doxycycline (1μg/ml) or vehicle for 4 days prior to being treated with BSA or palmitate-conjugated BSA. Cell viability was determined by Annexin/PI staining after 2 days of treatment. Viability for palmitate-treated cells, relative to BSA treated cells, is shown.

B) A498 cells expressing dox-inducible shDGAT1-9 or shDGAT1_1 were treated as described in (A).

C) Parental A498 cells were pre-treated with DGAT1 inhibitor T863 for 1 day prior to treatment with 250μM palmitate or BSA vehicle for 2 days. Cell viability was determined by Annexin/PI staining after 2 days of treatment. p-values were determined by student's t-test. *** $p<0.001$.

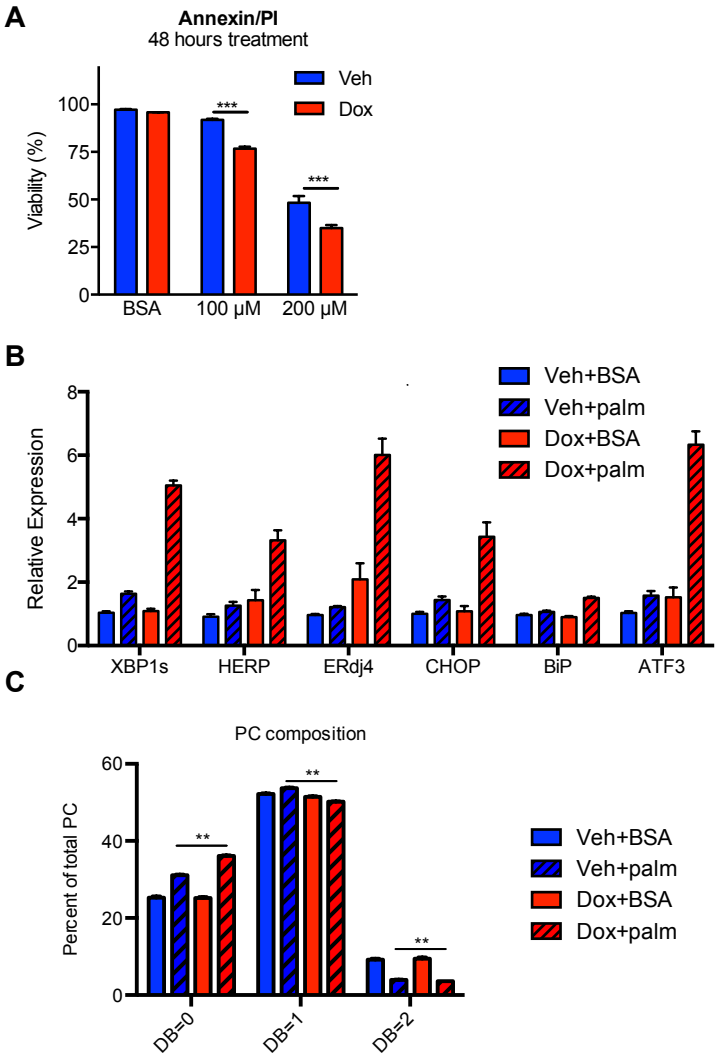

Figure 25: DGAT1/2 double ablation enhances palmitate-induced lipotoxicity

A) A498 cells expressing dox-inducible shDGAT2_5 and shDGAT1_1 were treated for 4 days of doxycycline (1µg/ml) prior to incubation with BSA or palmitate-conjugated BSA. Cell viability was determined by Annexin/PI staining after 2 days of treatment.

B) qRT-PCR analysis of cells from (A) treated for 24 hours with BSA and 100µM palmitate. *TBP* and *ACTB* were utilized as endogenous control genes and relative mRNA expression was determined by normalizing to expression in cells treated with vehicle and BSA.

C) LC-MS analysis of lipids extracted from cells in (B). For each condition, peaks corresponding to phosphatidylcholine (PC) were identified. The percentrage of total species with zero, one, or two double bonds is shown. n=5 per condition. p-values were determined by student's t-test. ** $p<0.01$, *** $p<0.001$.

DGAT ablated cells are more sensitive to serum and oxygen deprivation

Next, we determined the effect of DGAT ablation on ccRCC cell sensitivity to unsaturated lipid deprivation. Our lab previously demonstrated that oxygen-dependent unsaturated lipid synthesis becomes critical for transformed cells grown under low serum conditions (Young et al., 2013). In these studies, cytotoxic effects of hypoxia were recapitulated by pharmacologic inhibition of SCD1, suggesting that unsaturated lipid deprivation is a key component of hypoxic tumor cell stress. We found that DGAT1/2 ablated cells exhibited increased cell death when grown under hypoxia or combined serum and oxygen deprivation (Fig. 26A). Consistent with our previous studies, we found that DGAT1/2 ablated cells were also more sensitive to pharmacologic SCD1 inhibition, with a more pronounced effect noted in cells growth under low serum conditions in which exogenous unsaturated lipids are scarce (Fig. 26B). Lastly, the increased sensitivity to combined serum deprivation and SCD1 inhibition was associated with greater induction of UPR genes in DGAT1/2 ablated cells (Fig. 26C). Our results thus far suggest that DGAT activity protects against disruption of phospholipid desaturation index (i.e. upon exposure to palmitate or deprivation of unstaruated lipids).

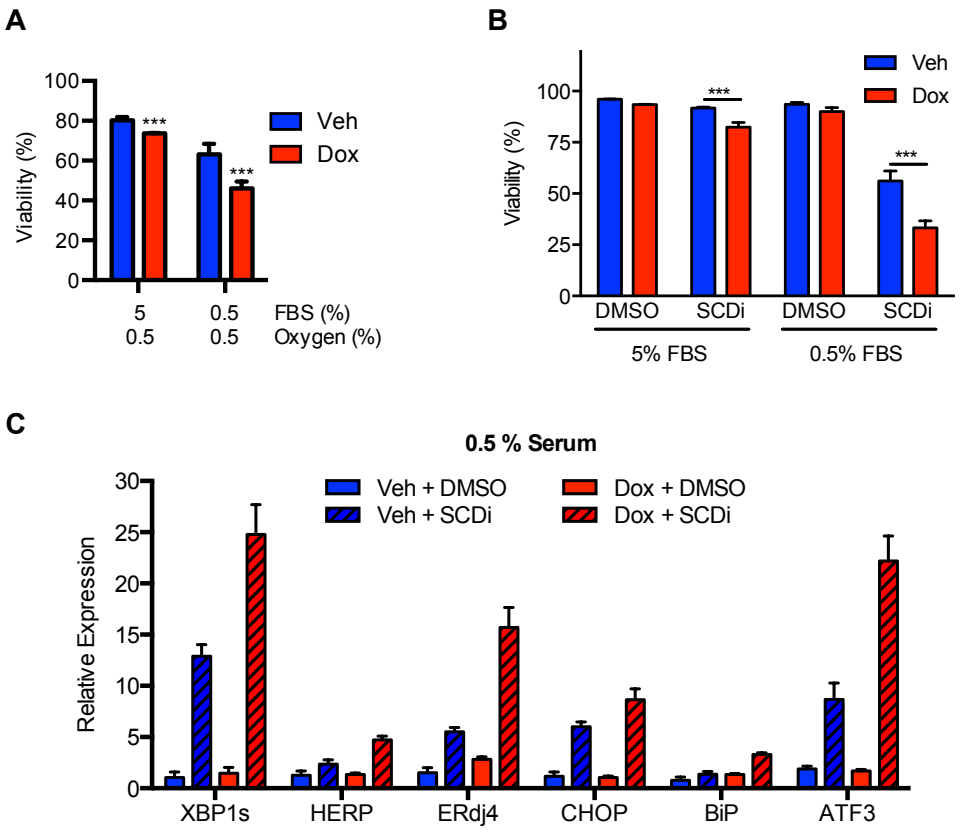

Figure 26: DGAT activity protects against unsaturated lipid deprivation

A) A498 cells expressing dox-inducible shDGAT2_5 and shDGAT1_1 were treated for 4 days of doxycycline (1µg/ml) prior to exposure to the indicated serum and oxygen growth conditions. Cell viability was determined by annexin/PI after 4 days under the indicated conditions.

B) A498 cells expressing dox-inducible shDGAT2_5 and shDGAT1_1 were treated for 4 days of doxycycline (1µg/ml) prior to exposure to the indicated serum and SCD1 inhibitor (CAY10566, 1µM) growth conditions. Cell viability was determined by annexin/PI after 3 days under the indicated conditions.

C) qRT-PCR analysis of cells from (B) under the 0.5% serum conditions. *TBP* and *ACTB* were utilized as endogenous control genes and relative mRNA expression was determined by normalizing to expression in tumors from vehicle treated animals. p-values were determined by student's t-test. *** $p<0.001$.

DGAT activity protects against pharmacologic ER stress

Our results suggested that DGAT activity was adaptive in the setting of lipotoxic stresses that directly perturb the cellular phospholipid profile. Interestingly, exposure to the proteotoxic ER stress-inducing agents tunicamycin (an inhibitor of N-linked glycoslation that impairs protein folding) and bortezomib (a proteasome inhibitor) actually increased TAG synthesis and neutral lipid storage in both cultured cells and in mouse tissues *in vivo* (Lee et al., 2012; Rutkowski et al., 2008). However, the function of enhanced lipid storage in these settings is unknown. To determine if TAG synthesis is protective against ER stress that emerges from mis-folded protein load, DGAT1/2 ablated cells were treated with tunicamyin or bortezomib. Remarkably, DGAT1/2 suppression enhanced cell death in cells treated with either drug (Fig. 27A-B). Collectively, our findings suggest that DGAT-dependent TAG synthesis is adaptive under conditions of ER stress triggered by perturbations in either lipid or protein metabolism.

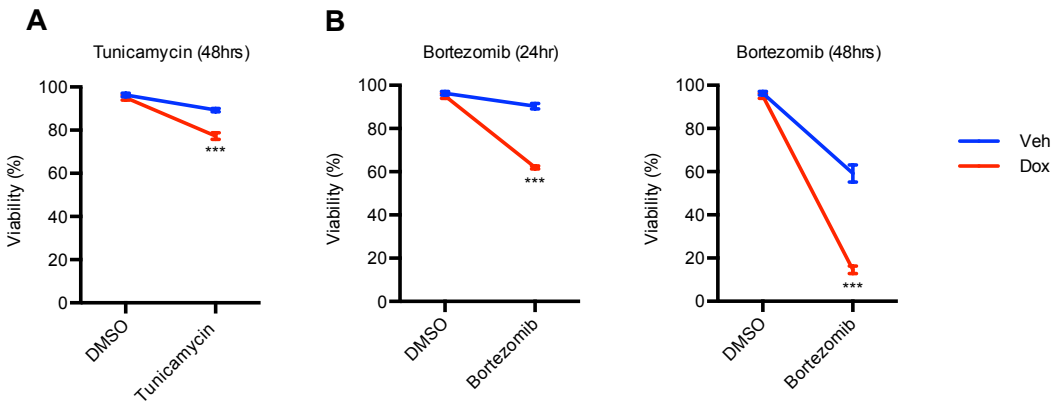

Figure 27: DGAT activity protects against pharmacological ER stress

A) A498 cells expressing dox-inducible shDGAT2_5 and shDGAT1_1 were treated for 4 days of doxycycline (1µg/ml) prior to exposure to DMSO or tunicamycin (5µg/ml). Cell viability was determined by Annexin/PI after 2 days.

B) A498 cells expressing dox-inducible shDGAT2_5 and shDGAT1_1 were treated for 4 days of doxycycline (1µg/ml) prior to exposure to DMSO or Bortezomib (50nM). Cell viability was determined by Annexin/PI after 1 or 2 days. p-values were determined by student's t-test. *** $p<0.001$.

DGAT activity promotes tumor growth and protects against ER stress in subcutaneous ccRCC xenografts

To proliferate and survive *in vivo,* tumor cells must overcome various sources of metabolic stress that arise from high metabolic demand and poor perfusion. With respect to lipid metabolism, cells must overcome fluctuations in serum delivery of exogenous lipids and/or the substrates to synthesize them. In addition, low oxygen availability impairs the synthesis of unsaturated fatty acids via the Δ9 stearoyl-CoA desaturase (SCD1), which requires molecular oxygen as an electron acceptor (Ariyama et al., 2010). Interestingly, DGAT1/2 ablation did not affect cell proliferation rate under nutrient and oxygen-replete conditions *in vitro* (Fig. 28A). To determine the requirement for DGAT activity *in vivo,* sub-cutaneous tumors expressing Dox-inducible shRNAs against both *DGAT1* and *DGAT2* were generated. After tumors reached 300mm^3, a cohort of animals was placed on doxycycline containing chow. We found that DGAT ablation inhibited tumor growth (Fig. 28B). Dox-induced DGAT1/2 ablation was also associated with a reduction in proliferation index, as measured by Ki67 immunohistochemistry (Fig. 28C). However, cell death, as measured by cleaved caspsase 3 staining, was not observed in either group (data not shown). Lastly, DGAT1/2 ablation was associated with a modest increase UPR target gene expression in sub-cutaneous tumors (Fig. 28D). Notably, DGAT1/2 ablated cell did not exhibit UPR induction when grown under nutrient and oxygen replete conditions *in vitro* (data not shown), suggesting stresses associated with *in vivo* tumor growth enhanced the requirement for DGAT activity.

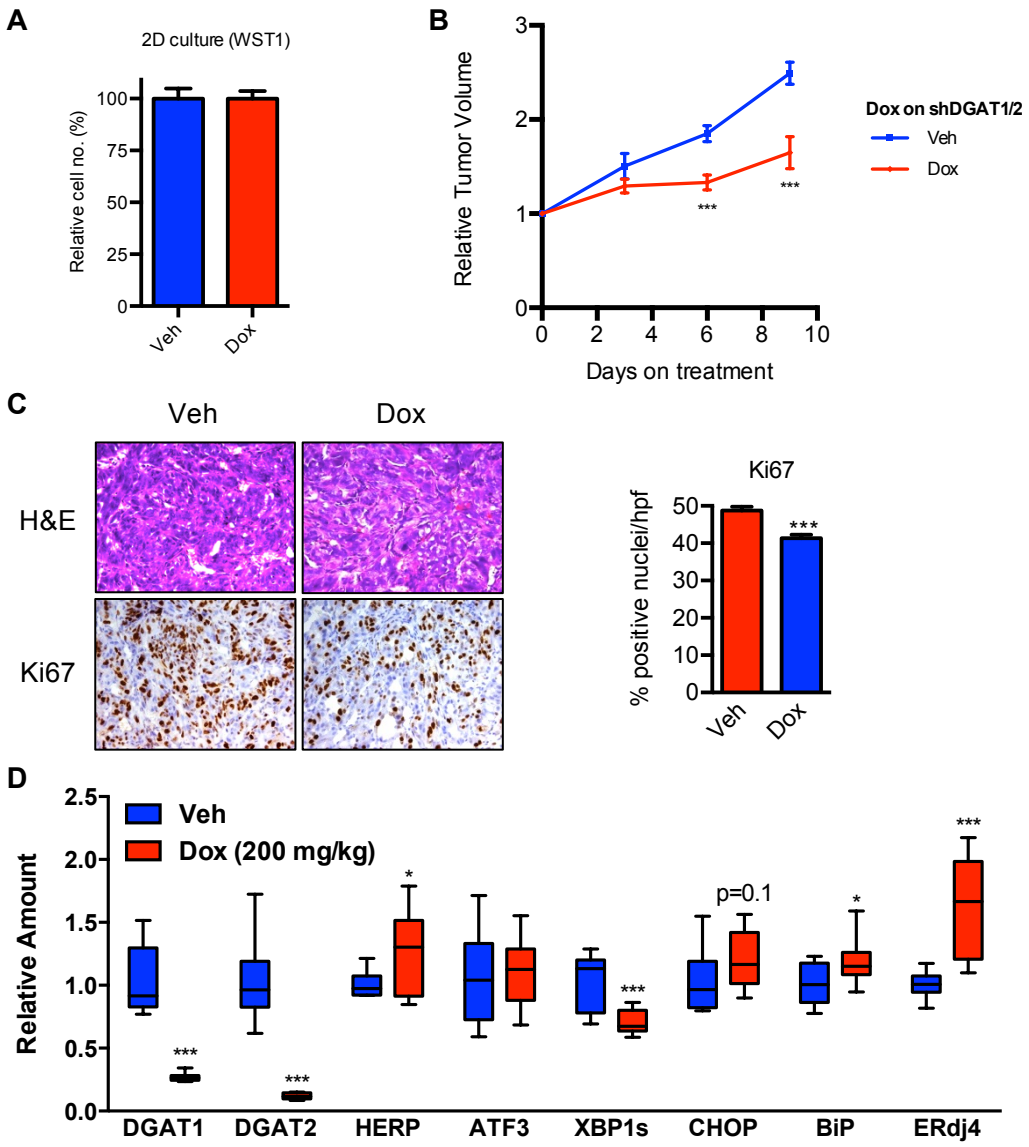

Figure 28: DGAT activity promotes ccRCC xenograft tumor growth

A) A498 cells expressing dox-inducible shDGAT2_5 and shDGAT1_1 were treated for 4 days of doxycycline (1µg/ml). Equal numbers of vehicle and doxycycline treated cells were plates into 96 well plates and relative cell number was determined after 3 days of growth by the WST1 colorometric assay.

B) Sub-cutaneous tumors of A498 cells expressing Dox-inducible shDGAT2_5 and shDGAT1_1 were generated in NIH-III nude mice. Once tumor volume reached 300mm^3, a cohort received Dox-chow (200 mg/kg). Relative tumor volume was monitored.

C) H&E and immunohistochemical staining of tumors from (B). Quantification of percentage of nuclei staining for Ki67 is shown (right)

D) qRT-PCR analysis of tumors from (B). *TBP* and *ACTB* were utilized as endogenous control genes and relative mRNA expression was determined by normalizing to expression in tumors from vehicle treated animals. p-values were determined by student's t-test. * p<0.05, ** p<0.01, *** p<0.001.

Discussion

These findings suggest that TAG synthesis is adaptive under conditions that perturb the cellular fatty acid pool (palmitate exposure, hypoxia, SCD1 inhibition) or protein homeostasis (tunicamycin, bortezomib, hypoxia). Similar to our findings regarding PLIN2 function in Chapter 3, ER stress induction and activation of the UPR were common to each of the conditions examined upon DGAT ablation. These results suggest that DGAT-dependent TAG synthesis and storage contribute to ER homeostasis downstream of PLIN2-dependent lipid storage. The upregulation of UPR target genes observed upon DGAT ablation *in vivo* was modest in comparison to *in vitro* conditions of lipotoxic stress (palmitate exposure, serum and oxygen deprivation, serum deprivation and SCD1 inhibition). First of all, the maximal activation of UPR signaling may have occurred at an earlier time-point, as RNA was harvested after 9 days on Dox chow, while tumor growth was suppressed as early as 4 days on Dox chow. Indeed, the primary function of UPR activation is to overcome the ER stress that originally triggered the response. Secondly, we reasoned that the stresses simulated by these *in vitro* culture conditions are only found within zones of the tumor experiencing nutrient and oxygen deprivation, possibly explaining the modest overall induction across the entire tumor. Immunohistochemistry for UPR targets will provide insight into this hypothesis. Lastly, our *in vitro* data demonstrated that DGAT activity was protective against pharmacologic ER stress inducing agents (tunicamycin and Bortezomib). We predict that treatment of tumor bearing animals with Bortezomib will broaden the zones of the tumor experiencing ER stress and that DGAT ablation will enhance anti-tumor activity of this treatment.

In the case of palmitate exposure, the protective effect of DGAT activity was associated with maintenance of proper phospholipid desaturation. However, perturbations of cellular lipid content under the other conditions tested within this study (i.e. sub-cutaneous tumor growth, hypoxia) are likely more complex. For example, DGAT activity could affect cellular concentrations of lipid-derived signaling molecules, such as DAG and ceramides (Hannun and Obeid, 2008). For example, mitogenic and pro-survival signaling downstream of protein kinase C epsilon (PKCε),

which is activated by DAG, has been observed in various malignancies (Griner and Kazanietz, 2007). In addition, Benjamin et al. recently demonstrated that reduced DAG-mediated signaling accounted for anti-tumor effects of fatty acid synthase inhibitors (Benjamin et al., 2015). We observed that DAG content was actually increased in DGAT1/2 ablated ccRCC cells under replete culture conditions *in vitro*. Future studies will examine mitogenic signaling pathways and lipid composition in the other systems utilized here, where DGAT activity was cytoprotective (*in vivo* tumor growth, serum and oxygen deprivation). Another potential mediator of lipotoxicity is cytotoxic ceramide signaling. Indeed, ceramide concentration was elevated in palmitate-treated DGAT ablated cells (data not shown). Previous studies evaluating a role for ceramide signaling in lipotoxic cell death are conflicting, often yielding cell type or stress specific findings (Listenberger et al., 2001; Suzuki et al., 2011). Future studies will directly examine the function of ceramide signaling in DGAT ablated ccRCC cells. Ultimately, ER stress was a common feature of DGAT ablated cells in our study. Given the well-established functional connections between hypoxia, SCD1 inhibition, phospholipid composition, and ER stress, we anticipate that LC-MS analysis will reveal phospholipid changes that may account for the enhanced lipotoxicity in DGAT ablated cells.

The observation that TAG synthesis protected against proteotoxic ER stress (tunicamycin, bortezomib, hypoxia) suggests an active, adaptive function of enhanced lipid storage under ER stress. While increased lipid storage has previously been observed as a consequence of ER stress, its potential functional impact is largely unexplored. Future studies will address this question (see Chapter 5).

Chapter 5: Conclusion

Tumor promoting functions of lipid storage

Our results identify a mechanism for the development of the clear cell phenotype in ccRCC and indicate that enhanced lipid storage promotes ER homeostasis in this common renal malignancy. A prominent source of ER stress in ccRCC derives from activation of the mTORC1 pathway, which promotes both protein and lipid synthesis. Large scale sequencing studies by the TCGA initially reported activating mutations within the mTORC1 pathway in 30% of tumors (Cancer Genome Atlas Research, 2013). Subsequent studies involving multi-region sequencing of patients' tumors and metastases reveal that approximately 60% of all cases have mTORC1 pathway activating mutations (Gerlinger et al., 2014). In addition, immunohistochemical staining of a large number of primary ccRCC samples reveals mTORC1 pathway activation in >80% of all cases (Haddad et al., 2015). While pVHL loss and HIF pathway activation in murine renal tubular cells is not sufficient for ccRCC development, the absolute requirement for constitutive HIF signaling is this disease is well-established. Given the early biallelic inactivation of *VHL* in sporadic and hereditary ccRCC cases, our results suggest a model in which enhanced lipid storage develops early in disease progression and facilitates cellular transformation by maintaining ER homeostasis in the setting of oncogene-induced dysregulated growth, which induces ER stress via cell intrinsic (i.e. enhanced ER protein load) and extrinsic (poor nutrient/oxygen delivery) mechanisms. We refer you the the model presented at the end of Chapter 3 (Fig. 20)

mTORC1 activation is a feature of many human malignancies, but grossly enhanced lipid storage and the "clear cell" phenotype are not always observed in such tumors. Other malignancies likely acquire additional adaptations to maintain ER homeostasis. For example, Zhang et al recently demonstrated that mTORC1 increases proteasome activity to sustain intracellular amino acid levels in the setting of enhanced protein synthesis (Zhang et al., 2014). The requirement for mTORC1 dependent proteasome activity is likely enhanced by the fact that

mTORC1 suppresses autophagy, another primary mechanism for breakdown of intracellular proteins into constituent amino acids. While this study focused on maintenance of amino acid content, another function of the proteasome is suppression of proteotoxicity and ER stress. Indeed, mTORC1-driven protein synthesis induces ER stress and triggers the unfolded protein response (UPR). While it is established that UPR signaling enhances proteasome-dependent clearance of misfolded proteins via ERAD, it has not been tested whether mTORC1-activated tumors may rely more on proteasome activity for maintenance of ER homeostasis.

ccRCC represents an extreme example of tumor-promoting functions of lipid storage, yet it is increasingly evident that the LD may have tumor-promoting activities in a wide variety of cancers. For example, our unpublished work indicates that in A549 lung cancer cell lines, DGAT-dependent TAG synthesis is similarly adaptive under conditions of lipotoxic stress. Additionally, Bensaad et al recently identified cytoprotective functions for enhanced fatty acid uptake and lipid storage during ischemia/reperfusion injury in glioblastoma and breast cancer cell lines (Bensaad et al., 2014). The authors found that enhanced lipid storage, through unclear mechanisms, limited oxidative stress during the reperfusion phase of injury. Notably, the induction of genes involved in fatty acid uptake and lipid storage were identified by profiling mRNA expression in glioblastoma xenografts after treatment with the anti-angiogenic agent Bevacizumab. While enhanced lipid storage is a constitutive feature of ccRCC, it may also be an inducible adaptation under specific stresses in other malignancies.

Future directions

HIF-2α and PLIN2 expression: gene regulation and metabolic impacts

How does HIF-2α promote PLIN2 expression in ccRCC? One potential mechanism is direct activation of *PLIN2* transcription by a HIF-2α/ARNT transcriptional complex. Indeed, our analysis of published ChIP-seq data in the 786-O ccRCC cell line reveals association of HIF-2α and ARNT 35 kilobases (kb) upstream of the *PLIN2* promoter (Schodel et al., 2012). *PLIN2* is the nearest gene to these peaks, and long-range enhancer activity (i.e. >200kb for *CCND1*) have

been demonstrated for HIF-2α. Canonical hypoxia response elements (HREs) can be found within this genomic region associated with HIF-2α/ARNT. Future enhance-reporter studies will be performed to identify the functional HREs within this region. Furthermore, the endogenous function of these putative *PLIN2* enhancer(s) can be examined using CRISPR (clustered regularly interspaced short palindromic repeats) genome-editing technology. On the other hand, HIF-2α could indirectly regulate PLIN2 expression via its other effects on lipid metabolism. For example, recent work indicates that HIF-2α suppresses peroxisomal β-oxidation via induction of selective peroxisome degradation by autophagy (Walter et al., 2014). A subsequent increase in lipid availability could trigger *PLIN2* transcription. However, our results indicate that other potential mediators of PLIN2 expression in response to lipid availability, including PPARγ and PPARα, are unlikely to be responsible for PLIN2 expression in ccRCC.

Our results reveal that PLIN2 expression is sufficient to promote lipid storage in the absence of HIF-2α expression and suggest that enhanced TAG synthesis can account for part of PLIN2's function in ccRCC. Previous studies suggest that PLIN2 expression can have broader impacts on cellular metabolism (i.e. enhancing *de novo* fatty acid synthesis and/or suppressing lipolysis) (Imamura et al., 2002; Sun et al.). Thus, ER stress induction may explain only part of the anti-tumor effects of PLIN2 ablation in ccRCC. We have found that enhanced lipid storage in primary ccRCC patient samples is associated with robust repression of PPARα, PGC-1α, and the mitochondrial β-oxidation genes regulated by these two factors. Furthermore, recent literature suggests that suppression of PGC-1α-dependent mitochondrial biogenesis in ccRCC tumors reduces mitochondrial respiration and limits mitochondrial reactive oxygen species (ROS) generation (LaGory et al., 2015). Previous studies have indicated that PLIN2 is able to suppress ATGL-dependent lipolysis and reduce PPARα activity, presumably by reducing lipolysis-dependent release of PPARα ligands (Sapiro et al., 2009). While tumor-promoting functions of β-oxidation have been identified in other malignancies (Carracedo et al., 2013), the impact of PPARα activity and β-oxidation on ccRCC tumor growth are unknown. We hypothesize that suppression of mitochondrial fatty acid oxidation may protect ccRCC cells from mitochondrial

ROS. The established connection between PLIN2 expression, lipolysis, and PPARα activation provides a system for initial studies into the role of lipid oxidation in ccRCC.

Extending the cytoprotective functions of lipid storage to other settings

Our findings that PLIN2 expression and DGAT activity are protective against proteotoxic ER stress inducing agents, including tunicamycin and bortezomib, provides rationale for testing the broader function of enhanced lipid storage in additional settings. For example, in rodent models, treatment with tunicamycin induces robust lipid storage (Lee et al., 2012). In addition, acute renal ischemia is associated with induction of lipid storage in kidney tubule cells following injury (Zager et al., 2011). However, the function of enhanced lipid storage in these settings has not been explored. Under conditions of ER stress, vesicular transport is suppressed and *de novo* fatty acid synthesis is induced (Amodio et al., 2013; Lee et al., 2008), increasing ER lipid content. While ER membrane expansion may be necessary to accommodate an increased misfolded protein load, optimal ER lipid composition may be disrupted by such an increase in ER lipid content. TAG synthesis and storage may act as an overflow pathway to protect ER lipid composition under these conditions.

Enhanced lipid storage has been appreciated in histological analyses of primary human Burkitt's lymphoma (BL) samples (Wright, 1968), and immunohistochemical staining has revealed that PLIN2 is overexpressed specifically in BL cases, and not in other B cell malignancies (Ambrosio et al., 2012). Compared to other B cell malignancies, BL is distinguished by robust activation of MYC (Boxer and Dang, 2001). Our analysis of published MYC ChIP-seq data indicates that MYC can bind to the proximal promoter of *PLIN2* (Lin et al., 2012), suggesting a potential functional relationship between MYC activation and PLIN2-dependent lipid storage. However, the function of lipid storage in BL has not been explored. Our findings suggest a hypothesis that lipid storage may promote ER homeostasis in the setting of MYC-driven protein synthesis. As a transcriptional regulator of the overall translational machinery, MYC enhances global protein synthesis. This is required for transformation downstream of MYC (Barna et al.,

2008), but increased translation rates also generate metabolic stresses that must overcome to sustain tumor growth, including ER stress. Recently, Hart et al demonstrated that MYC dependent protein synthesis triggers UPR-mediated cytoprotective autophagy to support cell viability (Hart et al., 2012). Shin et al reported additional cross talk between the UPR and MYC-driven translation (Shin et al., 2013). These authors demonstrated that the IRE1α/XBP1 arm of the UPR induces the NAD+ dependent histone deacetylase SIRT7 to dampen MYC dependent transactivation of ribosomal genes, limit ER protein load, and ameliorate ER stress. Lastly, as was the case for mTORC1, MYC activation may also require the coordination of protein and lipid metabolism. Recent work by Carroll et al sheds light on how MYC stimulates various homeostatic processes, including lipogenesis, to sustain cell viability (Carroll et al., 2015). The authors demonstrate that MYC induces MondoA, a MYC superfamily member, which cooperates with MYC at a subset of loci, but also transactivates a variety of genes independently of MYC. Within the latter category are processes that limit metabolic stress downstream of MYC, including ER maintenance and lipid biosynthesis. Remarkably, MondoA ablation was selectively toxic in MYC activated cells. The importance of MondoA-dependent lipogenesis was underscored by the finding that provision of exogenous lipid in the form of the unsaturated fatty acid oleic acid was sufficient to rescue MondoA loss. While the authors did not address the mechanisms whereby lipid deprivation led to cell death in MondoA depleted cells, our work suggests that MYC-driven protein synthesis and ER stress may be involved. Ultimately, we hypothesize that MYC-dependent PLIN2 expression and lipid storage may provide an additional mechanism for sustaining ER homeostasis in the setting of MYC-driven protein synthesis.

Targeting oncogene-induced metabolic vulnerabilities

Oncogenic activation reprograms cellular metabolism to drive tumor growth, but also induces metabolic vulnerabilities, leading some to speculate that cancer treatment could be improved by targeting oncogene-induced metabolic stresses, rather than the oncogenes themselves. For instance, rapamycin analogs exhibit anti-tumor activity in various malignancies, including ccRCC, but are often cytostatic and tumor regrowth commonly occurs upon therapy cessation (Medvetz et

al., 2015). Our results suggest that ccRCC cells, which exhibit mTORC1 activation, require various homeostatic pathways to prevent ER stress and ensure cell viability, including enhanced lipid storage. In particular, our observation that multiple components of the ERAD machinery (*HERP, HRD1, ERdj4*) were induced in HIF-2α depleted tumors provides initial evidence for the rational combination of proteasome inhibitors and HIF-2α suppression, especially as HIF-2α specific inhibitors are currently under development for treatment of ccRCC (Clinical Trial No. NCT02293980).

Inhibition of DGAT-dependent TAG synthesis has been explored as a potential therapy for the treatment of fatty liver disease. The clinical utility of DGAT1 inhibitors may be limited by the exquisite requirement for intestinal DGAT1 activity for dietary lipid uptake (Haas et al., 2012). However, as discussed in Chapter 4, DGAT2 accounts for the majority of DGAT activity in murine liver, where suppression of DGAT2, but not DGAT1, reduced hepatic lipid storage and improved insulin sensitivity in murine models of fatty liver disease (Choi et al., 2007). Our results also suggest a dominant role for DGAT2 in ccRCC cell lines. DGAT2 specific small molecules are currently under development (Li et al., 2015). Our future work will explore the therapeutic potential of targeting DGAT2 in ccRCC tumors.

Bibliography

Ackerman, D., and Simon, M.C. (2014). Hypoxia, lipids, and cancer: surviving the harsh tumor microenvironment. Trends in cell biology *24*, 472-478.

Ambrosio, M.R., Piccaluga, P.P., Ponzoni, M., Rocca, B.J., Malagnino, V., Onorati, M., De Falco, G., Calbi, V., Ogwang, M., Naresh, K.N.*, et al.* (2012). The alteration of lipid metabolism in Burkitt lymphoma identifies a novel marker: adipophilin. PloS one *7*, e44315.

Amodio, G., Venditti, R., De Matteis, M.A., Moltedo, O., Pignataro, P., and Remondelli, P. (2013). Endoplasmic reticulum stress reduces COPII vesicle formation and modifies Sec23a cycling at ERESs. FEBS letters *587*, 3261-3266.

Ariyama, H., Kono, N., Matsuda, S., Inoue, T., and Arai, H. (2010). Decrease in membrane phospholipid unsaturation induces unfolded protein response. J Biol Chem *285*, 22027-22035.

Atkins, C., Liu, Q., Minthorn, E., Zhang, S.Y., Figueroa, D.J., Moss, K., Stanley, T.B., Sanders, B., Goetz, A., Gaul, N.*, et al.* (2013). Characterization of a novel PERK kinase inhibitor with antitumor and antiangiogenic activity. Cancer Res *73*, 1993-2002.

Barna, M., Pusic, A., Zollo, O., Costa, M., Kondrashov, N., Rego, E., Rao, P.H., and Ruggero, D. (2008). Suppression of Myc oncogenic activity by ribosomal protein haploinsufficiency. Nature *456*, 971-975.

Behrouzian, B., and Buist, P.H. (2002). Fatty acid desaturation: variations on an oxidative theme. Current opinion in chemical biology *6*, 577-582.

Benjamin, D.I., Li, D.S., Lowe, W., Heuer, T., Kemble, G., and Nomura, D.K. (2015). Diacylglycerol Metabolism and Signaling Is a Driving Force Underlying FASN Inhibitor Sensitivity in Cancer Cells. ACS chemical biology *10*, 1616-1623.

Bensaad, K., Favaro, E., Lewis, C.A., Peck, B., Lord, S., Collins, J.M., Pinnick, K.E., Wigfield, S., Buffa, F.M., Li, J.L.*, et al.* (2014). Fatty Acid Uptake and Lipid Storage Induced by HIF-1alpha Contribute to Cell Growth and Survival after Hypoxia-Reoxygenation. Cell reports *9*, 349-365.

Bickel, P.E., Tansey, J.T., and Welte, M.A. (2009). PAT proteins, an ancient family of lipid droplet proteins that regulate cellular lipid stores. Biochimica et biophysica acta *1791*, 419-440.

Bobrovnikova-Marjon, E., Grigoriadou, C., Pytel, D., Zhang, F., Ye, J., Koumenis, C., Cavener, D., and Diehl, J.A. (2010). PERK promotes cancer cell proliferation and tumor growth by limiting oxidative DNA damage. Oncogene *29*, 3881-3895.

Boxer, L.M., and Dang, C.V. (2001). Translocations involving c-myc and c-myc function. Oncogene *20*, 5595-5610.

Bozza, P.T., and Viola, J.P. (2010). Lipid droplets in inflammation and cancer. Prostaglandins, leukotrienes, and essential fatty acids *82*, 243-250.

Brewer, J.W., and Diehl, J.A. (2000). PERK mediates cell-cycle exit during the mammalian unfolded protein response. Proc Natl Acad Sci U S A *97*, 12625-12630.

Cancer Genome Atlas Research, N. (2013). Comprehensive molecular characterization of clear cell renal cell carcinoma. Nature *499*, 43-49.

Carracedo, A., Cantley, L.C., and Pandolfi, P.P. (2013). Cancer metabolism: fatty acid oxidation in the limelight. Nat Rev Cancer *13*, 227-232.

Carroll, P.A., Diolaiti, D., McFerrin, L., Gu, H., Djukovic, D., Du, J., Cheng, P.F., Anderson, S., Ulrich, M., Hurley, J.B.*, et al.* (2015). Deregulated Myc requires MondoA/Mlx for metabolic reprogramming and tumorigenesis. Cancer Cell *27*, 271-285.

Chang, B.H., Li, L., Paul, A., Taniguchi, S., Nannegari, V., Heird, W.C., and Chan, L. (2006). Protection against fatty liver but normal adipogenesis in mice lacking adipose differentiation-related protein. Mol Cell Biol *26*, 1063-1076.

Chang, B.H., Li, L., Saha, P., and Chan, L. (2010). Absence of adipose differentiation related protein upregulates hepatic VLDL secretion, relieves hepatosteatosis, and improves whole body insulin resistance in leptin-deficient mice. Journal of lipid research *51*, 2132-2142.

Chantranupong, L., Wolfson, R.L., and Sabatini, D.M. (2015). Nutrient-Sensing Mechanisms across Evolution. Cell *161*, 67-83.

Chen, F., Kishida, T., Yao, M., Hustad, T., Glavac, D., Dean, M., Gnarra, J.R., Orcutt, M.L., Duh, F.M., Glenn, G.*, et al.* (1995). Germline mutations in the von Hippel-Lindau disease tumor suppressor gene: correlations with phenotype. Human mutation *5*, 66-75.

Choi, C.S., Savage, D.B., Kulkarni, A., Yu, X.X., Liu, Z.X., Morino, K., Kim, S., Distefano, A., Samuel, V.T., Neschen, S.*, et al.* (2007). Suppression of diacylglycerol acyltransferase-2 (DGAT2), but not DGAT1, with antisense oligonucleotides reverses diet-induced hepatic steatosis and insulin resistance. J Biol Chem *282*, 22678-22688.

Clarke, H.J., Chambers, J.E., Liniker, E., and Marciniak, S.J. (2014). Endoplasmic reticulum stress in malignancy. Cancer Cell *25*, 563-573.

Commisso, C., Davidson, S.M., Soydaner-Azeloglu, R.G., Parker, S.J., Kamphorst, J.J., Hackett, S., Grabocka, E., Nofal, M., Drebin, J.A., Thompson, C.B.*, et al.* (2013). Macropinocytosis of protein is an amino acid supply route in Ras-transformed cells. Nature *497*, 633-637.

Cross, B.C., Bond, P.J., Sadowski, P.G., Jha, B.K., Zak, J., Goodman, J.M., Silverman, R.H., Neubert, T.A., Baxendale, I.R., Ron, D.*, et al.* (2012). The molecular basis for selective inhibition of unconventional mRNA splicing by an IRE1-binding small molecule. Proc Natl Acad Sci U S A *109*, E869-878.

Currie, E., Schulze, A., Zechner, R., Walther, T.C., and Farese, R.V., Jr. (2013). Cellular fatty acid metabolism and cancer. Cell Metab *18*, 153-161.

Duvel, K., Yecies, J.L., Menon, S., Raman, P., Lipovsky, A.I., Souza, A.L., Triantafellow, E., Ma, Q., Gorski, R., Cleaver, S.*, et al.* (2010). Activation of a metabolic gene regulatory network downstream of mTOR complex 1. Mol Cell *39*, 171-183.

Elorza, A., Soro-Arnaiz, I., Melendez-Rodriguez, F., Rodriguez-Vaello, V., Marsboom, G., de Carcer, G., Acosta-Iborra, B., Albacete-Albacete, L., Ordonez, A., Serrano-Oviedo, L.*, et al.* (2012). HIF2alpha acts as an mTORC1 activator through the amino acid carrier SLC7A5. Mol Cell *48*, 681-691.

Faller, W.J., Jackson, T.J., Knight, J.R., Ridgway, R.A., Jamieson, T., Karim, S.A., Jones, C., Radulescu, S., Huels, D.J., Myant, K.B.*, et al.* (2015). mTORC1-mediated translational elongation limits intestinal tumour initiation and growth. Nature *517*, 497-500.

Fels, D.R., Ye, J., Segan, A.T., Kridel, S.J., Spiotto, M., Olson, M., Koong, A.C., and Koumenis, C. (2008). Preferential cytotoxicity of bortezomib toward hypoxic tumor cells via overactivation of endoplasmic reticulum stress pathways. Cancer Res *68*, 9323-9330.

Folch, J., Lees, M., and Sloane Stanley, G.H. (1957). A simple method for the isolation and purification of total lipides from animal tissues. J Biol Chem *226*, 497-509.

Frew, I.J., and Moch, H. (2015). A clearer view of the molecular complexity of clear cell renal cell carcinoma. Annual review of pathology *10*, 263-289.

Fu, S., Yang, L., Li, P., Hofmann, O., Dicker, L., Hide, W., Lin, X., Watkins, S.M., Ivanov, A.R., and Hotamisligil, G.S. (2011). Aberrant lipid metabolism disrupts calcium homeostasis causing liver endoplasmic reticulum stress in obesity. Nature *473*, 528-531.

Gerlinger, M., Horswell, S., Larkin, J., Rowan, A.J., Salm, M.P., Varela, I., Fisher, R., McGranahan, N., Matthews, N., Santos, C.R.*, et al.* (2014). Genomic architecture and evolution of clear cell renal cell carcinomas defined by multiregion sequencing. Nature genetics *46*, 225-233.

Ghosh, R., Wang, L., Wang, E.S., Perera, B.G., Igbaria, A., Morita, S., Prado, K., Thamsen, M., Caswell, D., Macias, H.*, et al.* (2014). Allosteric inhibition of the IRE1alpha RNase preserves cell viability and function during endoplasmic reticulum stress. Cell *158*, 534-548.

Gordan, J.D., Lal, P., Dondeti, V.R., Letrero, R., Parekh, K.N., Oquendo, C.E., Greenberg, R.A., Flaherty, K.T., Rathmell, W.K., Keith, B.*, et al.* (2008). HIF-alpha effects on c-Myc distinguish two subtypes of sporadic VHL-deficient clear cell renal carcinoma. Cancer Cell *14*, 435-446.

Gossage, L., Eisen, T., and Maher, E.R. (2015). VHL, the story of a tumour suppressor gene. Nat Rev Cancer *15*, 55-64.

Greenberg, A.S., Coleman, R.A., Kraemer, F.B., McManaman, J.L., Obin, M.S., Puri, V., Yan, Q.W., Miyoshi, H., and Mashek, D.G. (2011). The role of lipid droplets in metabolic disease in rodents and humans. J Clin Invest *121*, 2102-2110.

Griffiths, B., Lewis, C.A., Bensaad, K., Ros, S., Zhang, Q., Ferber, E.C., Konisti, S., Peck, B., Miess, H., East, P.*, et al.* (2013). Sterol regulatory element binding protein-dependent regulation of lipid synthesis supports cell survival and tumor growth. Cancer & metabolism *1*, 3.

Griner, E.M., and Kazanietz, M.G. (2007). Protein kinase C and other diacylglycerol effectors in cancer. Nat Rev Cancer *7*, 281-294.

Gunaratnam, L., Morley, M., Franovic, A., de Paulsen, N., Mekhail, K., Parolin, D.A., Nakamura, E., Lorimer, I.A., and Lee, S. (2003). Hypoxia inducible factor activates the transforming growth factor-alpha/epidermal growth factor receptor growth stimulatory pathway in VHL(-/-) renal cell carcinoma cells. J Biol Chem *278*, 44966-44974.

Haas, J.T., Winter, H.S., Lim, E., Kirby, A., Blumenstiel, B., DeFelice, M., Gabriel, S., Jalas, C., Branski, D., Grueter, C.A.*, et al.* (2012). DGAT1 mutation is linked to a congenital diarrheal disorder. J Clin Invest *122*, 4680-4684.

Haddad, A.Q., Kapur, P., Singla, N., Raman, J.D., Then, M.T., Nuhn, P., Buchner, A., Bastian, P., Seitz, C., Shariat, S.F.*, et al.* (2015). Validation of mammalian target of rapamycin biomarker panel in patients with clear cell renal cell carcinoma. Cancer *121*, 43-50.

Hannun, Y.A., and Obeid, L.M. (2008). Principles of bioactive lipid signalling: lessons from sphingolipids. Nature reviews Molecular cell biology *9*, 139-150.

Hart, L.S., Cunningham, J.T., Datta, T., Dey, S., Tameire, F., Lehman, S.L., Qiu, B., Zhang, H., Cerniglia, G., Bi, M.*, et al.* (2012). ER stress-mediated autophagy promotes Myc-dependent transformation and tumor growth. J Clin Invest *122*, 4621-4634.

Hoffman, M.A., Ohh, M., Yang, H., Klco, J.M., Ivan, M., and Kaelin, W.G., Jr. (2001). von Hippel-Lindau protein mutants linked to type 2C VHL disease preserve the ability to downregulate HIF. Human molecular genetics *10*, 1019-1027.

Hu, C.J., Wang, L.Y., Chodosh, L.A., Keith, B., and Simon, M.C. (2003). Differential roles of hypoxia-inducible factor 1alpha (HIF-1alpha) and HIF-2alpha in hypoxic gene regulation. Mol Cell Biol *23*, 9361-9374.

Imai, Y., Boyle, S., Varela, G.M., Caron, E., Yin, X., Dhir, R., Dhir, R., Graham, M.J., and Ahima, R.S. (2012). Effects of perilipin 2 antisense oligonucleotide treatment on hepatic lipid metabolism and gene expression. Physiological genomics *44*, 1125-1131.

Imamura, M., Inoguchi, T., Ikuyama, S., Taniguchi, S., Kobayashi, K., Nakashima, N., and Nawata, H. (2002). ADRP stimulates lipid accumulation and lipid droplet formation in murine fibroblasts. American journal of physiology Endocrinology and metabolism *283*, E775-783.

Inoue, K., Kawahito, Y., Tsubouchi, Y., Kohno, M., Yoshimura, R., Yoshikawa, T., and Sano, H. (2001). Expression of peroxisome proliferator-activated receptor gamma in renal cell carcinoma and growth inhibition by its agonists. Biochemical and biophysical research communications *287*, 727-732.

Jones, J., Otu, H., Spentzos, D., Kolia, S., Inan, M., Beecken, W.D., Fellbaum, C., Gu, X., Joseph, M., Pantuck, A.J.*, et al.* (2005). Gene signatures of progression and metastasis in renal cell cancer. Clinical cancer research : an official journal of the American Association for Cancer Research *11*, 5730-5739.

Kammoun, H.L., Chabanon, H., Hainault, I., Luquet, S., Magnan, C., Koike, T., Ferre, P., and Foufelle, F. (2009). GRP78 expression inhibits insulin and ER stress-induced SREBP-1c activation and reduces hepatic steatosis in mice. J Clin Invest *119*, 1201-1215.

Kamphorst, J.J., Cross, J.R., Fan, J., de Stanchina, E., Mathew, R., White, E.P., Thompson, C.B., and Rabinowitz, J.D. (2013). Hypoxic and Ras-transformed cells support growth by scavenging unsaturated fatty acids from lysophospholipids. Proc Natl Acad Sci U S A *110*, 8882-8887.

Kaushik, S., and Cuervo, A.M. (2015). Degradation of lipid droplet-associated proteins by chaperone-mediated autophagy facilitates lipolysis. Nature cell biology *17*, 759-770.

Keith, B., Johnson, R.S., and Simon, M.C. (2012). HIF1alpha and HIF2alpha: sibling rivalry in hypoxic tumour growth and progression. Nat Rev Cancer *12*, 9-22.

Koliwad, S.K., Streeper, R.S., Monetti, M., Cornelissen, I., Chan, L., Terayama, K., Naylor, S., Rao, M., Hubbard, B., and Farese, R.V., Jr. (2010). DGAT1-dependent triacylglycerol storage by

macrophages protects mice from diet-induced insulin resistance and inflammation. J Clin Invest *120*, 756-767.

Kondagunta, G.V., Drucker, B., Schwartz, L., Bacik, J., Marion, S., Russo, P., Mazumdar, M., and Motzer, R.J. (2004). Phase II trial of bortezomib for patients with advanced renal cell carcinoma. Journal of clinical oncology : official journal of the American Society of Clinical Oncology *22*, 3720-3725.

Kondo, K., Kim, W.Y., Lechpammer, M., and Kaelin, W.G., Jr. (2003). Inhibition of HIF2alpha is sufficient to suppress pVHL-defective tumor growth. PLoS Biol *1*, E83.

Kondo, K., Klco, J., Nakamura, E., Lechpammer, M., and Kaelin, W.G., Jr. (2002). Inhibition of HIF is necessary for tumor suppression by the von Hippel-Lindau protein. Cancer Cell *1*, 237-246.

LaGory, E.L., Wu, C., Taniguchi, C.M., Ding, C.K., Chi, J.T., von Eyben, R., Scott, D.A., Richardson, A.D., and Giaccia, A.J. (2015). Suppression of PGC-1alpha Is Critical for Reprogramming Oxidative Metabolism in Renal Cell Carcinoma. Cell reports *12*, 116-127.

Laplante, M., and Sabatini, D.M. (2012). mTOR signaling in growth control and disease. Cell *149*, 274-293.

Latif, F., Tory, K., Gnarra, J., Yao, M., Duh, F.M., Orcutt, M.L., Stackhouse, T., Kuzmin, I., Modi, W., Geil, L.*, et al.* (1993). Identification of the von Hippel-Lindau disease tumor suppressor gene. Science *260*, 1317-1320.

Lee, A.H., Scapa, E.F., Cohen, D.E., and Glimcher, L.H. (2008). Regulation of hepatic lipogenesis by the transcription factor XBP1. Science *320*, 1492-1496.

Lee, J.S., Zheng, Z., Mendez, R., Ha, S.W., Xie, Y., and Zhang, K. (2012). Pharmacologic ER stress induces non-alcoholic steatohepatitis in an animal model. Toxicology letters *211*, 29-38.

Lee-Ying, R., Lester, R., and Heng, D. (2014). Current management and future perspectives of metastatic renal cell carcinoma. International journal of urology : official journal of the Japanese Urological Association *21*, 847-855.

Li, B., Qiu, B., Lee, D.S., Walton, Z.E., Ochocki, J.D., Mathew, L.K., Mancuso, A., Gade, T.P., Keith, B., Nissim, I.*, et al.* (2014). Fructose-1,6-bisphosphatase opposes renal carcinoma progression. Nature *513*, 251-255.

Li, C., Li, L., Lian, J., Watts, R., Nelson, R., Goodwin, B., and Lehner, R. (2015). Roles of Acyl-CoA:Diacylglycerol Acyltransferases 1 and 2 in Triacylglycerol Synthesis and Secretion in Primary Hepatocytes. Arteriosclerosis, thrombosis, and vascular biology *35*, 1080-1091.

Lin, C.Y., Loven, J., Rahl, P.B., Paranal, R.M., Burge, C.B., Bradner, J.E., Lee, T.I., and Young, R.A. (2012). Transcriptional amplification in tumor cells with elevated c-Myc. Cell *151*, 56-67.

Listenberger, L.L., Han, X., Lewis, S.E., Cases, S., Farese, R.V., Jr., Ory, D.S., and Schaffer, J.E. (2003). Triglyceride accumulation protects against fatty acid-induced lipotoxicity. Proc Natl Acad Sci U S A *100*, 3077-3082.

Listenberger, L.L., Ory, D.S., and Schaffer, J.E. (2001). Palmitate-induced apoptosis can occur through a ceramide-independent pathway. J Biol Chem *276*, 14890-14895.

Majmundar, A.J., Wong, W.J., and Simon, M.C. (2010). Hypoxia-inducible factors and the response to hypoxic stress. Mol Cell *40*, 294-309.

Mandriota, S.J., Turner, K.J., Davies, D.R., Murray, P.G., Morgan, N.V., Sowter, H.M., Wykoff, C.C., Maher, E.R., Harris, A.L., Ratcliffe, P.J.*, et al.* (2002). HIF activation identifies early lesions in VHL kidneys: evidence for site-specific tumor suppressor function in the nephron. Cancer Cell *1*, 459-468.

Martinez-Botas, J., Anderson, J.B., Tessier, D., Lapillonne, A., Chang, B.H., Quast, M.J., Gorenstein, D., Chen, K.H., and Chan, L. (2000). Absence of perilipin results in leanness and reverses obesity in Lepr(db/db) mice. Nature genetics *26*, 474-479.

Medvetz, D., Priolo, C., and Henske, E.P. (2015). Therapeutic targeting of cellular metabolism in cells with hyperactive mTORC1: a paradigm shift. Molecular cancer research : MCR *13*, 3-8.

Morrissey, J.J., Mellnick, V.M., Luo, J., Siegel, M.J., Figenshau, R.S., Bhayani, S., and Kharasch, E.D. (2015). Evaluation of Urine Aquaporin-1 and Perilipin-2 Concentrations as Biomarkers to Screen for Renal Cell Carcinoma: A Prospective Cohort Study. JAMA oncology *1*, 204-212.

Obeng, E.A., Carlson, L.M., Gutman, D.M., Harrington, W.J., Jr., Lee, K.P., and Boise, L.H. (2006). Proteasome inhibitors induce a terminal unfolded protein response in multiple myeloma cells. Blood *107*, 4907-4916.

Oslowski, C.M., and Urano, F. (2011). Measuring ER stress and the unfolded protein response using mammalian tissue culture system. Methods in enzymology *490*, 71-92.

Ozcan, U., Ozcan, L., Yilmaz, E., Duvel, K., Sahin, M., Manning, B.D., and Hotamisligil, G.S. (2008). Loss of the tuberous sclerosis complex tumor suppressors triggers the unfolded protein response to regulate insulin signaling and apoptosis. Mol Cell *29*, 541-551.

Peterson, T.R., Sengupta, S.S., Harris, T.E., Carmack, A.E., Kang, S.A., Balderas, E., Guertin, D.A., Madden, K.L., Carpenter, A.E., Finck, B.N.*, et al.* (2011). mTOR complex 1 regulates lipin 1 localization to control the SREBP pathway. Cell *146*, 408-420.

Porstmann, T., Santos, C.R., Griffiths, B., Cully, M., Wu, M., Leevers, S., Griffiths, J.R., Chung, Y.L., and Schulze, A. (2008). SREBP activity is regulated by mTORC1 and contributes to Akt-dependent cell growth. Cell Metab *8*, 224-236.

Purdue, M.P., Johansson, M., Zelenika, D., Toro, J.R., Scelo, G., Moore, L.E., Prokhortchouk, E., Wu, X., Kiemeney, L.A., Gaborieau, V.*, et al.* (2011). Genome-wide association study of renal cell carcinoma identifies two susceptibility loci on 2p21 and 11q13.3. Nature genetics *43*, 60-65.

Rankin, E.B., Rha, J., Selak, M.A., Unger, T.L., Keith, B., Liu, Q., and Haase, V.H. (2009). Hypoxia-inducible factor 2 regulates hepatic lipid metabolism. Mol Cell Biol *29*, 4527-4538.

Raval, R.R., Lau, K.W., Tran, M.G., Sowter, H.M., Mandriota, S.J., Li, J.L., Pugh, C.W., Maxwell, P.H., Harris, A.L., and Ratcliffe, P.J. (2005). Contrasting properties of hypoxia-inducible factor 1 (HIF-1) and HIF-2 in von Hippel-Lindau-associated renal cell carcinoma. Mol Cell Biol *25*, 5675-5686.

Roschinger, W., Muntau, A.C., Duran, M., Dorland, L., L, I.J., Wanders, R.J., and Roscher, A.A. (2000). Carnitine-acylcarnitine translocase deficiency: metabolic consequences of an impaired

mitochondrial carnitine cycle. Clinica chimica acta; international journal of clinical chemistry *298*, 55-68.

Rutkowski, D.T., Wu, J., Back, S.H., Callaghan, M.U., Ferris, S.P., Iqbal, J., Clark, R., Miao, H., Hassler, J.R., Fornek, J.*, et al.* (2008). UPR pathways combine to prevent hepatic steatosis caused by ER stress-mediated suppression of transcriptional master regulators. Developmental cell *15*, 829-840.

Sapiro, J.M., Mashek, M.T., Greenberg, A.S., and Mashek, D.G. (2009). Hepatic triacylglycerol hydrolysis regulates peroxisome proliferator-activated receptor alpha activity. Journal of lipid research *50*, 1621-1629.

Sato, Y., Yoshizato, T., Shiraishi, Y., Maekawa, S., Okuno, Y., Kamura, T., Shimamura, T., Sato-Otsubo, A., Nagae, G., Suzuki, H.*, et al.* (2013). Integrated molecular analysis of clear-cell renal cell carcinoma. Nature genetics *45*, 860-867.

Schmidt, E.K., Clavarino, G., Ceppi, M., and Pierre, P. (2009). SUnSET, a nonradioactive method to monitor protein synthesis. Nature methods *6*, 275-277.

Schodel, J., Bardella, C., Sciesielski, L.K., Brown, J.M., Pugh, C.W., Buckle, V., Tomlinson, I.P., Ratcliffe, P.J., and Mole, D.R. (2012). Common genetic variants at the 11q13.3 renal cancer susceptibility locus influence binding of HIF to an enhancer of cyclin D1 expression. Nature genetics *44*, 420-425, S421-422.

Shen, C., Beroukhim, R., Schumacher, S.E., Zhou, J., Chang, M., Signoretti, S., and Kaelin, W.G., Jr. (2011). Genetic and functional studies implicate HIF1alpha as a 14q kidney cancer suppressor gene. Cancer Discov *1*, 222-235.

Shen, C., and Kaelin, W.G., Jr. (2013). The VHL/HIF axis in clear cell renal carcinoma. Seminars in cancer biology *23*, 18-25.

Shin, J., He, M., Liu, Y., Paredes, S., Villanova, L., Brown, K., Qiu, X., Nabavi, N., Mohrin, M., Wojnoonski, K.*, et al.* (2013). SIRT7 represses Myc activity to suppress ER stress and prevent fatty liver disease. Cell reports *5*, 654-665.

Siegel, R., Ma, J., Zou, Z., and Jemal, A. (2014). Cancer statistics, 2014. CA: a cancer journal for clinicians *64*, 9-29.

Smith, S.J., Cases, S., Jensen, D.R., Chen, H.C., Sande, E., Tow, B., Sanan, D.A., Raber, J., Eckel, R.H., and Farese, R.V., Jr. (2000). Obesity resistance and multiple mechanisms of triglyceride synthesis in mice lacking Dgat. Nature genetics *25*, 87-90.

Son, S.H., Goo, Y.H., Chang, B.H., and Paul, A. (2012). Perilipin 2 (PLIN2)-deficiency does not increase cholesterol-induced toxicity in macrophages. PloS one *7*, e33063.

Stone, S.J., Myers, H.M., Watkins, S.M., Brown, B.E., Feingold, K.R., Elias, P.M., and Farese, R.V., Jr. (2004). Lipopenia and skin barrier abnormalities in DGAT2-deficient mice. J Biol Chem *279*, 11767-11776.

Sun, M., Lughezzani, G., Perrotte, P., and Karakiewicz, P.I. Treatment of metastatic renal cell carcinoma. Nat Rev Urol *7*, 327-338.

Sun, Z., Miller, R.A., Patel, R.T., Chen, J., Dhir, R., Wang, H., Zhang, D., Graham, M.J., Unterman, T.G., Shulman, G.I.*, et al.* (2012). Hepatic Hdac3 promotes gluconeogenesis by repressing lipid synthesis and sequestration. Nature medicine *18*, 934-942.

Suzuki, J., Akahane, K., Nakamura, J., Naruse, K., Kamiya, H., Himeno, T., Nakamura, N., Shibata, T., Kondo, M., Nagasaki, H.*, et al.* (2011). Palmitate induces apoptosis in Schwann cells via both ceramide-dependent and independent pathways. Neuroscience *176*, 188-198.

Sztalryd, C., Bell, M., Lu, X., Mertz, P., Hickenbottom, S., Chang, B.H., Chan, L., Kimmel, A.R., and Londos, C. (2006). Functional compensation for adipose differentiation-related protein (ADFP) by Tip47 in an ADFP null embryonic cell line. J Biol Chem *281*, 34341-34348.

Tansey, J.T., Sztalryd, C., Gruia-Gray, J., Roush, D.L., Zee, J.V., Gavrilova, O., Reitman, M.L., Deng, C.X., Li, C., Kimmel, A.R.*, et al.* (2001). Perilipin ablation results in a lean mouse with aberrant adipocyte lipolysis, enhanced leptin production, and resistance to diet-induced obesity. Proc Natl Acad Sci U S A *98*, 6494-6499.

Thiam, A.R., Farese, R.V., Jr., and Walther, T.C. (2013). The biophysics and cell biology of lipid droplets. Nature reviews Molecular cell biology *14*, 775-786.

Tun, H.W., Marlow, L.A., von Roemeling, C.A., Cooper, S.J., Kreinest, P., Wu, K., Luxon, B.A., Sinha, M., Anastasiadis, P.Z., and Copland, J.A. (2010). Pathway signature and cellular differentiation in clear cell renal cell carcinoma. PloS one *5*, e10696.

van Meer, G., Voelker, D.R., and Feigenson, G.W. (2008). Membrane lipids: where they are and how they behave. Nature reviews Molecular cell biology *9*, 112-124.

Volmer, R., van der Ploeg, K., and Ron, D. (2013). Membrane lipid saturation activates endoplasmic reticulum unfolded protein response transducers through their transmembrane domains. Proc Natl Acad Sci U S A *110*, 4628-4633.

Walter, K.M., Schonenberger, M.J., Trotzmuller, M., Horn, M., Elsasser, H.P., Moser, A.B., Lucas, M.S., Schwarz, T., Gerber, P.A., Faust, P.L.*, et al.* (2014). Hif-2alpha promotes degradation of Mammalian peroxisomes by selective autophagy. Cell Metab *20*, 882-897.

Walter, P., and Ron, D. (2011). The unfolded protein response: from stress pathway to homeostatic regulation. Science *334*, 1081-1086.

Walther, T.C., and Farese, R.V., Jr. (2012). Lipid droplets and cellular lipid metabolism. Annual review of biochemistry *81*, 687-714.

Wilfling, F., Wang, H., Haas, J.T., Krahmer, N., Gould, T.J., Uchida, A., Cheng, J.X., Graham, M., Christiano, R., Frohlich, F.*, et al.* (2013). Triacylglycerol synthesis enzymes mediate lipid droplet growth by relocalizing from the ER to lipid droplets. Developmental cell *24*, 384-399.

Wright, D.H. (1968). Lipid content of malignant lymphomas. Journal of clinical pathology *21*, 643-649.

Yao, M., Huang, Y., Shioi, K., Hattori, K., Murakami, T., Nakaigawa, N., Kishida, T., Nagashima, Y., and Kubota, Y. (2007). Expression of adipose differentiation-related protein: a predictor of cancer-specific survival in clear cell renal carcinoma. Clinical cancer research : an official journal of the American Association for Cancer Research *13*, 152-160.

Yen, C.L., Stone, S.J., Koliwad, S., Harris, C., and Farese, R.V., Jr. (2008). Thematic review series: glycerolipids. DGAT enzymes and triacylglycerol biosynthesis. Journal of lipid research *49*, 2283-2301.

Young, R.M., Ackerman, D., Quinn, Z.L., Mancuso, A., Gruber, M., Liu, L., Giannoukos, D.N., Bobrovnikova-Marjon, E., Diehl, J.A., Keith, B.*, et al.* (2013). Dysregulated mTORC1 renders cells critically dependent on desaturated lipids for survival under tumor-like stress. Genes Dev *27*, 1115-1131.

Yue, S., Li, J., Lee, S.Y., Lee, H.J., Shao, T., Song, B., Cheng, L., Masterson, T.A., Liu, X., Ratliff, T.L.*, et al.* (2014). Cholesteryl ester accumulation induced by PTEN loss and PI3K/AKT activation underlies human prostate cancer aggressiveness. Cell Metab *19*, 393-406.

Zager, R.A., Johnson, A.C., and Becker, K. (2011). Acute unilateral ischemic renal injury induces progressive renal inflammation, lipid accumulation, histone modification, and "end-stage" kidney disease. American journal of physiology Renal physiology *301*, F1334-1345.

Zhang, Y., Nicholatos, J., Dreier, J.R., Ricoult, S.J., Widenmaier, S.B., Hotamisligil, G.S., Kwiatkowski, D.J., and Manning, B.D. (2014). Coordinated regulation of protein synthesis and degradation by mTORC1. Nature *513*, 440-443.